Using Soils to Constrain Past and Future Terrestrial Climate Change

by

Jennifer M. Cotton

A dissertation submitted in partial fulfillment
of the requirements for the degree of
Doctor of Philosophy
(Earth and Environmental Sciences)
in the University of Michigan
2013

Doctoral Committee:

Assistant Professor Nathan D. Sheldon, Chair
Assistant Professor Sarah M. Aciego
Professor Kyger C. Lohmann
Assistant Professor David C. Lund
Professor Donald R. Zak

This thesis is dedicated to Boris Avdeev and Jillian Drow.

Friends lost during my time at the University of Michigan, but not forgotten.

Acknowledgements

This thesis would not be possible without the help of many people from the field to the lab to the writing process. First and foremost, I would like to thank my advisor for taking a chance on a mediocre chemistry major with little background in geology. Not only I have learned a great deal from Nathan, but he has always listened to my ideas and has been incredibly tolerant of my research "A.D.D." and constant threats to quit grad school and open a food truck. I would have little data without the help of many people in the field, especially my labmates Ethan Hyland, Tim Gallagher and Christie Wilkins. To call them field assistants would be a gross understatement. I am grateful for my co-authors Louise Jeffery, Mike Hren, Ethan and Tim, without whose knowledge and expertise these projects could never have been completed, and for my committee Sarah Aciego, Kacey Lohmann, Dave Lund and Don Zak for their guidance. I am also grateful for the many people who have taken the time to read my manuscripts and offer helpful comments, including Selena Smith, Rich Fiorella, Laura Waters, and countless reviewers. I would like to acknowledge my funding sources for work completed over the last five years: the National Science Foundation, the Geological Society of America, the Evolving Earth Foundation, the American Association of Petroleum Geologists, the Society for Sedimentary Geology, ExxonMobil, the University of Michigan Rackham Graduate School and the department of Earth and Environmental Sciences. I thank my family,

Mom, Dad, Jess and Den for their constant encouragement, especially my mother who never ceases to ask if I have finished my homework, even at the age of 27. And lastly, I thank all of my friends from C.C. Little for filling the last five years with dancing, climbing, building, brewing, and fun in general, including Nora, Alison, Nadja, Dan, Alex, Boris, Lydia, Louise, Meghan W., Meghan T., Tom, Steph, Tim, Allie, Will, Mike, Matt, Sarah and Larianna. I especially thank the past and present member of the GeoFrat: Ethan, Carli, Rich, Laura, Tara, Rohit, Clay, Sae, Ethan F., Mark, Attila, Cloey and Dancefloor. Thanks!

Table of Contents

Dedication ..... **ii**

Acknowledgements ..... **iii**

List of Figures ..... **vii**

List of Tables ..... **ix**

List of Appendices ..... **xi**

Abstract ..... **xii**

Chapter 1. Introduction **1**
1.1 Introduction to the Global Carbon Cycle 3
1.2 Stable Isotopes in the Environment 5
1.3 Proxy Reconstructions of Atmospheric pCO_2 8
1.4 Soils as a Proxy for Atmospheric pCO_2 10
1.5 Dissertation Structure 12
1.6 Publications and Abstracts Resulting From This Dissertation 18
1.7 References 20

Chapter 2. New constraints on using paleosols to reconstruct atmospheric pCO_2 24
2.0 Abstract 24
2.1 Introduction 25
2.2 Background 27
2.3 Methods 31
2.4 Results 34
2.5 Discussion 37
2.6 Application to the Geologic Past 40
2.6.1 Application to the Cenozoic 41
2.6.2 Application to the Mesozoic 45
2.6.3 Application to the Paleozoic 46
2.6.4 CO_2-Temperature Coupling in the Geologic Past 48
2.7 Implications for Paleosol Paleobarometry 50
2.8 Conclusions 55
2.9 Acknowledgements 57
2.10 References 68

Chapter 3. Climate controls on soil-respired CO_2 in the United States: Implications for 21st century chemical weathering rates in temperate and arid ecosystems 73
3.0 Abstract 73
3.1 Introduction 74
3.2 Background 77
3.3 Methods 80

3.3.1 Modern Soil CO_2 Spatial Variability 80
3.3.2 Future S(z) and [CO_{2aq}] predictions 83
3.4 Results 85
3.4.1 Modern Spatial Variability in S(z) 85
3.4.2 Predictions of Future Spatial Variability of S(z) and [CO_{2aq}] 86
3.5 Discussion 89
3.5.1 Modern Spatial Variability of S(z) 89
3.5.2 Implications for Future Chemical Weathering and CO_2 Consumption 91
3.5.3 Uncertainties in Future Spatial Variability of S(z) 93
3.5.4 Limitations of the Model 94
3.6 Conclusions 95
3.7 Acknowledgements 96
3.8 References 104

Chapter 4. Positive feedback drives carbon release from soils to atmosphere during Paleocene/Eocene warming 111
4.0 Abstract 111
4.1 Introduction 112
4.2 Methods 114
4.3 Results 117
4.4 Discussion 118
4.4.1 Increased Atmospheric pCO_2 118
4.4.2 Increased Temperature and Productivity 119
4.4.3 Changing Depth to Bk Horizon 122
4.4.4 Additional Carbon Source 123
4.4.5 Methane Cycling 124
4.4.6 Increased Surface Carbon Cycling 125
4.5 Implications for Carbon Cycle 129
4.6 Conclusions 143
4.7 Acknowledgements 143
4.8 References 143

Chapter 5. Summary of major results and conclusions 149
5.1 Chapter 2 149
5.2 Chapter 3 151
5.3 Chapter 4 153
5.4 Implications for Future Climate Change 154
5.5 Future Work 156
5.6 References 160

Appendices 163

List of Figures

Figure 1.1. The global carbon cycle..... 16

Figure 1.2. Stable isotopes in the terrestrial biosphere. 17

Figure 2.1. Soil CO_2 versus climatic variables.. 58

Figure 2.2. Relationship between summer minimum soil-respired CO_2 (*S(z)*) and mean annual precipitation for 23 soils forming pedogenic carbonate. 59

Figure 2.3. Field photographs from modern soils used in calibration and paleosols from the late Miocene Beaverhead locality.. 60

Figure 2.4. Atmospheric pCO_2 reconstruction for the late Miocene from the Beaverhead pedogenic carbonates using the new soil-respired CO_2 proxy compared to reconstructions from multiple other proxies from a variety of locations..... 61

Figure 2.5. Revised paleosol carbonate pCO_2 estimates compared with proxy and model results.. 62

Figure 2.6. Calculated *S(z)* values for modern validation soils, including $\Delta^{13}C$ values between 14–17‰. 63

Figure 2.7. Procedural guidelines to follow for use of pedogenic carbonates in atmospheric CO_2 reconstructions..... 64

Figure 3.1. Range of values of summer soil-respired CO_2 (*S(z)* by soil order 97

Figure 3.2. Relationship between summer average *S(z)* and mean annual precipitation in the continental United States for soils forming under 900 mm yr^{-1} precipitation or less..... 98

Figure 3.3. A: Calculated modern summer average *S(z)* for areas receiving 900 mm yr^{-1} precipitation or less in the central and Western United States..... 99

Figure 3.4. Plots of the five regional climate model simulations of current precipitation conditions from 1971 – 2000 compared to average observed precipitation conditions from the WorldClim dataset..... 100

Figure 3.5. Left: Summer average [CO_{2aq}] for the decade 2050–2060 in μmoles L^{-1} H_2O. [CO_{2aq}] and weathering rates are higher in the Great Plains and the in the southwestern United States. 101

Figure 3.6. A-C: Summer average [CO_{2aq}] for the decade 2050–2060 in μmoles L^{-1} H_2O for the three models that do not accurately simulate modern precipitation variability across the western United States. 102

Figure 4.1. $\Delta^{13}C$ anomalies for Polecat Bench, Tendruy, and Axhandle Canyon. 134

Figure 4.2. Atmospheric CO_2/*S(z)* ratios for each site calculated using Eq. 4.3.. 135

Figure 4.3. The isotopic composition of soil CO_2 with depth in a hypothetical soil. 136

Figure 4.4. $\Delta^{13}C$ anomaly vs. %C for each PETM site. 137

Figure 4.5. Predicted $\delta^{13}C_s$ and $\delta^{13}C_s$ recorded by the isotopic composition of pedogenic carbonates from Polecat Bench and Tendruy for the pre/post PETM. 138

Figure A1. Location of soil sites used in literature review based proxy derivation and modern soil carbonate calibration. 164

Figure A2. Comparison between the summer minimum soil-respired CO_2 and summer average soil-respired CO_2 proxies. 165

Figure A3. Plot of summer minimum soil-respired CO_2 (*S(z)*) and monthly precipitation during the time of soil CO_2 measurement. 166

Figure A4. Summer minimum soil-respired CO_2 vs. MAP for arid to sub-humid soils. 167

Figure B1. Basic geologic map of the western United States highlighting the regions dominated by limestone bedrock.. 252

Figure C1. $\delta^{13}C_{calcite}$ record analyzed in this study compared to the record previously published by Bowen and Bowen (2008). 271

List of Tables

Table 2.1. Isotopic data from Montana paleosols used to reconstruct pCO_2 of the late Miocene..... 65

Table 2.2. Previously published estimates as well as revised estimates for both *S(z)* and atmospheric pCO_2 for Mesozoic and Paleozoic case studies..... 67

Table 3.1 Summary of the soil CO_2 data derived from literature review.. 103

Table 4.1. $\delta^{13}C_{org}$ values used to calculate $\delta^{13}C_s$ with varying contributions of respiration from surface litter..... 142

Table A1. Summer minimum soil-respired CO_2 data used in the linear regression to derive the new *S(z)* proxy 168

Table A2. Isotopic and climatic data from modern soils used to validate new *S(z)* proxy.. 170

Table A3. Descriptions of individual soils from Beaverhead locality used in Miocene atmospheric pCO_2 reconstruction 172

Table A4. Calculations of partial derivatives for Gaussian error propagation according to equations derived by Retallack (2009). 173

Table A5. Individual summer soil CO_2 measurements..... 174

Table B1. Summer Average *S(z)* for sites in the United States forming under 900 mm yr^{-1} 253

Table B2. Comparison between different regional climate models..... 254

Table B3. Individual measurements from soils located in the United States forming under 900 mm yr^{-1}..... 255

Table C1. Carbon isotopic compositions of preserved organic material and pedogenic carbonates from paleosols at Axhandle Canyon, Utah. 272

Table C2. Carbon isotopic data from preserved organic material and pedogenic carbonates in paleosols from Polecat Bench in the Bighorn Basin, Wyoming.. 274

Table C3. Carbon isotopic data from preserved organic material and pedogenic carbonates in paleosols from Tendruy in the Southeastern Pyrenees, Spain.…..... 276

Table C4. Carbon and oxygen isotopic composition of pedogenic carbonates from paleosols at Axhandle Canyon, Utah measured at the University of Michigan for this study.…..... 277

List of Appendices

Appendix A **163**
Appendix B **250**
Appendix C **270**

Abstract

Future ecosystem and climatic changes due to anthropogenic emissions of CO_2 are of increasing importance to society. Soils are the largest terrestrial reservoir of carbon, have the potential to become new sources or sinks of carbon to the atmosphere, and can also record information about climate and environment. In this dissertation, I use modern and ancient soil to constrain past and future terrestrial climate and environmental change. To better determine the sensitivity of ecosystems to changes in atmospheric CO_2 and climate, we must first increase the precision of past atmospheric CO_2 reconstructions. I have developed a new proxy for soil-respired CO_2 based on its relationship with precipitation to reduce the uncertainties in the soil carbonate paleobarometer, the most widely applicable method of atmospheric CO_2 reconstructions. Using this new method of paleobarometry, I have refined previous estimates of atmospheric CO_2 and find that estimates now support CO_2-temperature coupling throughout the Phanerozoic. This new respired CO_2 proxy is also useful for predictions of carbon cycle changes. Silicate weathering consumes atmospheric CO_2, and the concentration of soil CO_2 is an important factor in weathering rates. I couple the newly derived relationship to precipitation simulations from regional climate models to predict future changes to soil CO_2 and the concentration of dissolved CO_2. I find large increases in dissolved CO_2 for the central Great Plains region and moderate decreases for the Southwestern United States for the

decade of 2050-2060, indicating that the Great Plain soils may become a new sink for atmospheric CO_2 in the future. While increased chemical weathering in soils may act to buffer anthropogenic CO_2 emissions on decadal time scales, on longer hundred to thousand year time scales warming may destabilize the carbon pool stored in soils. Here, I use paleosols from the Paleocene-Eocene Thermal Maximum to determine how soils respond to rapid climate warming on thousand year time scales. The carbon isotopic compositions of pedogenic carbonates and soil organic matter indicate increases to soil respiration that likely reduced carbon burial and increased fluxes of carbon to the atmosphere. Results from this dissertation have important implications for changes to climate, environment and carbon cycling in the next century and beyond.

Chapter 1

Introduction

Anthropogenically driven climate change is one of the most pressing concerns facing humanity. To predict better future climatic and environmental changes and their effect on human populations world wide, we must first understand how sensitive Earth's climate is to changes in atmospheric composition as well as how sensitive ecosystems are to climatic changes in the geologic past. The concentration of atmospheric CO_2 is the main control of the Earth's temperature over geologic time (Royer et al., 2004); however, the precise relationship between CO_2 and temperature is not fully understood (IPCC, 2007). In order to determine precisely the relationship between atmospheric pCO_2 and temperature, it is necessary to quantify the concentration of atmospheric pCO_2 in the geologic past for comparison to temperature records. The major goal of this research is to reconstruct more precisely the atmospheric CO_2 levels and temperature during times in the geologic past analogous to future climate change in order to provide better constraints on the magnitude of future climate and on predictions of likely environmental changes.

According to the IPCC (2007), a 1.5–4.5°C temperature increase is expected per doubling of CO_2. This temperature range is not precise enough to accurately predict future environmental changes associated with current climate change, and with CO_2 set to approach double preindustrial values by the year 2050 (IPCC, 2007), it is imperative to

be able to anticipate and prepare for the coming changes. Until recently, most estimates of CO_2-temperature sensitivity were derived using records from the past few thousand to hundreds of thousands of years, when CO_2 was low and similar to today's values (Royer et al., 2007; Paleosens Project Members, 2012). It is unclear whether the Earth's climate behaves similarly during times of high atmospheric CO_2 analogous to conditions in the near future. While the concentration of atmospheric CO_2 can be directly measured through gases trapped in ice cores back to roughly 800,000 years (Lüthi et al., 2008), the Earth has had low concentrations of atmospheric CO_2 similar to today's value for at least the last 5 Ma (Royer et al., 2004). Therefore, it is necessary to look to deep time using geochemical proxies to constrain CO_2-temperature sensitivity and also environmental changes that arise from associated warming at times of elevated CO_2 analogous to future climate change. Recent work has included Cenozoic paleoclimatic reconstructions into climate sensitivity estimates and finds a 2.2–4.8°C increase in surface temperature per doubling of CO_2 (Paleosens Project Members, 2012). This variability in temperature change is due in part to the errors associated with proxy reconstructions of atmospheric pCO_2, highlighting the need for more precise estimates in deep time.

Changes to the composition of the atmosphere, the climate and environment in deep time can be investigated using geochemical proxies. This dissertation focuses on using light stable isotopes as a method for tracing the cycling of elements within the biosphere. Stable isotopes are non-radioactive species of the same chemical element that have differing atomic masses due to the number of neutrons in the nucleus. Carbon has two stable isotopes, ^{12}C, which makes up 98.9% of all carbon, and ^{13}C, which makes up 1.1% of all carbon. The stable isotopic composition, or the ratio of $^{13}C/^{12}C$ in different

carbon reservoirs on Earth is highly variable. These differences can be used to track changes to Earth's surficial environments in the geologic past, including the transfer of carbon to the atmosphere and changing composition of the vegetation in a particular environment. The following work focuses on using these different stable isotopic compositions of carbon pools to understand changes to the atmosphere and terrestrial biosphere in deep time. In particular, this work uses the carbon isotopic composition of preserved organic material and pedogenic (soil) carbonates to constrain atmospheric CO_2 concentrations and changes to the terrestrial carbon cycle during times of rapid climate change, as well as making predictions about changes to the carbon cycle in the future.

1.1 Introduction to the Global Carbon Cycle

The main control on Earth's climate through time is the concentration of greenhouse gases, and CO_2 is the primary greenhouse gas whose concentration varies substantially through time (due to natural and anthropogenic processes) to influence climate. In order to constrain climate change associated with CO_2 in the atmosphere we must understand the sources and sinks of atmospheric CO_2. Carbon stored in many different reservoirs on Earth, including the Earth's interior, atmosphere, the biosphere, oceans and sediments. On short (annual to decadal) timescales, carbon is moved to the atmosphere through respiration and oxidation of plant litter and soil carbon in the biosphere, as well as through the release of carbon from the surface ocean. This release of carbon is balanced by the uptake of CO_2 through photosynthesis in the terrestrial biosphere and the absorption of CO_2 into the surface ocean equal to the amount of CO_2 released to the atmosphere. Unless there is a change to these fluxes, the concentration of

CO_2 in the atmosphere over short time scales is in a steady state. A summary of the modern global carbon cycle is shown in Figure 1.1.

Over long time scales, carbon is released to the atmosphere from sediments and rocks through volcanism. Carbon is removed from the atmosphere through the process of terrestrial silicate chemical weathering as shown by this schematic "Urey" equation:

$$CaSiO_3 + H_2CO_3 \rightarrow CaCO_3 + SiO_2 + H_2O \text{ (Eq. 1.1)}$$

The rate at which CO_2 is released to the atmosphere through volcanism is dependent on sea floor spreading rates (Berner et al., 1983). The rate at which CO_2 is removed from the atmosphere via weathering is dependent on a number of factors including the amount of exposed silicate bedrock on Earth and climate. According to the Arrhenius equation, the rates of chemical reactions are generally faster at higher temperatures (Engel and Reid, 2012), and thus chemical weathering and CO_2 drawdown from the atmosphere increases with increasing mean annual temperature (Brady et al., 1999). Because temperature is controlled by atmospheric CO_2 content, chemical weathering of silicate minerals is a negative feedback on the climate system, where high CO_2 and high temperatures increase weathering and the rate of drawdown and consumption of CO_2 from the atmosphere (Berner et al., 1983; Berner and Kothavala, 2001; Berner, 2006). The rates of volcanism and weathering are not necessarily balanced, and differences between these rates of CO_2 release and drawdown form the long-term control on the concentration of CO_2 in the atmosphere and Earth's climate. However, perturbations in the larger fluxes of carbon to and from the terrestrial biosphere and oceans, or the introduction of a new flux (e.g., the burning of fossil fuels by humans) can cause rapid climate change events. Determining how these reservoirs and fluxes change in the geologic past is important for

understanding ecosystem response to rapid warming events, and stable carbon isotopes provide a method to trace these changes to the carbon cycle.

1.2 Stable Isotopes in the Environment

The differences in stable isotopic compositions of carbon reservoirs arise from equilibrium and kinetic isotope fractionation processes. Equilibrium is defined as the state in which chemical substances have not necessarily stopped reacting, but are present in concentrations that do not change further with time. Fractionation, or the separation of heavy and light isotopes, can also occur while a reaction is proceeding towards equilibrium. The equilibrium isotopic composition of reacting substances is dependent on temperature, with the largest fractionations occurring at low temperatures and the smallest fractionations occurring at high temperatures (Kim and O'Neil, 1997). An increase or decrease in temperature can cause a shift in the equilibrium isotopic composition of reactants and products. When two substances in equilibrium are in different phases, the heavier isotope is also preferentially incorporated into the liquid or solid phase (Faure and Mensing, 2005).

Equilibrium isotope processes are the dominant fractionation processes in inorganic reactions. For example, water vapor in equilibrium with liquid water will undergo isotopic exchange between the two phases according to the following equation.

$$H_2{}^{18}O_v + H_2{}^{16}O_l \leftrightarrow H_2{}^{16}O_v + H_2{}^{18}O_l \quad \text{(Eq. 1.2)}$$

^{18}O is preferentially incorporated into the liquid phase of water, and the equilibrium ratio of ^{18}O in liquid to ^{18}O in vapor is dependent on temperature (Dansgaard, 1964; Faure and Mensing, 2005). On the other hand, in biological reactions, the kinetic isotope effect

dominates fractionation of stable isotopes. The kinetic isotope effect is defined as fractionation that occurs during a chemical reaction due to the mass difference of different isotopes in a molecule affecting the rates in which those molecules are involved in that chemical reaction. For a given element, a chemical bond involving the heavier isotope has a lower zero point energy and is stronger, and requires more energy to break than a chemical bond involving the lighter isotope (Park and Epstein, 1960; Bigeleisen, 1965). Therefore, molecules containing the lighter isotope of a given element typically react faster than molecules containing the heavier isotope. For irreversible chemical reactions such as photosynthesis, fractionation due to the kinetic isotope effect tends to produce products that are isotopically lighter than the reactants.

Differences in the isotopic composition of materials are measured as ratios of the heavy to light isotope in a sample and are compared to that ratio in a standard according to the following equation:

$$\delta^{heavy}X = \left(\frac{R_{sample}}{R_{std}} - 1\right) \times 1000 \text{ (Eq. 1.3)}$$

where R is the ratio of the heavy to the light isotope of element X ($^{heavy}X/^{light}X$) and $\delta^{heavy}X$ represents the isotopic composition of element X compared to that of a standard. Isotopic ratios are reported in units of per mil (‰), which is similar to percent, but represents units of per thousand.

Carbon has two stable isotopes, ^{12}C that makes up 99% of carbon, and ^{13}C that makes up 1% of carbon. For carbon, $R=^{13}C/^{12}C$ and $\delta^{13}C$ represents the isotopic composition of a sample with respect to the international standard Vienna Pee Dee Belemnite (Coplen, 2011). $\delta^{13}C$ values are highly variable within different carbon-

containing materials on Earth due to fractionations associated with both equilibrium and kinetic processes. For example, the process of photosynthesis acts to fractionate carbon in the biosphere. Terrestrial C_3 plants use RuBisCo to capture and fix atmospheric CO_2 into sugars. However, due to the kinetic isotope effect, RuBisCo preferentially binds to $^{12}CO_2$, making plant carbon depleted in ^{13}C relative to the atmosphere (Tipple and Pagani, 2007). The average depletion is -19‰ less than atmospheric CO_2 (Koch, 1998), and under current atmospheric conditions, the average $\delta^{13}C$ of terrestrial C_3 plants is ~-27‰ (Cerling et al. 1997; Cerling and Harris, 1999). C_4 photosynthesis, which evolved and spread in the Miocene (Tipple and Pagani, 2007) employs a carbon concentrating mechanism though the use of PEP-carboxylase. This enzyme discriminates less against ^{13}C than RuBisCo, such that biomass derived from C_4 photosynthesis is only an average of -5.5‰ more depleted in ^{13}C than the atmosphere. The average $\delta^{13}C$ of C_4 plants is -13‰ (Cerling et al., 1997).

Carbon generated from photosynthesis can then be transferred to different terrestrial carbon pools. For example, leaf litter becomes partially degraded and buried to become soil organic matter, and the further degradation of that litter and soil organic matter produces CO_2 in the soil atmosphere. Soil CO_2 can then be involved in the formation of carbonates within the soil. Pedogenic carbonates are calcium carbonate nodules that often precipitate in isotopic equilibrium with soil CO_2. Soil CO_2 is predominantly derived from the respiration of organic material, but also includes a component of atmospheric CO_2 equal to the concentration in the atmosphere (Cerling, 1991). Soil CO_2 experiences a +4.4‰ enrichment in ^{13}C compared to respired organic material due to the faster diffusion of ^{12}C out of the soil. The difference between the $\delta^{13}C$

of pedogenic carbonates and the $\delta^{13}C$ of the soil CO_2 is controlled by temperature dependent equilibrium fractionation processes (Romanek et al. 1992). This temperature dependent fractionation is on the order of 10‰, and is smaller at higher temperatures. Combined with the 4.4‰ enrichment from diffusion in soil CO_2, pedogenic carbonates are typically +14–17‰ more enriched in ^{13}C than the organic material from which the respired CO_2 is generated (Cerling and Quade, 1993). Figure 1.2 summarizes how carbon fractionates through the terrestrial biosphere for the C_3 and C_4 photosynthetic pathways.

1.3 Proxy Reconstructions of Atmospheric *p*CO_2

In order to determine precisely the climate sensitivity during times of high CO_2 analogous to future climate change, we must first be able to reconstruct atmospheric CO_2 concentrations accurately and precisely in deep time. Several geochemical and paleobotanical proxies exist for determining past atmospheric CO_2 reconstructions, including the carbon isotopic composition of marine alkenones, the boron isotopic composition of marine foraminifera, the carbon isotopic composition of pedogenic carbonates, and the number of stomatal cells in ginkgo leaves (Royer et al., 2004; Royer 2007; Paleosens Project Members, 2012).

The carbon isotopic composition of alkenones produced by marine algae has been used to reconstruct the concentration of atmospheric CO_2 in the Miocene (Freeman and Hayes, 1992; Pagani et al. 1999). The offset between the $\delta^{13}C$ of dissolved CO_2 and the $\delta^{13}C$ of alkenones is controlled by the concentration of dissolved CO_2 in the ocean, and the concentration of dissolved CO_2 in the ocean is directly proportional to the concentration of CO_2 in the atmosphere. However, the $\delta^{13}C$ of these alkenones is also

influenced significantly by algal growth rates and cell geometries, which can cause large uncertainties in atmospheric CO_2 reconstructions. This method is also not useful prior to the Cenozoic because the specific algae (haptophytes) used in this method did not evolve until then. Thus, large uncertainties due to vital effects and a small timespan of applicability keep this proxy from being widely usable.

The boron isotopic composition of marine foraminifera is thought to be controlled by the pH of the ocean (Spivack et al., 1993; Demicco et al., 2003). Boron is incorporated into foraminifera during the precipitation of their calcium carbonate shells, preserving the isotopic composition and pH of the ocean at the time of cell growth. Because ocean pH is controlled by the concentration of CO_2 in the atmosphere, preserved foraminifera can be used to reconstruct past concentrations of atmospheric CO_2. However, the reconstruction of atmospheric pCO_2 depends on knowledge of the starting boron isotopic composition of the ocean, which can change dramatically depending on rates of continental weathering (Sheldon and Tabor, 2009). There currently is no proxy for reconstructing initial boron isotopic composition of the ocean, which imparts large errors in atmospheric pCO_2 reconstructions and substantially reduces the usefulness of this method.

Stomata are pores in plant leaves that allow for gas exchange with the atmosphere, such as the uptake of CO_2 and the release of O_2. Stomatal cells open to allow CO_2 to enter the leaves for photosynthesis and close to prevent water from evaporating. The number of stomata in leaves varies with the concentration of CO_2 in the atmosphere. Under higher atmospheric pCO_2, plants need less stoma to obtain sufficient CO_2 to grow because of increased diffusion of CO_2 into each cell. *Ginkgo biloba* leaves have been used as a proxy for atmospheric pCO_2 (Retallack, 2001; Royer, 2001) because they are

common in the geologic record and date back to the Carboniferous period. Calculation of atmospheric pCO_2 from the ratio of stomata to epidermal cells (stomatal index) requires a calibration of modern Ginkgo leaves growing under greenhouse conditions. These calibrations only correlate atmospheric pCO_2 to stomatal index up to ~800 ppm (Beerling and Royer, 2002 Retallack, 2009) atmospheric CO_2, and extending the relationship past the calibration limit contributes to large errors in this method of atmospheric pCO_2 reconstruction. Because the concentration of atmospheric CO_2 was higher than 800 ppm for much of the Phanerozoic, especially during the Mesozoic and early Cenozoic, this method may not produce precise estimates of CO_2 during warming events analogous to future climate change.

1.4 Soils as a Proxy for Atmospheric pCO_2

Pedogenic (soil) carbonates are common throughout the geologic record and are the most widely applicable method of atmospheric pCO_2 reconstruction. Because pedogenic carbonates form in isotopic equilibrium with soil CO_2, the $\delta^{13}C$ of total soil CO_2 is recorded by the $\delta^{13}C$ of pedogenic carbonates. The concentration of CO_2 in the soil atmosphere is equal to the sum of C_a, the concentration of CO_2 derived from the atmosphere (which is equal to the concentration of atmospheric CO_2) and *S(z)*, the concentration of CO_2 from respired organic material according to Eq. 1.4 published by Cerling (1991):

$$C_s = S(z) + C_a \quad \text{(Eq. 1.4)}$$

One can calculate the concentration of atmospheric CO_2 from pedogenic carbonates using the isotopic differences between atmospheric CO_2 and CO_2 derived from respired organic material by the following equation published by Cerling (1999):

$$pCO_2 = S(z)\left(\frac{\delta^{13}C_s - 1.0044\delta^{13}C_r}{\delta^{13}C_a - \delta^{13}C_s}\right) \text{(Eq. 1.5)}$$

where $\delta^{13}C_s$, $\delta^{13}C_r$, and $\delta^{13}C_a$ represent the carbon isotopic composition of soil CO_2, respired CO_2 and atmospheric CO_2, respectively. Because $\delta^{13}C$ of pedogenic carbonates record the ratio of CO_2 derived from the atmosphere to CO_2 derived from the respiration of organic material (*S(z)*), it is necessary to know the value of *S(z)* to accurately estimate atmospheric pCO_2. Past studies (Ekart et al., 1999; Cleveland et al., 2008; Montañez et al. 2007 and others) have assumed values of *S(z)* for atmospheric pCO_2 reconstructions. Because the analytical uncertainty is low in measured isotopic values, the assumption of *S(z)* values is the largest source of uncertainty in this method of atmospheric pCO_2 reconstruction. These assumptions have lead to estimates of high levels of atmospheric pCO_2 during key times in the geologic past with extensive evidence for globally cool climates (Ekart et al., 1999; Montañez et al., 2007), suggesting CO_2-temperature decoupling at many times during the Phanerozoic. To reduce the uncertainty associated with the most widely applicable pedogenic carbonate paleobarometer, and determine if climate has been coupled to CO_2 throughout the Phanerozoic, a method for the accurate estimation of *S(z)* at the time of carbonate formation must be determined.

1.5 Dissertation Structure

In Chapter 2 of this dissertation (Cotton et al. 2012), I have calibrated a new proxy for the amount of soil-respired CO_2 (*S(z)*) in the soil atmosphere at the time of carbonate formation to reduce the uncertainty associated with the widely applicable pedogenic carbonate paleobarometer. Because *S(z)* is controlled by soil productivity, and soil productivity is controlled by climate (Raich and Schlesinger, 1992) this new proxy correlates *S(z)* to mean annual precipitation. First derived through a literature review of respired CO_2 measurements from calcareous soils and then validated using isotopic measurements of modern soils in the United States along a precipitation transect, this new proxy increases the precision on the pedogenic carbonate paleobarometer by introducing a method for *S(z)* estimation for each individual soil used for atmospheric pCO_2 reconstructions. Of equal importance to constraining uncertainty and increasing precision of atmospheric pCO_2 reconstructions is determining the conditions in which pedogenic carbonates should not be used for these reconstructions. This chapter also presents a set of guidelines necessary for accurate atmospheric pCO_2 reconstructions, including not only the use of a unique value of *S(z)* for each soil, but also the measurement of the carbon isotopic composition of preserved organic material occluded in pedogenic carbonates for each soil as an estimation of $\delta^{13}C_r$ in Eq. 1.5. Application of these new constraints will increase the precision on CO_2-temperature sensitivity estimates in deep time.

Over million year time scales, the main control on the concentration of CO_2 in the atmosphere is the release of CO_2 through volcanism and the sequestration of CO_2 into the ocean through terrestrial silicate weathering (Berner et al., 1983; Berner, 1992).

However, recent studies (Gislason et al., 2009; Beaulieu et al., 2012) have shown that changes in silicate weathering can affect carbon fluxes on human timescales as well. The primary driver of chemical weathering is carbonic acid, which forms from the dissolution of CO_2 in water. Because the concentration of CO_2 is many times higher in soils than in the atmosphere (de Jong and Shappert, 1972, Rightmire, 1978; Brook et al., 1983), the majority of chemical weathering of silicate minerals occurs in soils (West et al. 2012). The concentration of soil-respired CO_2 (*S(z)*) controls the concentration of carbonic acid in soils, and is sensitive to changes in climate (Cotton et al. 2012; Chapter 2). In Chapter 3 of this dissertation, I use an expanded dataset including non-calcareous soils obtained through the same literature review discussed in Chapter 2 to derive a relationship between average summer *S(z)* and MAP for the United States. I then use this relationship combined with projections of MAP changes from regional climate models to predict changes to *S(z)* and the concentration of dissolved CO_2 in soils for the decade of 2050–2060. The Great Plains region of the United States, especially the northern Great Plains is expected to become wetter in the coming decades, and this increase in precipitation should increase chemical weathering rates in this region. In addition to increases in soil productivity, this region may become a new sink for atmospheric CO_2 in the future. This work highlights the importance of identifying regions in which changes to precipitation and soil productivity may cause changes to regional carbon cycling and ultimately impact atmospheric CO_2 concentrations.

Because soils contain the largest reservoir of carbon in the terrestrial biosphere (Fig. 1.1, Schlesinger, 1997), understanding changes to soil carbon as a result of climate change is important for determining feedback mechanisms under climatic warming. In

Chapter 4 of this dissertation, I explore the controls on the carbon isotopic composition of pedogenic carbonates as well as soil organic material and demonstrate how carbon isotopes in soils can be used as a proxy for environmental change during the Paleocene – Eocene Thermal Maximum (PETM).

The PETM was the most dramatic global warming event in recent geologic history and is analogous to future climate change. The PETM is thought to be caused by a massive release of carbon to the atmosphere that resulted in a 5-10°C increase in global temperatures as well as major ecological change (Zachos et al., 2001; McInerney and Wing, 2011). The warming event is associated with a negative carbon isotope excursion in nearly all carbon pools on Earth (McInerney and Wing, 2011), however, the magnitude of these carbon isotope excursions is highly variable, especially within soil carbon pools. I find that pedogenic carbonates at three sites in different regions of the world record a larger magnitude carbon isotope excursion than corresponding preserved organic matter, lowering the $\Delta^{13}C$ values during the warming event. This decrease in $\Delta^{13}C$ values is likely caused by changing soil respiration and increased carbon turnover rates as a result of global warming. Due to time limitations, modern studies have yet to reach a consensus on the impact of climatic warming on soil carbon stocks. This work suggests that under warming conditions, surface carbon turnover rates will increase, which will decrease carbon burial rates and eventually cause an increase in atmospheric pCO_2. This chapter also shows the usefulness of paleosols for reconstructions of changes to the carbon cycle on hundred to thousand year timescales.

The final chapter of this dissertation (Chapter 5) summarizes the major conclusions from each chapter, and places conclusions within a boarder context for

implications for future carbon cycling and climate and environmental change. The complete data tables for the soil-respired CO_2 measurements and additional isotopic analyses are located in three appendices at the end of this dissertation.

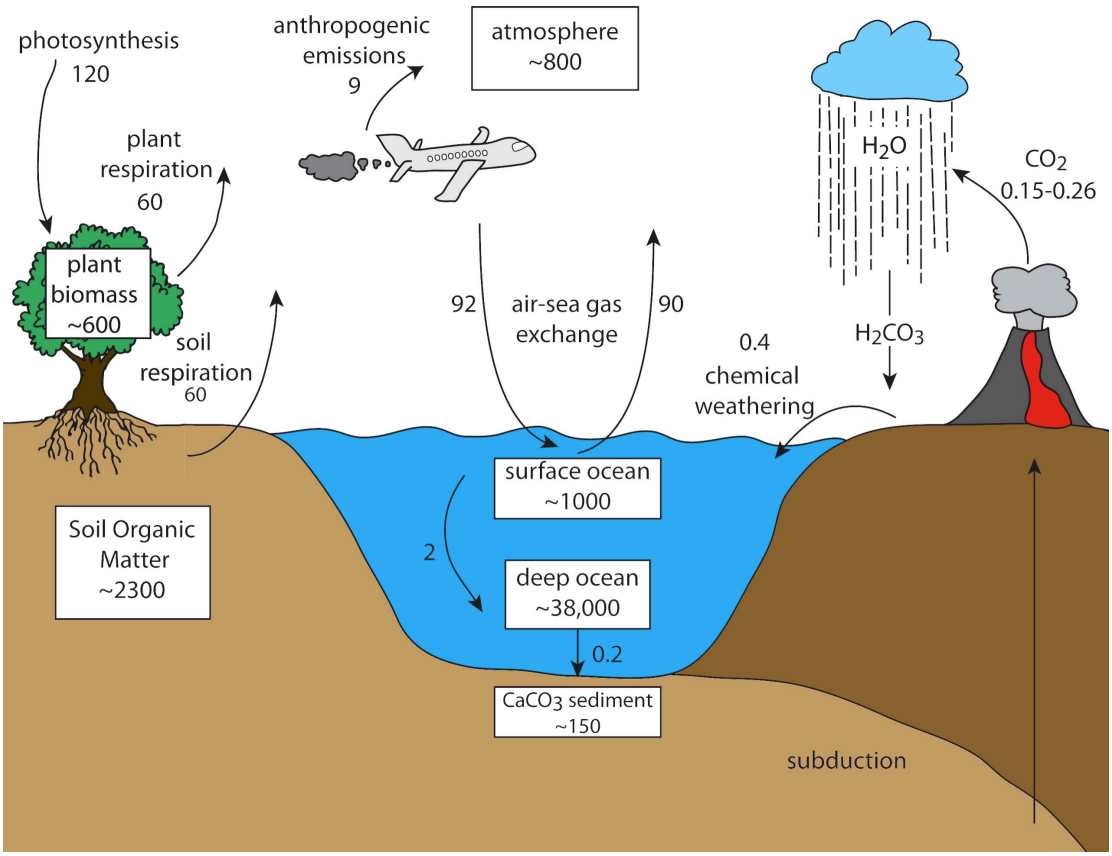

Figure 1.1. The global carbon cycle. The boxes represent permanent reservoirs of carbon in gigatonnes and the arrows represent fluxes of carbon in gigatonnes per year. Sizes of reservoirs and fluxes are from Schlesinger (1997), Gerlach, (2011) and NASA (2011).

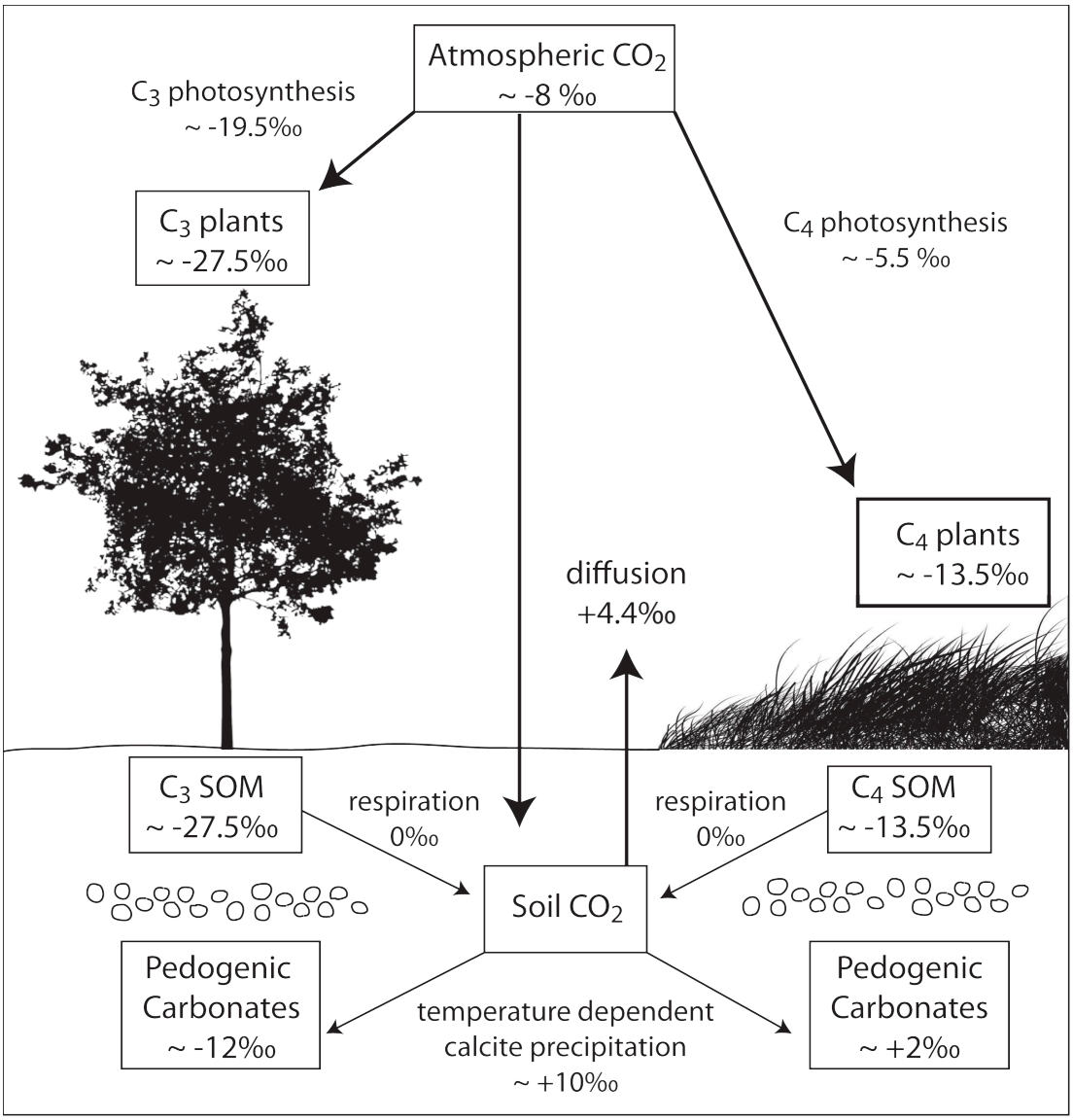

Figure 1.2. Stable isotopes in the terrestrial biosphere adapted from Koch (1998). The boxes represent the stable carbon isotopic composition of carbon reservoirs and the arrows represent fractionations that occur as carbon moves between reservoirs.

1.6 Publications and Abstracts Resulting From This Dissertation

Publications (peer reviewed)

Cotton, J.M., and Sheldon, N.D., 2012. New constraints on using paleosols to reconstruct atmospheric pCO_2. Geological Society of America Bulletin 124, 1411–1423. **(Chapter 2)**

Cotton, J.M., Jeffery, M.L., and Sheldon, N.D. Climate controls on soil-respired CO_2 in the United States: Implications for 21st century chemical weathering rates in temperate and arid ecosystems. In Review, Chemical Geology 2/13. **(Chapter 3)**

Cotton, J.M., Sheldon, N.D., Hren, M.T. and Gallagher, T.M. Positive feedback drives carbon release from soils to atmosphere during Paleocene/Eocene warming. In Preparation for submission to Nature, 4/13. **(Chapter 4)**

Additional Publications Completed During Tenure

Cotton, J.M., Hyland, E.G., and Sheldon, N.D. Multi-proxy evidence for tectonic control on the expansion of C_4 grasses in northwest Argentina . In Review, Earth and Planetary Science Letters 3/13.

Cotton, J.M. and Sheldon, N.D., 2013. Using stable isotopes to teach about sustainable agriculture through active learning. Journal of Geoscience Education 61, 59–67.

Cotton, J.M., Sheldon, N.D. and Strömberg, C.A.E. 2012. High resolution isotopic record of C_4 photosynthesis of a Miocene grassland. Palaeogeography, Palaeoclimatology, Palaeoecology 337-338, 88-98.

Published Abstracts

Cotton, J.M., Sheldon, N.D., Hren, M.T., and Gallagher, T.M., 2012. Variable magnitude of carbon isotope excursions in organic and inorganic terrestrial carbon pools during the Paleocene/Eocene Thermal Maximum. American Geophysical Union Meeting, San Francisco, CA.

Cotton, J.M. and Sheldon, N.D., 2012. Revised atmospheric pCO_2 estimates from pedogenic carbonates support CO_2-temperature coupling throughout the Phanerozoic Geological Society of America Annual Meeting, Charlotte, NC.

Cotton, J.M., Jeffery, M.L., and Sheldon, N.D., 2011. Modern and future spatial variability of soil-respired CO_2 across the United States. American Geophysical Union Meeting, San Francisco, CA.

Cotton, J.M. and Sheldon, N.D., 2010. Derivation of a new soil-respired CO_2 proxy and application to paleo-CO_2 reconstruction of the late Miocene. Geological Society

of America Meeting, Denver CO.

Cotton, J.M. Hyland, E.G., and Sheldon, N.D., 2011. Organic carbon isotopic reconstruction of C_3/C_4 photosynthesis and implications for the tectonic evolution of the Santa María basin, Northwest Argentina. Geological Society of America Annual Meeting, Minneapolis, MN.

Cotton, J.M. and Sheldon, N.D., 2010. Derivation of a new soil-respired CO_2 proxy for application to paleo-CO_2 reconstruction. Goldschmidt Annual Meeting, Knoxville, TN.

Cotton, J.M. and Sheldon, N.D., 2009. High resolution isotopic record of C_4 photosynthesis of a mid-Miocene grassland. Geological Society of America Meeting, Portland, OR.

1.7 References

Beaulieu, E., Godderis, Y., Donnadieu, Y., Labat, D., and Roelandt, C., 2012. High sensitivity of the continental-weathering carbon dioxide sink to future climate change. Nature Climate Change 2, 346–349.

Beerling, D.J., and Royer, D.L., 2002. Reading a CO_2 signal from fossil stomata. New Phytologist 153, 387–397.

Berner, R.A., 1992. Weathering, plants, and the long term carbon cycle. Geochimica et Cosmochimica Acta 56, 3225–3231.

Berner, R.A., 2006. GEOCARBSULF: A combined model for Phanerozoic atmospheric O_2 and CO_2. Geochimica et Cosmochimica Acta 70, 5653–5664.

Berner, R.A., Lasaga, A.C., Garrels, R.M., 1983. The carbonate-silicate geochemical cycle and its effect on atmospheric carbon dioxide over the last 100 million years. American Journal of Science 283, 641–683.

Berner, R.A., Kothavala, Z., 2001. GEOCARB III: A revised model of atmospheric CO_2 over Phanerozoic time. American Journal of Science 301, 182–204.

Bigeleisen, J., 1965. Chemistry of isotopes. Science 147, 463–471.

Brady, P.V., Dorn, R.I., Brazel, A.J., Clark, J., Moore, R.B., and Glidewell, T., 1999. Direct measurement of the combined effects of lichen, rainfall, and temperature on silicate weathering. Geochimica et Cosmochimica Acta 63, 3293–3300.

Brook, G.A., Folkoff, M.E., Box, E.O., 1983. A world model for soil carbon dioxide. Earth Surface Processes and Landforms 8, 79–88.

Cerling, T.E., 1991. Carbon dioxide in the atmosphere: evidence from Cenozoic and Mesozoic paleosols: American Journal of Science 291, 377–400.

Cerling, T.E., 1999. Stable carbon isotopes in paleosol carbonates. In: Thiry, M., and Simon-Coinco, R. (eds) Palaeoweathering, Palaeosurfaces and Continental Deposits. International Association for Sedimentology Special Publication 27, 43–60.

Cerling, T.H., and Harris, J.M., 1999. Carbon isotope fractionation between diet and bioapatite in ungulate mammals and implications for ecological and paleoecological studies. Oecologia 120, 347–363.

Cerling, T.E., Harris, J.M., MacFadden, B.J., Leakey, M.G., Quade, J., Eisenmann, V., Ehleringer, J. R., 1997. Global vegetation change through the Miocene/Pliocene boundary. Nature 389, 153–157.

Cerling, T.E. and Quade, J., 1993. Stable carbon and oxygen isotopes in soil carbonates. In: Swart, P.K., Lohmann, K.C., McKenzie, J.A., and Savin S. (eds) Climate change in continental isotopic records. Washington, D.C., American Geophysical Union, 217–231.

Cleveland, D.M., Nordt, L.C., Dworkin, S.I., and Atchley, S.C., 2008. Pedogenic carbonate isotopes as evidence for extreme climatic events preceding the Triassic-Jurassic boundary: Implications for the biotic crisis? Geological Society of America Bulletin 120, 1408–1415.

Coplen, T.B., 2011. Guidelines and recommended temrs for expression of stable-isotope-ratio and gas-ratio measurement results. Rapid Communications in Mass Spectrometry 25, 2538–2560.

Cotton, J.M., and Sheldon, N.D., 2012. New constraints on using paleosols to reconstruct atmospheric pCO_2. Geological Society of America Bulletin 124, 1411–1423.

de Jong, E., Schappert, H.J.V., 1972. Calculation of soil respiration and activity from CO_2 profiles in the soil. Soil Science 113, 328–333.

Dansgaard, W. 1964. Stable isotopes in precipitation. Tellus 16, 436–468.

Demicco, R.V., Lowenstein, T.K., and Hardie, L.A., 2003. Atmospheric pCO_2 since 60 Ma from records of seawater pH, calcium, and primary carbonate mineralogy. Geology 31, 793–796.

Ekart, D.D., Cerling, T.E., Montañez, I.P. and Tabor, N.J. 1999. A 400 million year carbon isotopic record of pedogenic carbonate: implications for paleoatmospheric carbon dioxide. American Journal of Science 299, 805–827.

Engel, T. and Reid, P., 2012. Physical Chemistry. 3rd edition. Prentice Hall, Upper Saddle River, 1128 pp.

Faure, G. and Mensing, T.M., 2005. Isotopes: Principles and Applications. 3rd edition. Wiley, Hoboken , NJ, 928 pp.

Freeman, K.H., Hayes, J.M., 1992. Fractionation of carbon isotopes by phytoplankton and estimates of ancient CO_2 levels. Global Biogeochemical Cycles 6, 185–198.

Gerlach, T., 2011. Volcanic versus anthropogenic carbon dioxide. EOS, transactions of the American Geophysical Union 92, 201–208.

Gislason., S.R., Oelkers, E.H., Eiriksdottir, E.S., Karjilov, M.I., Gisladottir, G., Sigfusson, B., Snorrason, A., Elefsen, S., Hardardottir, J., 2009. Earth and Planetary Science Letters 277, 213–222.

IPCC, 2007. Climate Change 2007: Synthesis Report. IPCC, Geneva, Switzerland, 104 pp.

Lüthi, D., Le Floch, M., Bereiter, B., Blunier, T., Barnola, J., Siegenthaler, U., Raynaud, D., Jouzel, J., Fischer, H., Kawamura, K., and Stocker, T., 2008. High-resolution carbon dioxide concentration record 650,000–800,000 years before present. Nature 453, 379–382.

Kim, S.-T., and O'Neil, J.R., 1997. Equilibrium and nonequilibrum oxygen isotope effects in synthetic carbonates. Geochimica et Cosmochimica Acta 61, 3461–3475.

Koch, P.L., 1998. Isotopic reconstruction of past continental environments. Annual Review of Earth and Planetary Science 26, 573–613.

McInerney, F.A. and Wing, S.L., 2011. The Paleocene-Eocene Thermal Maximum: A perturbation of carbon cycle, climate, and biosphere with implications for the future. Annual Review of Earth and Planetary Sciences 39, 489–516.

Montañez, I.P., Tabor, N.J., Niemeier, D., DiMichele, W.A., Frank, T.D., Fielding, C.R., Isbell, J.L., Birgenheier, L.P. and Rygel, M.C., 2007. CO_2-forced climate and vegetation instability during late Paleozoic glaciation. Science 315, 87–91.

NASA, 2011. Earth Observatory: The Carbon Cycle. http://earthobservatory.nasa.gov/Features/CarbonCycle/ accessed December, 2012.

Pagani, M., Aurthur, M.A., and Freeman, K.H., 1999. Miocene evolution of atmospheric carbon dioxide. Paleoceanography 14, 273–292.

Paleosens Project Members, 2012. Making sense of paleoclimate sensitivity. Nature 491, 683–691.

Park, R., and Epstein, S., 1960. Carbon isotope fractionation during photosynthesis. Geochimica et Cosmochimica Acta 21, 110–126.

Raich, J.W., Schlesinger, W.H., 1992. The global carbon dioxide flux in soil respiration and its relationship to vegetation and climate. Tellus B, 44, 81–99.

Retallack, G.J., 2001. A 300 million year record of atmospheric carbon dioxide from fossil plant cuticles. Nature 411, 287–290.

Retallack, G.J., 2009. Greenhouse crises of the past 300 million years. Geological Society of America Bulletin 121, 1441–1455.

Rightmire, C.T., 1978. Season variation in pCO_2 and ^{13}C content of soil atmosphere. Water Resources Research 14, 691–692.

Romanek, C.S., Grossman, E.L., and Morse, J.W., 1992. Carbon isotopic fractionation in synthetic aragonite and calcite: Effects of temperature and precipitation rate. Geochimica et Cosmochimica Acta 56, 419–430.

Royer D.L. 2001. Stomatal density and stomatal index as indicators of paleoatmospheric CO_2 concentration. Review of Palaeobotany and Palynology 114, 1–28.

Royer, D.L., Berner, R.A. and Park, J., 2007. Climate sensitivity constrained by CO_2 concentrations over the past 420 million years. Nature 446, 530–532.

Royer, D.L., Berner, R.A., Montañez, I.P., Tabor, N.J., and Beerling, D.J. 2004. CO_2 as a primary driver of phanerozoic climate. GSA Today 14, 4–10.

Schlesinger, W.H. 1997. Biogeochemistry: An Analysis of Global Change. Academic Press, San Diego

Sheldon, N.D., Tabor, N.J., 2009. Quantitative paleoenvironmental and paleoclimatic reconstruction using paleosols. Earth–Science Reviews 95, 1–52.

Spivack, A.J., You, C.-H., Smith, H.J., 1993. Foramaniferal boron isotope ratios as a proxy for surface ocean pH over the past 21 Myr. Nature 363, 149–151.

Tipple, B.J. and Pagani, M., 2007. The early origins of terrestrial C_4 photosynthesis. Annual Review of Earth and Planetary Sciences 35, 435–461.

Urey, H.C., 1947. The thermodynamic properties of isotopic substances. Journal of the Chemical Society 1947, 526–581.

West, A.J., 2012. Thickness of the chemical weathering zone and implications for erosional and climatic drivers of weathering and for carbon-cycle feedbacks. Geology 40, 811–815.

Zachos, J., Pagani, M., Sloan, L., Thomas, E., and Billups, K., 2001. Trends, rhythms and aberrations in global climate 65Ma to present. Science 292, 686–693.

Chapter 2

New constraints on using paleosols to reconstruct atmospheric pCO_2[1]

2.0 Abstract

Ecosystem and climatic changes due to anthropogenic emissions of CO_2 are of increasing importance to society. One way to predict these changes in the future is to study warming events in the geologic past. The main control of the Earth's temperature over geologic time is the concentration of atmospheric CO_2, however, the precise relationship between CO_2 and temperature is not fully understood. Therefore, it is essential to be able to quantify atmospheric CO_2 concentrations in the geologic past, especially at times of rapid climate change analogous to current atmospheric changes. One widely applied proxy relates the carbon isotopic composition of pedogenic carbonates to atmospheric pCO_2, however, one of the key variables (soil-respired CO_2; $S(z)$) is not well constrained. This study presents a new proxy where soil-respired CO_2 is related to mean annual precipitation by the following equation:

$$S(z) = 5.67(MAP) - 269.9 \quad R^2 = 0.59, \text{ SE} = 681 \text{ ppm}$$

This proxy, validated for modern atmospheric pCO_2 levels, constrains the primary source of uncertainty in the soil carbonate paleobarometer. We apply this proxy to make

[1]Cotton, J.M., and Sheldon, N.D., 2012. New constraints on using paleosols to reconstruct atmospheric pCO_2. Geological Society of America Bulletin 124, 1411–1423.

atmospheric pCO_2 reconstructions for examples from the Cenozoic, Mesozoic, and Paleozoic and calculate CO_2 estimates that are in better agreement with estimates from other independent proxies and model results than previous pedogenic carbonate reconstructions. The implications of the uncertainties attributed to pedogenic carbonate paleobarometry as well as guidelines for using this method are discussed. Making individual measurements rather than assumptions for each isotopic value and combining those analyses with an *S(z)* estimate for each paleosol considered using our new proxy described herein allows for increased precision of atmospheric pCO_2 reconstructions.

2.1 Introduction

Although proxies exist for paleo-atmospheric CO_2 concentration, they are either limited to Cenozoic systems (alkenones; Pagani, 2002), are not widely applicable (goethites; Sheldon and Tabor, 2009), are compromised by being assumption driven (pedogenic carbonate paleobarometer; Cerling, 1984; 1999, $\delta^{11}B$ of marine carbonates; Demicco et al., 2003; Sheldon and Tabor, 2009), or are subject to vital effects of organisms (alkenones, $\delta^{11}B$ of marine carbonates, stomatal indices; Royer et al., 2004). Paleosols (fossil soils) containing carbonate nodules are abundant globally in modern environments and date back to at least 2.6 billion years ago **(**Wantanabe et al., 2000). In practice, the pedogenic carbonate paleobarometer method can be applied back to the early Silurian (i.e., advent of land plants and "modern" soil carbon dynamics), making it potentially the most widely applicable proxy for paleo-atmospheric CO_2 concentrations. However, a key variable has previously been assumed when calculating paleo-

atmospheric pCO_2, which has commonly led to overestimates for some key intervals of geologic history, reducing the reliability of the pedogenic carbonate paleobarometer.

To reduce the uncertainty associated with Cerling (1984; 1999) paleobarometer, a new proxy has been calibrated for soil-respired CO_2 for modern soils using its relation to precipitation for application to paleosols. Soil-respired CO_2 (*S(z)*), the biologically contributed portion of CO_2 to the soil atmosphere, is a measure of soil productivity (microbial and plant respiration), which is influenced mainly by precipitation (Rosenzweig, 1968; Wanner, 1970; Brook et al., 1983). Deriving a relationship between *S(z)* and mean annual precipitation (MAP) can improve estimates of *S(z)*, and when applied to paleosols will improve past atmospheric pCO_2 estimates. Past precipitation can be estimated from paleosols using the depth to Bk horizon (Retallack, 2005), the chemical index of alteration without potassium (CIA-K) for most paleosol types (Sheldon et al, 2002), and the calcium and magnesium oxide weathering index (CALMAG) for Vertisols (Nordt and Driese, 2010). Therefore, a relationship between *S(z)* and MAP is useful for predicting *S(z)* during carbonate formation for a wide variety of paleosol types. This study also aims to demonstrate the significance of determining specific values of *S(z)* for each paleosol, as well as the importance of choosing paleosols suitable for reconstructions in quantifying uncertainty in the pedogenic carbonate paleobarometer. To meet these goals, we have performed a literature review of *S(z)* measurements in soils containing pedogenic carbonates, expanding upon a previous study by Brook et al. (1983). This new literature derived *S(z)*-MAP proxy was then validated through isotopic analysis of modern carbonate bearing soils from a variety of locations in the western

United States, and applied to three case studies to revise atmospheric pCO_2 estimates from the Cenozoic, Mesozoic and Paleozoic.

2.2 Background

The extensively applied pedogenic carbonate paleobarometer introduced by Cerling (1984; 1991; 1999) calculates the concentration of atmospheric CO_2 based on the carbon isotopic ratio of pedogenic carbonates precipitating in equilibrium with soil CO_2 from the following equation:

$$pCO_2 = S(z)\left(\frac{\delta^{13}C_s - 1.0044\delta^{13}C_r - 4.4}{\delta^{13}C_a - \delta^{13}C_s}\right) \quad \text{(Eq. 2.1)}$$

where *S(z)* is the concentration of soil-respired CO_2, $\delta^{13}C$ is the carbon isotopic composition of the total soil CO_2 in the soil air (s), respired CO_2 (r) and atmospheric CO_2 (a). The 1.0044 is the mixing ratio of diffusion coefficients of $^{12}CO_2$ to $^{13}CO_2$ and the 4.4 is the fractionation associated with the faster diffusion of lighter $^{12}CO_2$ out of the soil. For soils not parented by limestone or some other carbonate-rich material, pedogenic carbonates record the carbon isotopic composition of total soil CO_2, which is determined by the ratio of heavier (^{13}C-rich) atmospheric CO_2 to lighter (^{12}C-rich) microbial- and plant-respired CO_2.

Carbonate-rich parent materials are excluded because the weathering of limestone parent material releases CO_2 into the soil atmosphere that is isotopically different than the biologically and atmospherically derived CO_2. The introduction of this limestone derived CO_2 creates a three component system in which the atmospheric contribution to soil CO_2 cannot be determined without knowing the isotopic composition of the parent material

and the amount of CO_2 released from weathering (Hsieh and Yapp, 1999; Tabor et al., 2004; Tabor and Yapp, 2005; Sheldon and Tabor, 2009 and others). Limestone parented soils should also be avoided because pieces of the parent material may be occluded in and contaminate pedogenic carbonate nodules. Typically, stage 2 and 3 carbonates (Machete, 1985) are ideal for atmospheric pCO_2 calculations, while stage 4 and 5 carbonates integrate significantly more time and are not useful for high resolution reconstructions. Stage 5 carbonates are petrocalcic, and would also behave similarly to a limestone parented soil.

Due to small analytical uncertainties for isotopic measurements, the primary source of uncertainty in this paleobarometer is the amount of soil-respired CO_2 (*S(z)*) in the soil at the time that the pedogenic carbonates were formed. $\delta^{13}C_s$ and $\delta^{13}C_r$ can be measured by isotopic analysis of pedogenic carbonates and organic material, and $\delta^{13}C_a$ can be estimated by proxies using the isotopic composition of marine carbonates (Tipple et al., 2010) or of C_3 plants (Arens and Jahren, 2000; Gröcke, 2002). *S(z)* is dependent on many factors such as biological productivity, soil porosity, and tortuosity (Cerling 1991; Royer et al., 2001). At steady state conditions, *S(z)* may be calculated from the following equation:

$$S(z) = C_s - C_a \quad \text{(Eq. 2.2)}$$

where C_s represents the total concentration of CO_2 in the soil air and C_a represents the concentration of CO_2 in the atmosphere (Cerling, 1991; Royer et al., 2001). The generalizations made in Eq. 2 are necessary for reconstructions in the geologic past where soil characteristics like porosity (see Sheldon and Retallack (2001) for ways to address this) and tortuosity are not preserved. According to Eq. 2.1, *S(z)* is directly proportional

to the predicted atmospheric value, so assuming an incorrect *S(z)* value can lead to large errors in estimates of atmospheric CO_2.

As an example of this issue, Ekart et al. (1999) compiled a paleo-atmospheric pCO_2 reconstruction for most of the Phanerozoic that used a static value of 5000 ppm for all estimates of *S(z)*, regardless of paleosol type or climatic regime. The choice of 5000 ppm was based on previous studies of modern soils (Brook et al., 1983; Solomon and Cerling, 1987), which estimated average *S(z)* values to be 4000–7000 ppm for well-drained soils receiving less than 1000 mm yr^{-1} of precipitation (i.e., broadly speaking, soil conditions conducive to forming carbonates). However, more recent studies have shown that pedogenic carbonate growth is seasonal and occurs in warm, dry periods, and that carbonate does not form during mean growing season conditions (Breecker et al., 2009). Breecker et al. (2010) found that the soil-respired CO_2 concentration during time of carbonate growth is much lower than previously thought and ranges from 1034 to 6139 ppm, with an average of 2800 ppm suggesting that Ekart et al. (1999) and subsequent studies assuming values of *S(z)* > 2800 ppm may have overestimated paleo-atmospheric pCO_2 in their reconstructions. Breecker et al. (2010) also report a wide range of modern *S(z)* values from different soil types, demonstrating the importance of determining the specific value of *S(z)* for each individual soil used in atmospheric pCO_2 reconstructions rather than assuming a single value.

Because *S(z)* represents the amount of soil-respired CO_2 at the time of carbonate formation, this time must be constrained to improve estimates of *S(z)* and atmospheric pCO_2 reconstructions. Breecker et al. (2009) found that isotopic equilibrium between the carbonates and the soil water, and thus precipitation of carbonate nodules, occurred

during a warm and dry period in May for soils in New Mexico. The solubility of calcite in water decreases when the temperature increases and the concentration of dissolved CO_2 decreases, so while soil carbonates may not form strictly in May everywhere, it is likely that summer is the season of formation. Carbonate formation during the summer months is also supported by many recent studies including Mintz et al. (2011), Passey et al. (2010), and Quade et al (2011).

In order to be able to assign a specific *S(z)* value for atmospheric pCO_2 reconstruction using pedogenic carbonates, the global and seasonal variation in *S(z)* during the time of carbonate formation must be understood. The first study that attempted to quantify the relationship between soil CO_2 and climate was conducted by Brook et al. (1983) and showed that the concentration of total soil CO_2 is proportional to many climatic variables (Fig. 2.1) such as mean annual precipitation (MAP) and mean annual temperature (MAT). In a study of 19 soils worldwide, Brook et al. (1983) found logarithmic relationships between the concentration of mean growing season soil CO_2 and MAP (Fig 2.1A), MAT (Fig 2.1B), potential evapotranspiration (PET), and actual evapotranspiration (AET), with AET having the strongest relationship and MAP having the weakest relationship. These relationships were the basis for the original estimates of *S(z)* used in the atmospheric pCO_2 reconstructions published by Ekart et al. (1999) and later papers. This study aims to improve our understanding of modern concentrations of soil CO_2 to improve paleo-atmospheric pCO_2 estimates.

2.3 Methods

A literature review was performed to assemble an extensive *S(z)* dataset to understand better how *S(z)* changes with climatic conditions. Because measurements published in the literature reported total soil CO_2, *S(z)* was calculated by subtracting the monthly atmospheric CO_2 level in the year the measurement was taken according to Eq. 2.2 (Cerling, 1991; Retallack, 2009). Atmospheric pCO_2 values were taken from the NOAA Mauna Loa Observatory dataset (from website ftp://ftp.cmdl.noaa.gov/ccg/co2/trends/co2_annmean_mlo.txt: accessed November, 2009).

From this literature review, only measurements below a depth of 30 cm were included in the data compilation because only carbonates formed below that depth have reached a constant isotopic composition according to CO_2 diffusion models (Cerling, 1984; 1991; Koch, 1998; Sheldon and Tabor, 2009). At steady state, there is a constant atmospheric component of CO_2 in the soil equal to the partial pressure of CO_2 in the atmosphere. For soils with low respiration rates (typically coarse-grained soils in arid regions), the depth at which isotopic equilibrium is reached should be greatest as well as isotopically most enriched (Amundson et al., 1998), because the atmospheric contribution to soil CO_2 is proportionally larger. Isotopic analyses from Breecker et al. (2009) confirm constant isotopic compositions of carbonates by a depth of 30 cm from Entisols and Inceptisols forming in arid areas with MAP ranging from 210 to 375 mm yr^{-1}. The isotopic composition of CO_2 in the soil above 30 cm is not representative of the conditions of carbonate formation to be used in atmospheric pCO_2 reconstructions.

Measurements from the literature without an accompanying depth were not included in the regression.

Minimum summer soil CO_2 measurements from the compiled literature were used because these measurements meet the criteria of warm temperature and low soil CO_2 outlined by Breecker et al. (2009) necessary for calcite precipitation. Minimum soil-respired CO_2 values were determined by choosing the lowest value of soil CO_2 measured during the summer months (June 21 – September 21) at each site. These measurements were compared with MAT and MAP. MAP and MAT estimates were acquired from three different sources: temperature or precipitation estimates published along with the soil CO_2 measurements, NOAA and Environment Canada weather stations, and for remote sites without climatic data available, WorldClim global climatic data model for ArcGIS (Hijmans et al., 2005) was used to predict both MAT and MAP.

The literature-based proxy for *S(z)* was validated through the isotopic analysis of pedogenic carbonate nodules collected from modern (<10,000 years) carbonate-bearing soil series in Arizona, New Mexico, Colorado, South Dakota, and Minnesota (Fig. 2.2; Fig. 2.3A-B). These modern soils were determined to be Holocene in age from the size of the pedogenic carbonates forming within. These soil carbonates were less than 5 cm in diameter, which, according to the transfer function of Retallack (2005), represents growth from the last 10,000 years. The Industrial Revolution is a small proportion of this total time and though we do not know exactly how much carbonate has accumulated or has been dissolved and reprecipitated since then, this growth would likely only be found at the outermost part of the nodules. The inner areas of nodules were sampled to avoid carbonate formed since the industrial revolution when atmospheric CO_2 was higher than

280 ppm. Because the exact time of carbonate formation is unknown, *S(z)* at the time of carbonate formation cannot be measured. In order to determine *S(z)* at the time of carbonate formation for these modern soils, isotopic and temperature data were used to calculate *S(z)* from the pedogenic carbonate paleobarometer by setting atmospheric pCO_2 in Eq. 2.1 to the preindustrial value of 280 ppm (Appendix A, Table A2). These calculated *S(z)* values were then compared to the predicted value from the soil-respired CO_2 proxy. Once validated, the proxy was applied to paleosol carbonates for an atmospheric pCO_2 reconstruction of the late Miocene using carbonate-bearing paleosols from a new site in Montana, and to case studies from the literature from the Mesozoic (Cleveland et al., 2008a-b) and Paleozoic (Montañez et al., 2007) that could be compared to independent pCO_2 estimates (compilation of Breecker et al., 2010) and to model results (i.e., GEOCARBSULF; updated values from Berner, pers. comm. 2011).

For carbonate isotopic analyses, micritic nodules were microsampled to avoid spar and analyzed on a ThermoFinnigan MAT 253 isotope ratio mass spectrometer with KielIV autosampler at the University of Michigan. Primary carbonate (micrite) was distinguished from secondary spar through petrographic analysis of thin sections. Micrite was identified as particles having a diameter less than 4 μm, where secondary spar was much larger grained crystalline material (Folk, 1959). Carbon and oxygen isotopic ratios are reported in units of per mil (‰) relative to the international standard Vienna Pee Dee Belemnite (VPDB). The internal standards used to normalize measured values to VPDB were IAEA sucrose and caffeine for organic carbon analysis and NBS 19 for carbonate analysis. The analytical error is 0.03‰ for inorganic carbon and 0.05‰ for oxygen isotopes.

The average isotopic composition of multiple measurements of soil organic carbon below 30 cm depth was used to represent $\delta^{13}C_r$ in Eq. 2.1. For modern $\delta^{13}C_{org}$ analysis, samples were treated with a 2% HCl solution to remove any residual carbonate and rinsed with deionized water. The dried samples were then homogenized and loaded into tin capsules and analyzed using a Costech elemental analyzer attached to a Thermo Delta V+ isotope ratio mass spectrometer. For paleosol $\delta^{13}C_{org}$ analyses, organic material occluded in nodules was analyzed. Samples were ultrasonically cleaned and dissolved in 7% HCl to remove carbonate. Samples were then processed identically to the modern samples as described above. The analytical error for organic carbon measurements is <0.10‰ with a mean standard deviation of 0.26‰ and 0.24‰, respectively for duplicate and triplicate analyses of each sample.

2.4 Results

The literature review produced 932 soil-respired CO_2 measurements from 60 soils worldwide comprising every soil order except Histosols and Vertisols. Of those, 594 measurements from 23 soils were identified as containing pedogenic carbonates. The locations of these 23 soils are given in Appendix A, Table A1; the CO_2 and climatic data are available in Appendix A, Tables A1 and A3. There is only a weak relationship between MAP or MAT and soil CO_2 within the expanded dataset when all 932 data points are included in the regression (Fig 2.1A and 1B black circles). These results are not in agreement with the Brook et al. (1983) study that indicated strong relationships between soil CO_2 and these two climatic variables (Fig 2.1A and 1B, gray circles). Upon inclusion of more data, the correlation coefficient becomes reduced, the significance

decreases and the standard error increases. Globally, soils are too variable to all respond to precipitation or temperature in a uniformly predictable way, while soils containing pedogenic carbonates (constrained to form in climatic regimes that generally receive less than ~750 mm yr^{-1} precipitation (Royer, 1999; Retallack, 2000)), are typically much more characteristically similar. When we focus on only pedogenic carbonate forming soils, a statistically significant relationship between *S(z)* and MAP emerges (Fig. 2.2), but no relationship exists between *S(z)* and MAT ($R^2 = 0.06$). Figure 2.2 shows the linear relationship between summer minimum soil-respired CO_2 measurements and MAP for the 23 soils containing pedogenic carbonates, with *S(z)* related to MAP as:

$$S(z) = 5.67(MAP) - 269.9 \quad \text{(Eq. 2.3)}$$

where $R^2 = 0.59$, SE = ± 681 ppm ($t = 5.5$, $F = 30.15$, $p < 0.0001$) and *S(z)* represents the summer minimum soil-respired CO_2. It should be noted that the same linear relationship also exists between MAP and summer minimum soil-respired CO_2 at the depth of the Bk horizon. This is likely because minimum *S(z)* measurements are typically located at shallow depths similar to the depth of Bk horizons in arid to semi-arid regions. We found a similar linear relationship between average summer soil-respired CO_2 and MAP, though this relationship most likely does not represent the time of carbonate formation (Breecker et al., 2009) and may over estimate true *S(z)* values during precipitation of carbonate (see Appendix A, Fig. A2). Because of the lack of data from carbonate-bearing soils in humid climates in this dataset, Eq. 2.3 is only valid for paleosols with MAP estimates up to 600 mm yr^{-1}, though potentially, it may be extended modestly up to the precipitation limit for pedogenic carbonate formation (i.e., 750 mm yr^{-1}; Royer, 1999; Retallack, 2000). This dataset also does not include any soil CO_2 measurements from Vertisols, so it is unknown

whether or not this soil order behaves similarly, but preliminary observations of modern soils suggest that Vertisols behave uniquely relative to other soil orders, probably either as a result of forming in strongly seasonal climates, due to their very high clay contents (*D. Breecker, pers. comm.*), or due to seasonal saturation that minimizes the role of atmosphere in the formation of some carbonate phases (Mintz et al., 2011).

Though pedogenic carbonates do not precipitate during mean summer conditions (Breecker et al., 2009), *S(z)* seems to be well correlated to MAP. However, and perhaps surprisingly, *S(z)* is not related to seasonal precipitation ($R^2 = 0.07$, Appendix A, Fig. A3). Even if such a relationship were present in the data, it would not provide a useful constraint for pCO_2 reconstructions from paleosols because presently, no proxy exists for monthly precipitation in the geologic past, whereas various proxies exist for MAP (Sheldon et al., 2002; Retallack, 2005; Nordt and Driese, 2010).

The new *S(z)*-MAP proxy (Eq. 2.3) was subsequently validated using modern soils as described in the methods. Calculated *S(z)* values are very similar to the *S(z)* values predicted by the *S(z)* proxy. Figure 2.2 also shows the results of these validation experiments, with most of the calculated *S(z)* values falling very close to the linear regression line for summer minimum soil-respired CO_2 derived from the literature review, and all of the data except for one point plot well within the range of the standard error for the proxy. The *S(z)* value calculated from these modern soils demonstrates the new summer minimum soil-respired CO_2 proxy's ability to predict *S(z)* accurately, thus reducing the major source of uncertainty in the pedogenic carbonate paleobarometer. Based upon the validation from the soils in this modern dataset, this new *S(z)* proxy could

be applied to paleosols classified as comparable to modern Aridisols, Inceptisols and Mollisols, and potentially Alfisols and Entisols as well.

2.5 Discussion

The necessity of an *S(z)* proxy rather than an assumed value has been recognized by several previous studies (Retallack, 2009; Sheldon and Tabor, 2009; Breecker et al., 2009; 2010), in which each considered potential solutions. For example, Retallack (2009) introduced an *S(z)* proxy relating soil-respired CO_2 to the depth to Bk horizon. However, this proxy is less widely applicable than the *S(z)* proxy presented in this study for several reasons. First, the use of the depth to Bk horizon measurement as a proxy for anything, be it *S(z)* (Retallack, 2009) or MAP (Retallack, 2005), requires the preservation of the entire soil profile. If erosion of the top of the profile has occurred, then the depth to the Bk horizon will be decreased and the reconstructed *S(z)* will be too low. For our *S(z)*-MAP relationship, the paleosol may still be used to reconstruct atmospheric pCO_2 even if the entire soil profile is not preserved because precipitation estimates can be acquired from geochemical methods only relying on the presence of a B horizon (CIA-K, Sheldon et al., 2002; CALMAG, Nordt and Driese, 2010), or alternatively, from paleobotanical MAP proxy estimates based on fossil leaves preserved in paleosols. A second issue with the *S(z)*-depth to Bk horizon proxy is that it uses summer average soil-respired CO_2 measurements, which do not reflect the time of carbonate formation (Breecker et al., 2009; *this study*), as previously mentioned, and therefore have a tendency to overestimate atmospheric pCO_2 reconstructions. Therefore, our new proxy is more widely applicable

and more accurate than the previously published *S(z)*-Bk horizon depth proxy published by Retallack (2009).

Breecker et al. (2009) find that soil CO_2 is generally low during the time of carbonate formation. Of the four soils in New Mexico that were monitored in their study, three were Entisols that lack distinct Bk horizons and that contained only carbonate-coated clasts. Given that these soils are poorly developed and lack the type of Bk horizons typically preserved in the geologic record (e.g., Sheldon and Tabor, 2009), assuming a generalized low *S(z)* value may not be broadly applicable to all soils because most are more developed and reflect higher productivity ecosystems. Furthermore, many of the carbonate-bearing soils in this study forming under higher precipitation regimes have a higher measured *S(z)* value than Breecker et al. (2009) would predict (Fig. 2.2). However, when considered in conjunction with MAP data, the result from Entisols in the earlier study are in agreement with the linear regression including all the data from other soil orders, showing that while the Breecker et al. (2009) soils alone cannot be used to predict *S(z)*, they are part of a larger set of data that define a consistent *S(z)*-MAP relationship.

It is clear that *S(z)* at the time of carbonate formation is highly variable across all soil types and precipitation regimes, but the relationship between *S(z)* and MAP becomes much stronger when considering only soils containing pedogenic carbonates. The strength of this relationship for soils containing carbonates could be due to the fact that specific soil CO_2 conditions are necessary for carbonate formation. Soils forming pedogenic carbonates must have low soil CO_2 and have a high pH above 7 (Cerling, 1984; Breecker et al., 2009) at the time of carbonate precipitation. Soils with higher

productivity and higher *S(z)* values will not form carbonates. There is likely a minimum pH and thus, a maximum concentration of CO_2 that can be found in a soil above which formation of carbonate is not possible. Therefore, the conditions required for precipitation of carbonate characteristically separate these soils from soils with higher productivity that lack carbonate, and non-calcareous soils would have a different relationship with MAP than calcareous soils. The strength of the relationship between *S(z)* and MAP for soils forming carbonate may also be explained by the fact that soils that precipitate calcite are soils in which respiration is limited by summer precipitation. In wetter climates, respiration may be limited by another factor such as nutrient levels or temperature, and respiration in these soils would not be expected to be correlated to precipitation. Both of these hypotheses are supported by the data (Appendix A, Fig. A4), which shows that summer minimum *S(z)* is higher and more variable in non-calcareous soils.

This study demonstrates a robust relationship between summer minimum soil-respired CO_2 and MAP for soils forming up to 600 mm yr^{-1} (Fig. 2.2). However, there is considerable variability about that mean regression, due to the heterogeneity in the soils. The standard error (681 ppm) for the linear regression includes the error associated with apparent outliers. These outlier *S(z)* measurements could occur for multiple reasons. For example, the measurement pair at 374 mm yr^{-1} and 318 ppm (Fig. 2.2, Appendix A, Table A1) was taken from a soil described as a Mollisol, but which also contained a large amount of clay and experienced severe cracking (de Jong and Schappert, 1972). Therefore, it is possible that this measurement could represent a time after cracking occurred, dramatically reducing the concentration of CO_2 in the soil and thus causing this

site to deviate significantly from the mean relationship. While these outliers do not affect the slope or intercept of the linear regression, they do represent real sample variability to be expected when reconstructing past atmospheric CO_2 concentrations from pedogenic carbonates. Thus, we suggest making multiple reconstructions of atmospheric pCO_2 using different paleosols (where possible) and multiple analyses from the same paleosol (where possible) to remove the influence of any outlier soils that may not be able to be identified in the geologic record. With the previous outlier example, if the pedogenic carbonate was precipitating only when cracks had formed in the soil, the $\Delta^{13}C$ (difference between $\delta^{13}C$ of carbonate and organic material) would likely be greater than 17‰ and thus unsuitable for atmospheric pCO_2 reconstructions with this new *S(z)* proxy (see "implications for paleosol paleobarometry" section for an in depth discussion of $\Delta^{13}C$ values).

2.6 Application to the Geologic Past

It is clear that the pedogenic carbonate data, largely made up of data published by Ekart et al. (1999), overestimates atmospheric pCO_2 compared to other proxies for much of the 400 Ma record and are most likely not accurate. These high CO_2 estimates during key times with substantial evidence for globally cool temperatures (i.e., the Permian and Cenozoic) suggest CO_2-temperature decoupling. Our new *S(z)*-MAP proxy makes it possible to revise atmospheric pCO_2 estimates from pedogenic carbonates and to re-assess these cases of CO_2-temperature decoupling. In the following sections atmospheric pCO_2 has been reconstructed using the new *S(z)*-MAP proxy presented above with pedogenic carbonates from the Cenozoic, as well as revised previously published atmospheric pCO_2 estimates from the Mesozoic and Paleozoic to determine if individual

estimates of *S(z)* will reduce atmospheric pCO_2 estimates to support lower values estimated by other proxies.

2.6.1 Application to the Cenozoic

Cenozoic climate change is characterized by a gradual decrease in atmospheric CO_2 concentrations punctuated by warming events (Royer et al., 2004). By the latest Miocene, many atmospheric pCO_2 proxies indicate that concentrations had reached Preindustrial values (Pagani et al., 1999; Kürschner et al., 2001; Demicco et al., 2003). These low values coincide with the expansion of the West Antarctic Ice Sheet as well as ice sheets in Greenland around Miocene/Pliocene boundary (Zachos et al., 2001), coincident with the rapid global spread of C_4 grasses between 8 and 3 Ma ago (Cerling et al., 1997; Fox and Koch, 2003; Behrensmeyer et al., 2007). Pedogenic carbonates were used to reconstruct atmospheric pCO_2 during the late Miocene, a time when other CO_2 proxies are in agreement, to test the new *S(z)* proxy's ability to reconstruct accurately past atmospheric pCO_2.

Pedogenic carbonates were collected from the Beaverhead locality in southwestern Montana (45° 26' 4.6"N, 112° 26' 35.6"W). Four previously undescribed paleosols from the Sixmile Creek Formation were sampled (Fig. 2.3C-D). Detailed descriptions of paleosol morphology can be found in Appendix A, Table A3. The section is dated by biostratigraphy to be late Hemphillian in age (Hoffman, 1971; Kuenzi and Fields, 1971), though individual ages could not be assigned to each paleosol due to the lack of better age constraint. For this reconstruction, the depth to Bk horizon (Retallack,

2005) measurements were used, with care to include data only from intact profiles with no erosional features to estimate precipitation using the following equation:

$$P = 137.24 + 6.45D - 0.013D^2 \quad \text{(Eq. 2.4)}$$

where $R^2 = 0.52$ and SE = ± 147 mm yr^{-1}. While Royer (1999) found no significant relationship between the depth to Bk horizon and precipitation, Retallack (2000) points out that Royer's (1999) data compilation included many soils without nodular carbonate. When the same dataset is reduced to include only soils containing pedogenic nodules, Retallack (2005) calculated the relationship above, whose results are generally consistent with chemistry-based climofunctions and with paleobotanical data. Care was taken to avoid paleosols with erosional surfaces that could cause underestimation of MAP as described above by sampling paleosols with clear Bk horizonation and well-defined paleosol tops and bottoms (Fig. 2.3C) indicated by features such as branching organic-rich root traces and vertical burrow terminations (Fig. 2.3D). The Beaverhead section contains 16 paleosols, but only 4 are used in this reconstruction due to possible erosional surfaces, so this reconstruction is as conservative as possible. Precipitation estimates for this section ranged from 324 to 374 mm yr^{-1}. A mean annual temperature estimate of 9.5°C used in the paleo-atmospheric CO_2 reconstruction was obtained from the climate reconstruction published by Retallack (2007) using the molecular weathering ratio of Na_2O and K_2O to Al_2O_3 MAT proxy (Sheldon et al., 2002). This temperature estimate may not exactly represent the temperature at depth in the soil at the time of pedogenic carbonate formation, which is probably slightly warmer than the MAT (Passey et al., 2010). Thus, due to the effect of temperature on atmospheric pCO_2 calculations (Eq. 2.1), these pCO_2 values likely represent minimum estimates.

Table 2.1 shows the isotopic compositions, temperature and precipitation variables used in the atmospheric pCO_2 calculation for the late Miocene. While the $\delta^{13}C_{org}$ shows a possible component of C_4 photosynthesis or of water stressed C_3 vegetation, this signal does not pose a problem for the atmospheric reconstruction as long as this $\delta^{13}C_{org}$ value is used in the reconstruction and not the global average isotopic composition of C_3 plants derived from the fossil record of marine carbonates and the offset between the plants and the atmosphere as applied by Ekart et al., (1999). The respiration of C_4 or water stressed C_3 organic material will produce isotopically enriched soil CO_2, and therefore isotopically enriched pedogenic carbonates, but the offset will still be the same 14–17‰ (Cerling and Quade, 1993; Koch, 1998) as in pure C_3 systems with no water limitations. These pedogenic carbonates may be used for atmospheric pCO_2 reconstructions as long as the offset between the pedogenic carbonates and the soil CO_2 from which they were precipitated can be measured. Using the $\delta^{13}C$ of occluded organic material in each pedogenic carbonate nodule as $\delta^{13}C_r$ in Eq. 2.1 instead of the global average isotopic composition of C_3 plants allows for the true $\Delta^{13}C$ value to be analyzed for these paleosols. Table 2.1 also shows the $\Delta^{13}C$ values for these palsosols are well within the normal range of 14–17‰ established by Cerling and Quade (1993), thus we do not suspect microbial isotopic enrichment of the organic matter (e.g., Wynn, 2007). If this organic matter were isotopically enriched due to microbial degradation, we would expect the $\Delta^{13}C$ to be lower, which would cause an underestimation in atmospheric pCO_2.

Figure 2.4 shows the comparison between the atmospheric pCO_2 estimates from the Beaverhead pedogenic carbonates and other proxies (alkenones: Pagani et al., 1999,

geothites: Yapp and Poths, 1996; marine boron: Demicco et al., 2003; stomatal index: Kürschner et al., 2001) as well as the original Ekart et al. (1999) estimates using an assumed value for *S(z)* and $\delta^{13}C_{org}$. Our paleo-atmospheric pCO_2 reconstruction using the pedogenic carbonates collected at Beaverhead yield four estimates ranging from 215 ± 147 to 376 ± 251 ppm, with an average of 282 ± 183 ppm (Table 2.1; Fig. 2.4). The error for these estimates was calculated by Gaussian error propagation using equations derived by Retallack (2009). This error includes the errors associated with all isotopic measurements, as well as the standard errors associated with transfer functions used to calculate precipitation, temperature (used in the determination of $\delta^{13}C_s$) and *S(z)*. For the 7.0–5.0 Ma time period, estimates based on alkenones (Pagani et al., 1999) yield an average atmospheric pCO_2 value of 282 ppm, marine boron (Demicco et al., 2003) estimates yield an average of 251 ppm, and estimates based on the stomatal index of oak and birch leaves (Kürschner et al., 2001) yields an average of 314 ppm. One goethite measurement produces an estimate of 350 ppm, whereas the original Ekart et al. (1999) pedogenic carbonate reconstruction estimates an average of 770 ppm. Thus, using an arbitrary value of 5000 ppm for *S(z)* in the Ekart et al. (1999) calculation results in more than double preindustrial atmospheric pCO_2 during this time period, a value greatly overestimated compared to other proxies.

Using the pedogenic carbonate paleobarometer method with our isotopic data from the Beaverhead section combined with the Retallack (2009) depth to Bk horizon-*S(z)* proxy, we calculate atmospheric pCO_2 for the late Miocene ranging from 363 to 637 ppm with an average of 465 ppm. As expected, this proxy based on mean growing season soil-respired CO_2 overestimates atmospheric pCO_2 compared to other previously

published estimates from this time period. Our reconstruction using the Cerling (1984; 1991) paleobarometer combined with the new soil-respired CO_2 proxy produces the same low atmospheric pCO_2 values estimated by the other proxies, which demonstrates that this new proxy can accurately determine past atmospheric CO_2 concentrations.

2.6.2 Application to the Mesozoic

Cleveland et al. (2008a-b) investigated the CO_2 and climatic changes leading up the to the Triassic/Jurassic boundary using paleosols from the Chinle formation of the Southwestern United States. These studies found that the concentration of atmospheric CO_2 increased from the late Norian to the Rhaetian, while precipitation remained relatively constant at semi-arid levels (~300–500 mm yr^{-1}).

We have refined pCO_2 estimates for this time period using the isotopic data from pedogenic carbonates published by Cleveland et al (2008a) combined with precipitation estimates from the same paleosols published by Cleveland et al (2008b) to apply our new *S(z)*-MAP proxy (Fig. 2.5C). For these atmospheric pCO_2 revisions, we used both the depth to Bk horizon precipitation proxy (Fig. 2.5C circles) as well as the CIA-K precipitation proxy (Fig. 2.5C squares) to examine differences in the reconstructed pCO_2 value using different MAP proxies. *S(z)* was originally estimated to be 4000 ppm and 3000 ppm for the Ghost Ranch and Montoya members of the Chinle formation, respectively. There are no error estimates for these *S(z)* values in the original paper, because these values have been assumed. For the Ghost Ranch member, we calculate an average *S(z)* value of 3782 ppm using the *S(z)*-MAP proxy with precipitation estimates from geochemical data using the CIA-K proxy and an average *S(z)* value of 2163 ppm

using the depth to Bk horizon precipitation proxy. For the Montoya member, we calculate an average *S(z)* value of 3237 ppm using the CIA-K precipitation proxy and an average *S(z)* value of 2246 using the depth to Bk horizon precipitation proxy. Thus, the original *S(z)* estimates and atmospheric pCO_2 estimates published by Cleveland et al.(2008) are similar to but higher than our refined estimates for atmospheric pCO_2. In this case, the revision of atmospheric pCO_2 values were minor because the original estimates of *S(z)* by Cleveland et al. (2008) were reasonable, but this is not likely to always be true. Figure 2.5C (red circle and square) shows the revised atmospheric pCO_2 estimates compared to pCO_2 curve from pedogenic carbonate paleobarometry estimates (dashed gray), the pCO_2 curve from other proxies (blue; Breecker et al., 2010) as well as the GEOCARBSULF model of Berner (pers. comm. 2011). Revised pCO_2 estimates using lower *S(z)* values are now within the error window for the reconstructions from other proxies and have smaller errors than the previous reconstruction, showing that our new *S(z)*-MAP proxy produces more accurate and more precise pCO_2 estimates (Fig. 2.5).

2.6.3 Application to the Paleozoic

Montañez et al. (2007) reconstructed atmospheric pCO_2 and paleotemperature from the latest Carboniferous to Middle Permian using pedogenic carbonates from multiple formations from the Southwest United States and found an increase in atmospheric pCO_2 from present day values up to 3500 ppm by the middle Permian. These CO_2 changes were accompanied by an increase in tropical sea surface temperature of 4–7°C that the authors link to a transition to an ice free world. The atmospheric pCO_2

reconstruction originally published by Montañez et al. (2007) using assumed *S(z)* values estimate an increase in atmospheric CO_2 of roughly 600 ppm from 300 to 285Ma (Fig. 2.5A-B). We refined atmospheric pCO_2 estimates using the isotopic data published by Montañez et al. (2007) combined with precipitation data from soils matched to the same formation and age published by Retallack (2009) and found a negligible CO_2 rise from 300 to 285Ma (Fig. 2.5C-D). These new revised pCO_2 estimates (also shown in Table 2.2) are reduced and are closer to estimates produced by other proxies as well as the revised GEOCARBSULF model (Berner, per. comm., 2011).

Ekart et al. (1999) also reconstructed pCO_2 using pedogenic carbonates from multiple formations dating to the early Permian. These reconstructions incorporated assumed values for *S(z)* (5000 ppm) as well as assumed temperatures and $\delta^{13}C_{org}$. We revised the pCO_2 estimates from the early Permian by matching the paleosols to precipitation estimates from paleosols of the same formation and age from Retallack (2009). Figure 2.5C and d show that these revised pCO_2 estimates still plot much higher than what other proxies estimate and what is predicted by GEOCARBSULF. The $\Delta^{13}C$ values for the three pedogenic carbonates for this time period published by Ekart et al. (1999) range from 18.3 to 19.9‰, outside of the acceptable limits for pedogenic carbonate paleobarometry (described in detail below) and are not expected to produce accurate pCO_2 reconstructions.

Figure 2.5 shows that using precipitation estimates from the same soil gives atmospheric pCO_2 estimates closer to the pCO_2 curve produced by all other proxies other than pedogenic carbonates. These estimates are also closer to modeled atmospheric CO_2 concentrations. Our refined pCO_2 estimates using the data published by Montañez et al.

(2007) do not have precipitation estimates from the exact paleosols in which the pedogenic nodules were sampled, and these estimates are higher than what is predicted by other proxies and models. The refined estimates for the Permian using the data published by Ekart et al. (1999) are still much higher than would be expected based on glacial records preserved and do not agree with values estimated from other proxies as well as models (GEOCARBSULF results of Berner; Horton et al., 2010), demonstrating the importance of measuring $\delta^{13}C_{org}$ as well as estimating an *S(z)* value for each soil used in atmospheric pCO_2 reconstructions.

2.6.4 CO_2-Temperature Coupling in the Geologic Past

Though CO_2-temperature coupling has been validated on some time scales (Royer et al., 2004), there is still a question of whether or not CO_2 has been coupled to climate throughout the entirety of geologic time. For example, Pagani et al. (1999) find low concentrations of CO_2 throughout the Miocene, suggesting a CO_2-temperature decoupling during the Middle Miocene Climatic Optimum. Reconstructions using pedogenic carbonates and our new *S(z)*-MAP proxy produce low estimates of atmospheric pCO_2 for the late Miocene that are in agreement with other terrestrial and marine proxies. Given that temperature reconstructions from this time period are not much warmer than today (Zachos et al., 2001; Billups and Schrag, 2002), the Ekart et al. (1999) estimate of high pCO_2 would suggest a temperature-CO_2 decoupling for the late Miocene. The revised atmospheric pCO_2 values from the Beaverhead site in Montana instead support CO_2-temperature coupling, at least for the late Miocene.

For the early Permian, our revised atmospheric pCO_2 reconstruction shows no detectable pCO_2 increase in the early Permian (Table 2.2), which is in general agreement with pCO_2 estimates from the stomatal index proxy as well as GEOCARBSULF. Geochemical temperature reconstructions from Utah (Retallack, 2009) show no absolute temperature change between 300 to 285 Ma. Temperature estimates from pedogenic phyllosilicates and Fe-oxides published by Montañez et al. (2007) show significant variation between 300 to 285 Ma, but the absolute change in temperature between these dates (corresponding to the dated atmospheric pCO_2 estimates) is small (~4°C) and within error of the proxy. The rock record also contains extensive glacial features during this time, and recent modeling results show that late Paleozoic Ice Age conditions are triggered at relatively low CO_2 levels, between 420 and 840 ppm (Horton et al., 2010). The agreement of multiple proxies and model results as well as temperature reconstructions that indicate relatively stable temperature between 300 and 285 Ma and suggest CO_2-temperature coupling in the early Permian. Additionally, the high CO_2 estimates >3000 ppm from Ekart et al. (1999; Table 2.2) are at odds with the rock record, multiple other atmospheric pCO_2 proxies (Montañez et al., 2007; *this study*) as well as multiple model results, and should be considered unreliable. It should be noted that other climatic reconstructions do find significant variability in temperatures and precipitation over the late Carboniferous to early Permian (Tabor and Montañez, 2005; Tabor, 2007; Tabor et al., 2008), though no directional change in climate was found during this time period, which indicates regional temperature variability during this time period.

Thus, the CO_2-temperature decoupling implied for some time periods by the Ekart et al. (1999) pCO_2 reconstruction does not hold up to scrutiny. Instead, revised paleosol

paleobarometer pCO_2 estimates closely match other pCO_2 proxy results (e.g., compiled in Royer et al., 2004), indicating CO_2-temperature coupling during both the late Cenozoic and Paleozoic.

2.7 Implications for Paleosol Paleobarometry

From the modern soil validation study, not all soils were in agreement with the predicted *S(z)*-proxy regression. These soils had $\Delta^{13}C$ values (defined as $\delta^{13}C_{cc}$-$\delta^{13}C_{org}$) that were greater than 17‰ or less than 14‰, outside of the normal range for modern soils described by Cerling and Quade (1993). When the value of *S(z)* is calculated as described in the methods section using measured isotopic compositions (Eq. 2.1), as the soil $\Delta^{13}C$ increases, the calculated *S(z)* decreases. If the $\Delta^{13}C$ is less than ~14‰ (depending on temperature), then the calculated *S(z)* value will be negative, implying precipitation of carbonates from a one component soil CO_2 system (Tabor et al., in press). Figure 2.6 and Appendix A, Table A2 include data from five soil series in South Dakota, two in Minnesota and one in New Mexico that clearly do not fall on the *S(z)*-MAP relationship defined based upon the literature data. These modern soils have $\Delta^{13}C$ values falling outside the range of 14–17‰, with low *S(z)* values from soils with a $\Delta^{13}C > 17$‰ and negative *S(z)* values from soils with $\Delta^{13}C < 14$‰. Soils with $\Delta^{13}C$ values greater than 17‰ can arise from low productivity ecosystems where *S(z)* is low and pedogenic carbonates exhibit a greater influence from the diffusion of isotopically heavier atmospheric CO_2 into the soil (Sheldon and Tabor, 2009). Modern soils with $\Delta^{13}C$ values less than 14‰ can occur in a system in which the fractionation caused by diffusion is small or absent. Low $\Delta^{13}C$ values have been observed to occur in areas with groundwater

saturation (Mintz et al., 2011), or with soils that do not exhibit gravity-driven hydrologic flow, which lowers diffusivity and decreases the diffusive enrichment factor (Tabor et al., in press). Water saturated soils may undergo advection as well as diffusion. Because the 4.4‰ diffusive enrichment factor (Eq. 2.1) described by Cerling (1991) is calculated based on diffusion at 25°C, advection processes in the soil may alter this enrichment. This diffusive enrichment of $^{13}CO_2$ in soils itself may also lead to variation in $\Delta^{13}C$ values, because it is a modeled value that may vary in soils depending on a variety of factors such as the offset between $\delta^{13}C_r$ and $\delta^{13}C_a$ (Davidson, 1995) as well as temperature (Cerling, 1991), but without experimental data it is unclear how much this term will vary. A diffusive enrichment of less than 4.4‰ could also lead to low $\Delta^{13}C$ values.

This new *S(z)* proxy cannot be used with soils that fall outside of the range of 14–17‰. We recommend that soils with a $\Delta^{13}C$ of greater than 17‰ only be used for atmospheric pCO_2 reconstructions if an independent constraint on productivity is available. We recommend that soils with a $\Delta^{13}C$ value of less than 14‰ never be used for atmospheric pCO_2 reconstructions because it is not likely that these soils are behaving according to the diffusive model necessary for calculation of atmospheric pCO_2 with the pedogenic carbonate paleobarometer. The Permian atmospheric pCO_2 estimates published by Ekart et al. (1999) used carbonates with $\Delta^{13}C$ values of 18.3–19.9‰. Given that high $\Delta^{13}C$ values are associated with low productivity ecosystems and low *S(z)* values, pCO_2 reconstructions using a *S(z)* value of 5,000 ppm overestimated atmospheric pCO_2 for this time period compared to all other proxies as well as other pCO_2 reconstructions using pedogenic carbonates and measured $\delta^{13}C_{org}$ (i.e., Montañez et al.,

2007). Even after the Ekart et al. (1999) values were revised using our *S(z)*-MAP proxy, the reconstruction still overestimates Permian pCO_2 due to the large $\Delta^{13}C$ values.

The soils that fall off the *S(z)*-MAP line due to high or low $\Delta^{13}C$ demonstrate the importance of measuring both the isotopic composition of the carbonate as well as organic material occluded in the carbonates for each soil rather than assuming a single $\delta^{13}C_{org}$ value for an entire section or time period as has been done in the past (e.g., Ekart et al., 1999). These measurements allow for the calculation of $\Delta^{13}C$ for each specific soil. Using an estimate of the $\delta^{13}C$ of the organic matter at the surface is not useful because the isotopic composition of organic material at the surface of the soil does not always match that of the organic matter at depth due to microbial decomposition (Wynn, 2007). The magnitude of the difference between the $\delta^{13}C$ of organic material at the surface and at depth in the soil is highly variable, and dependent on many different factors such as grain size and climate (Garten et al., 2000; Wynn, 2007). While the A horizon has more labile organic material than the B horizon and may be respired more quickly than the organic material at depth, this CO_2 is unlikely to diffuse down the soil profile against the flux of soil CO_2 moving towards the soil surface to the atmosphere. The isotopic composition of both soil organic matter and soil-respired CO_2 reaches equilibrium at roughly 30 cm depth in the soil (Cerling and Quade, 1993; Amundson et al., 2000) and therefore, the soil organic matter occluded in carbonate nodules is more representative of soil CO_2 at depth than the soil organic material from the O or A horizons. Assuming a value of $\delta^{13}C$ of organic matter rather than measuring it increases uncertainties in pCO_2 reconstructions (Royer et al., 2001). If the specific $\Delta^{13}C$ value is unknown, then paleosols that are potentially unsuitable for paleobarometry could be used

and produce incorrect reconstructions. This may be the case for much of the data compiled by Ekart et al. (1999) and some of the data used in the revised Breecker et al. (2010) atmospheric pCO_2 curve that relied upon the same isotopic data (though Breecker et al. (2010) culled some of the obviously unreliable data). The $\delta^{13}C_{org}$ value for the Ekart et al. (1999) reconstructions was based on a proxy derived from marine carbonates and not from measured organic material. Thus, the true $\Delta^{13}C$ value for each of these paleosols is unknown and the accuracy of the results is questionable.

In the pedogenic carbonate atmospheric pCO_2 curve revised by Breecker et al. (2010), the value of *S(z)* used in each CO_2 reconstruction was lowered from 5000 ppm to 2500 ppm. An *S(z)* value of 2500 equates to a MAP value of about 500 mm yr^{-1}, which would be an overestimation for all soils forming under drier conditions, the majority of the carbonate forming precipitation range. The use of 2500 ppm would also underestimate atmospheric pCO_2 using soils forming in areas wetter than 500 mm yr^{-1}. Assuming that pedogenic carbonate forms at or below 750 mm yr^{-1}, the maximum *S(z)* value that our new proxy (Eq. 2.3) predicts is 3982 ppm, substantially lower than the 5000 ppm used by Ekart et al. (1999), which means that it is likely that every pCO_2 estimate published in that study is overestimated. Because the value of *S(z)* is highly variable and greatly influences the final atmospheric pCO_2 estimate, the most accurate reconstructions of past atmospheric pCO_2 can be made if each pedogenic carbonate nodule analyzed has an accompanying *S(z)* value.

The errors for the estimates from the late Miocene above are considerably larger than the error estimates produced by the same Gaussian error propagation used by Retallack (2009), which is due to the fact that the standard error associated with the proxy

relationship for MAP was taken into consideration. A closer investigation of the Gaussian error propagation (Appendix A, Table A4) reveals that the uncertainties in atmospheric CO_2 reconstruction are largely due to the uncertainties in *S(z)*, showing the importance of the *S(z)*-MAP proxy introduced by this study. The uncertainties associated with atmospheric pCO_2 reconstructions using pedogenic carbonates are typically estimated and not calculated. In our Miocene case study, we quantify the uncertainty in pCO_2 estimates using this pedogenic carbonate paleobarometer. While the error may seem larger for this reconstruction than other proxies, many of the other proxies report errors from analytical uncertainty only (i.e., alkenones, marine boron). The uncertainties associated with revised atmospheric pCO_2 estimates in this study have been significantly reduced compared to the estimated uncertainties in previous pedogenic carbonate reconstructions (i.e. Ekart et al., 1999; Montañez et al., 2007). Four reconstructions of atmospheric CO_2 concentrations from separate paleosols from the same time period were made in an effort to average out the variability in *S(z)* across different soils. Due to its higher sensitivity at higher levels of atmospheric CO_2 than other proxies, the pedogenic carbonate paleobarometer is most useful at times of in the geologic past when atmospheric CO_2 was high (Royer et al., 2001; Montañez et al., 2007), though it also may produce accurate results for times of lower atmospheric pCO_2 as well (Fig. 2.5) if applied carefully.

To produce the most accurate atmospheric CO_2 reconstructions using paleosols, we present a set of guidelines for the use of the pedogenic carbonate paleobarometer that expand upon the work of various other studies (e.g., Cerling, 1991; Royer et al., 2001; Montañez et al., 2007) but which have yet to be compiled into a useful set of criteria

published in a single paper. Figure 2.7 describes the methods that should be followed at each step, including fieldwork sampling, laboratory observations and analyses to exclude samples unsuitable for reconstructions. Combined with careful carbonate collection and laboratory work, organic matter occluded in pedogenic carbonates should be analyzed for $\delta^{13}C_{org}$ to determine $\Delta^{13}C$ as has been suggested by other studies (Duetz et al., 2001; Royer et al., 2001; Montañez et al., 2007). We propose that each individual $\delta^{13}C_{org}$ value must be combined with a specific value of *S(z)* for each paleosol used to make an atmospheric CO_2 reconstruction. To reduce uncertainties and the effects of outlier isotopic measurements, replicate samples from each paleosol as well as multiple paleosols from the time period of interest should be analyzed. The new *S(z)*-MAP proxy described here provides a useful way to assign a specific value of *S(z)* to individual palesols and significantly increases the precision of paleo-atmospheric CO_2 reconstructions using the pedogenic carbonate paleobarometer.

2.8 Conclusions

We present an empirical relationship between summer minimum soil-respired CO_2 (*S(z)*) and precipitation. This new *S(z)* proxy, validated by modern soil and paleosols, allows for the estimation of unique values of *S(z)* for each soil used in atmospheric pCO_2 reconstruction, thus constraining the assumption driven source of uncertainty in the pedogenic carbonate paleobarometer. While this new proxy has been shown to predict *S(z)* accurately for some modern soils and to produce reasonable results for the geologic past, it cannot be used for all paleosols. Thus, care must be taken in choosing the right paleosols and climatic conditions for use with this proxy. Due to the

lack of data from soils forming in humid areas, this proxy should only be applied to paleosols with precipitation estimates up to 600 mm yr^{-1}, though this is the majority of the precipitation range in which pedogenic carbonates are found. The useful range of this proxy could be extended to 750 mm yr^{-1} to include the entire precipitation range for soil carbonates, but further proof of concept would be needed. Our literature review does not include any soil-respired CO_2 data from Vertisols, so we cannot confirm that the same relationship will hold true for this soil order. However, we can confirm based on our modern dataset that this proxy works for Aridisols, Mollisols and Inceptisols, and it may potentially work for Alfisols and Entisols as well. Assumptions about the isotopic composition of plant material inputs are not valid because fractionations between the surface organic material and the organic material at depth are highly variable. Because of this variability, we also conclude that care must be taken to analyze both inorganic and organic carbon isotopic compositions in order to determine the $\Delta^{13}C$ value for each paleosol. If the value falls out of the range of 14–17‰, these paleosols should not be used with this *S(z)* proxy. We also suggest that due to the inherent variability within soils and *S(z)* values at the time of carbonate formation, it is best to analyze multiple paleosols containing pedogenic carbonates for a given time period to reduce the influence of possible outlier soils or carbonate nodules.

Our atmospheric pCO_2 reconstruction from the Miocene produces the same low CO_2 values as many other proxies. Our refined CO_2 estimates from the Mesozoic and Paleozoic are lower and more similar to CO_2 estimates reconstructed by other proxies as well as models than the originally published estimates. Temperature estimates from the early Permian as well as glacial evidence in the rock record suggest CO_2-temperature

coupling for this time period, as opposed to CO_2-temperature decoupling suggested by the higher pCO_2 estimates published by Ekart et al., 1999 and Montanez et al. (2007). The new *S(z)* proxy presented here reduces uncertainty and produces more accurate pCO_2 estimates than previous reconstructions using the pedogenic carbonate paleobarometer.

2.9 Acknowledgements

The authors would like to thank L. Wingate for performing isotopic analyses, as well as E. Hyland, C. Wilkins, J. and K. Kaufman for field assistance, and A. Sacarny for statistical consultation. Associate Editor A.Hope Jahren, reviewers D. Breecker and N. Tabor, and other anonymous reviewers made numerous helpful suggestions that significantly improved the manuscript. The authors also acknowledge the NSF (Award #1024535 to NDS), Geological Society of America (to JMC), the Evolving Earth Foundation (to JMC), and the Scott Turner Award (to JMC) for funding this research.

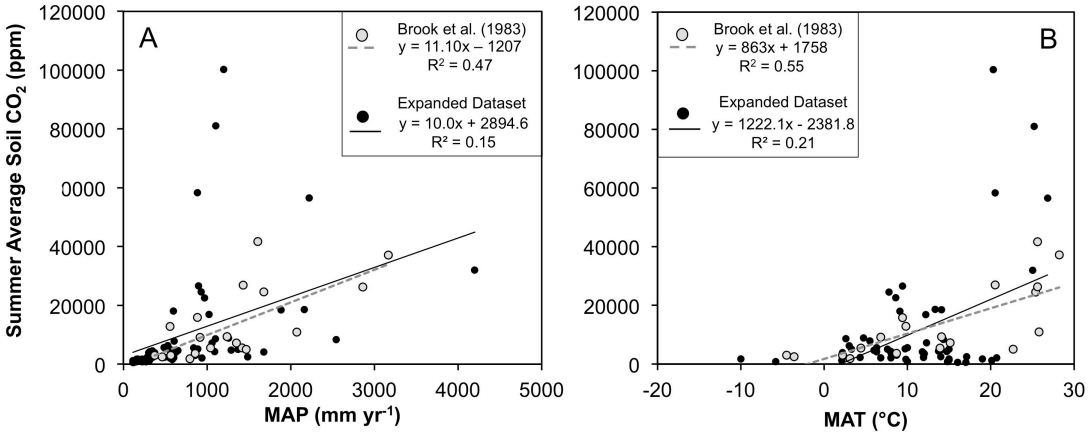

Figure 2.1. Soil CO_2 versus climatic variables. A. 19 original Brook et al. (1983) average soil CO_2 measurements (gray circles) and averages of measurements of soil CO_2 from 60 soils (this study, black circles) vs. MAP. B. 19 original Brook et al. (1983) average soil CO_2 measurements (gray circles) and measurements of soil CO_2 from 60 soils (this study, black circles) vs. MAT. With a large increase in the number of soil CO_2 measurements, the strength of the relationships observed by Brook et al. is weakened and the significance is reduced.

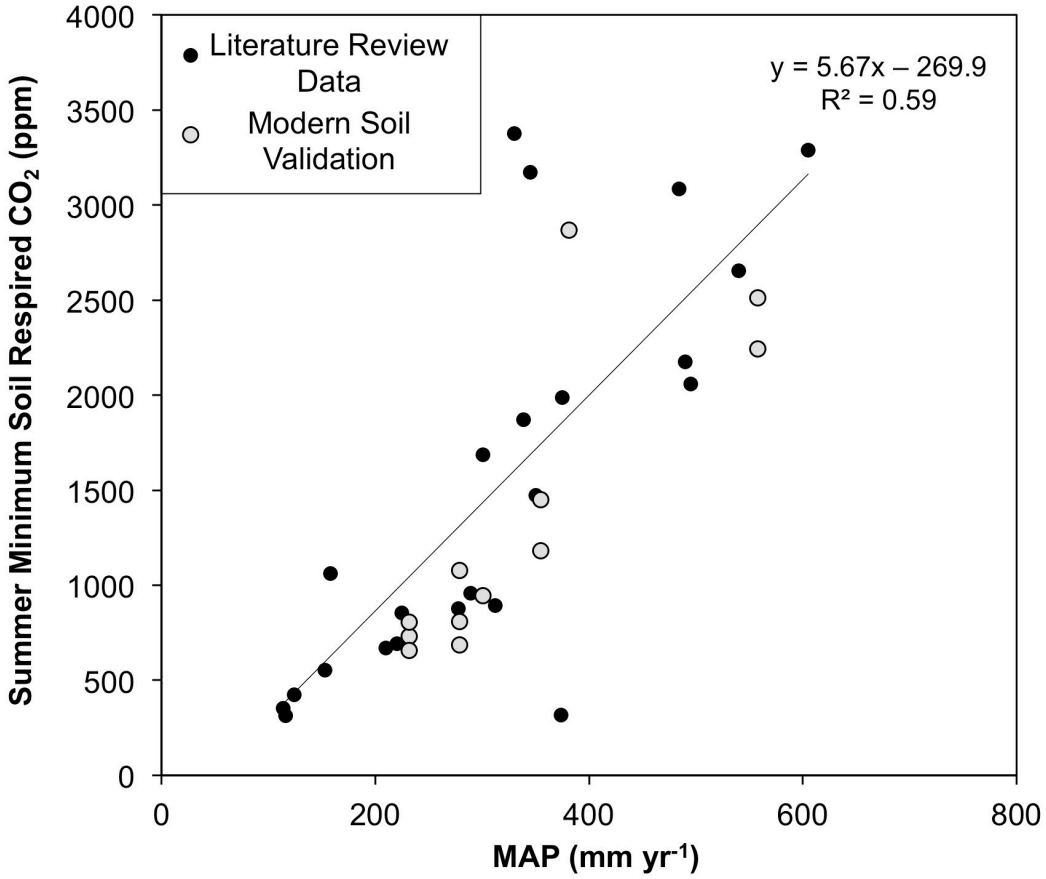

Figure 2.2. Relationship between summer minimum soil-respired CO_2 (*S(z)*) and mean annual precipitation for 23 soils forming pedogenic carbonate (black circles, $R^2 = 0.59$, SE = ± 681 ppm). Also shown are the calculated *S(z)* values from the sampled modern soil carbonates from Arizona, New Mexico, Colorado and South Dakota (gray circles). Most of these calculated *S(z)* values are within the standard error of the predicted values using the new *S(z)* proxy.

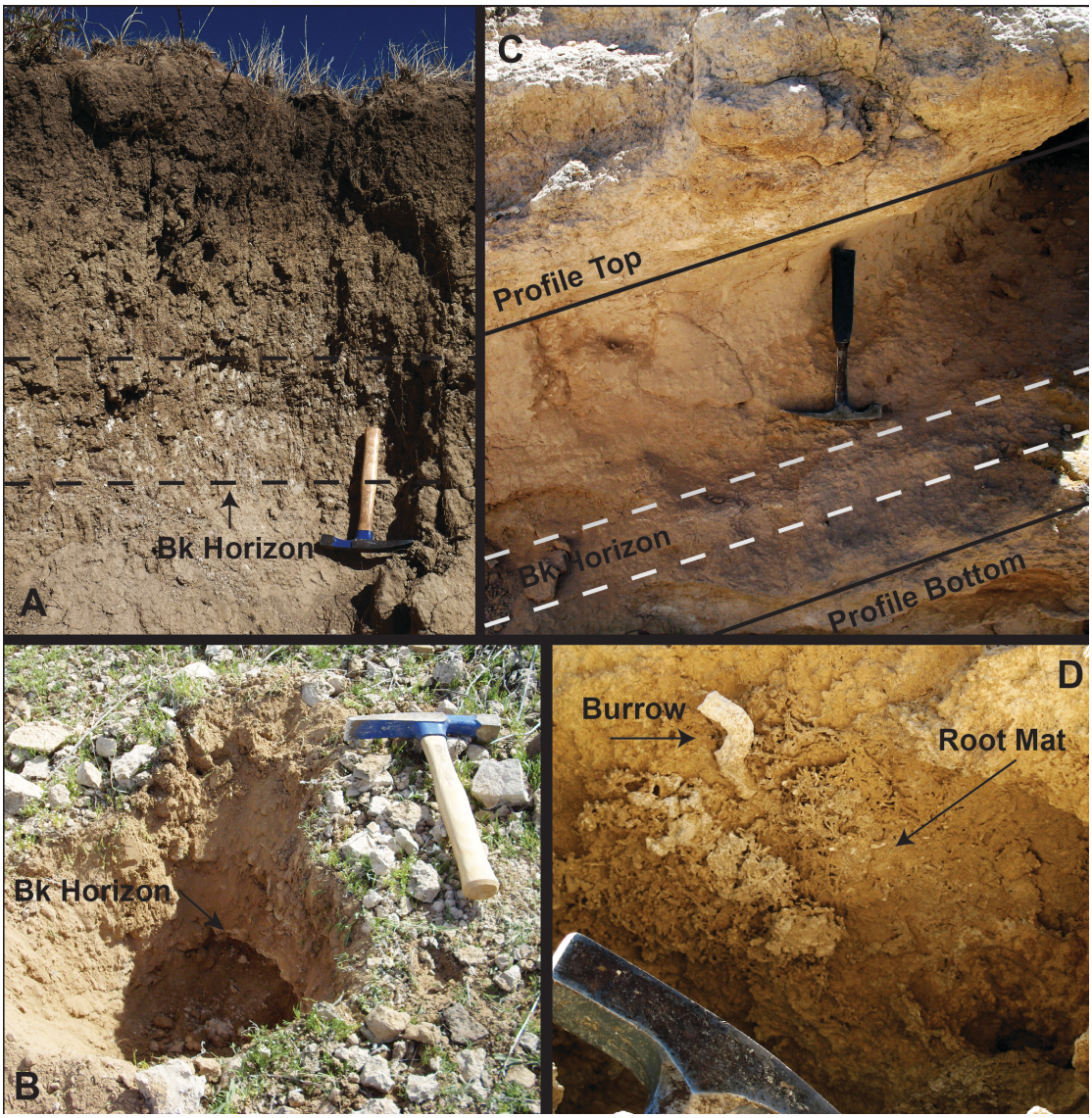

Figure 2.3. Field photographs from modern soils used in calibration and paleosols from the late Miocene Beaverhead locality. A: Bk horizon displayed in modern soil profile from the Plughat soil series in Colorado. B: Bk horizon from modern Cipriano soil series in Arizona. C: Complete preserved paleosol profile at the late Miocene Beaverhead locality in southwestern Montana, showing the top of soil profile and the Bk horizon. D: Trace fossil (burrow) and root mat preserved in a paleosol at the late Miocene Beaverhead locality.

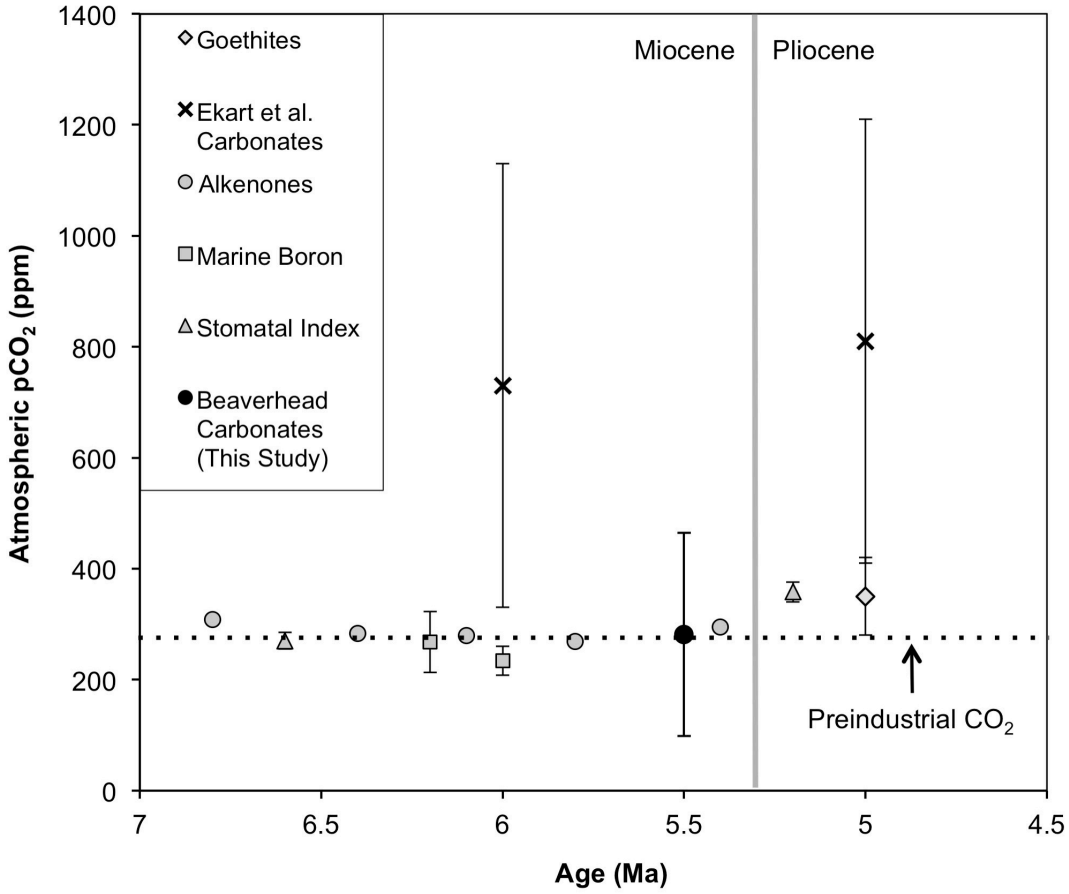

Figure 2.4. Atmospheric pCO_2 reconstruction for the late Miocene from the Beaverhead pedogenic carbonates using the new soil-respired CO_2 proxy compared to reconstructions from multiple other proxies from a variety of locations: Pedogenic carbonates (Ekart et al., 1999), Goethites (Yapp and Poths, 1996), Alkenones (Pagani et al., 1999), Marine Boron (Demicco et al., 2003) and Stomatal Index (Kürschner et al., 2001). Beaverhead samples are dated as late Hemphillian, and all four paleosols are displayed as the same age. Error of 151–260 ppm associated with the Beaverhead pCO_2 estimates was determined by Gaussian error propagation (see Appendix A, Table A4) using equations derived by Retallack (2009).

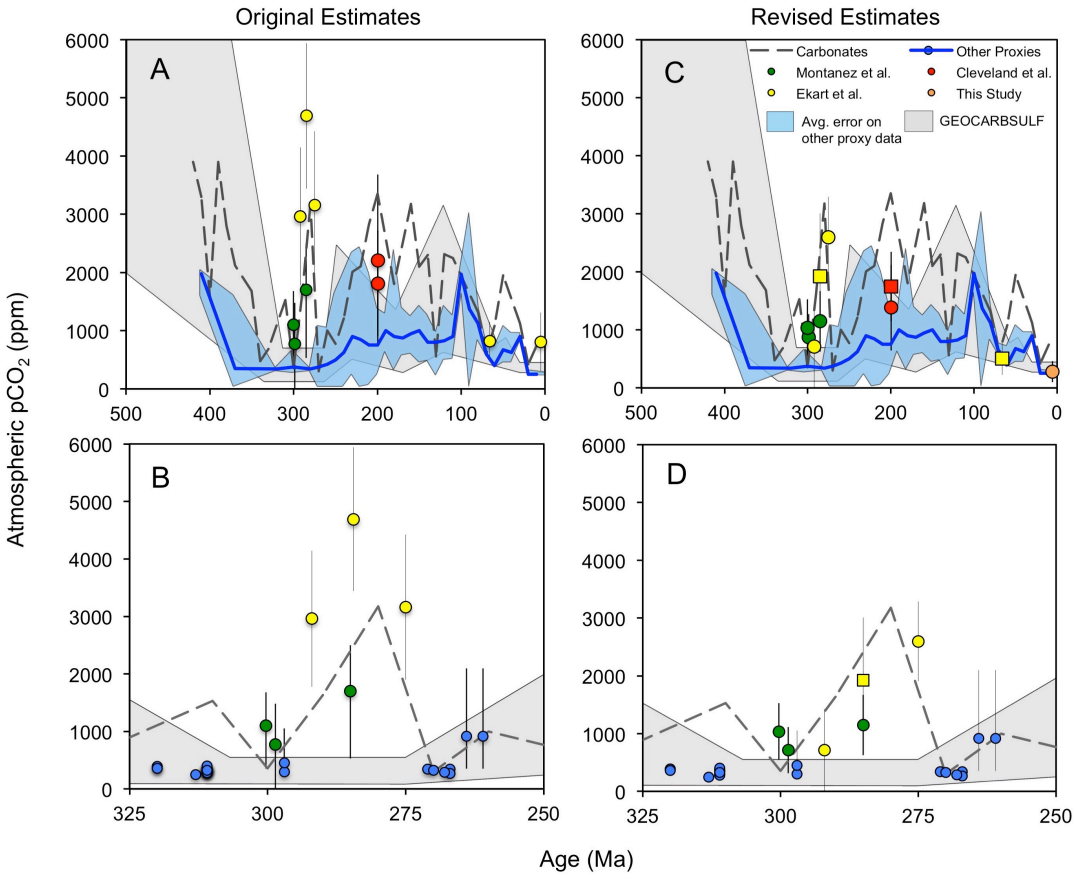

Figure 2.5. Revised paleosol carbonate pCO_2 estimates compared with proxy and model results. The proxy curve has been reproduced from Breecker et al. (2010), who reconstructed pCO_2 over the Phanerozoic using a multi-proxy dataset that was averaged in 10 Ma bins. The gray dashed line represents the paleosol carbonate reconstruction while the blue line represents the reconstruction based on all other proxies with the blue shaded area representing the average error associated with the proxies for 10Ma bin. The gray shaded area is the most recent revision of GEOCARBSULF (Berner, pers. comm., 2011). A: Original estimates published by Cleveland et al. (2008), Montañez et al. (2007), and Ekart et al. (1999). B: Original estimates displayed in A focusing on the late Carboniferous to early Permian. C: Revised estimates using precipitation reconstructions and the new *S(z)* proxy. Circle markers represent CO_2 revisions made using the depth to Bk horizon precipitation proxy while square markers represent CO_2 revisions made using the CIA-K precipitation proxy. D: Revised estimates displayed in C focusing on the late Carboniferous to early Permian.

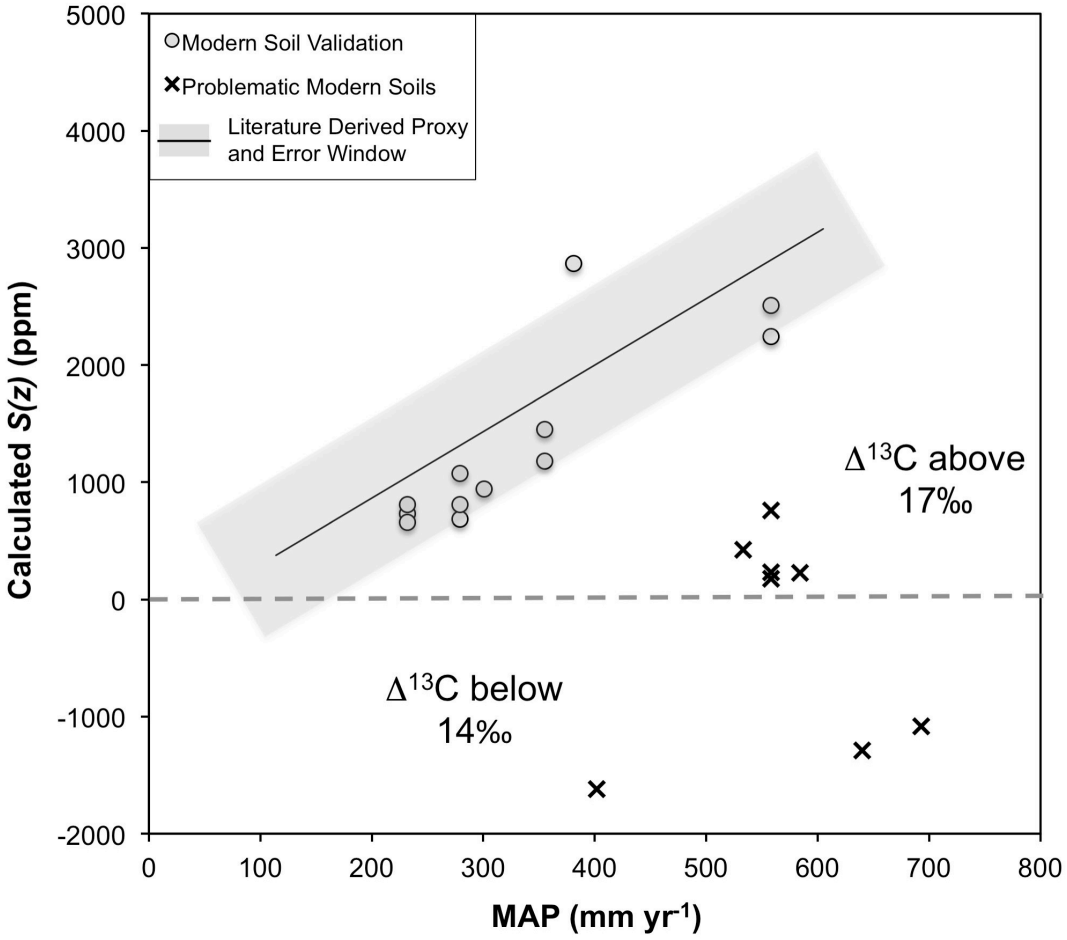

Figure 2.6. Calculated *S(z)* values for modern validation soils, with $\Delta^{13}C$ values between 14–17‰ shown as gray circles and soils falling outside the range of 14–17‰ shown as a black 'x'. Plotted in black is the proxy relationship for *S(z)* derived from the literature review. The gray box represents the standard error (± 681 ppm) associated with the linear regression. Soils with $\Delta^{13}C$ higher than 17‰ will have calculated *S(z)* values lower than those predicted by the proxy relationship, soils with $\Delta^{13}C$ lower than 14‰ will have negative calculated *S(z)* values.

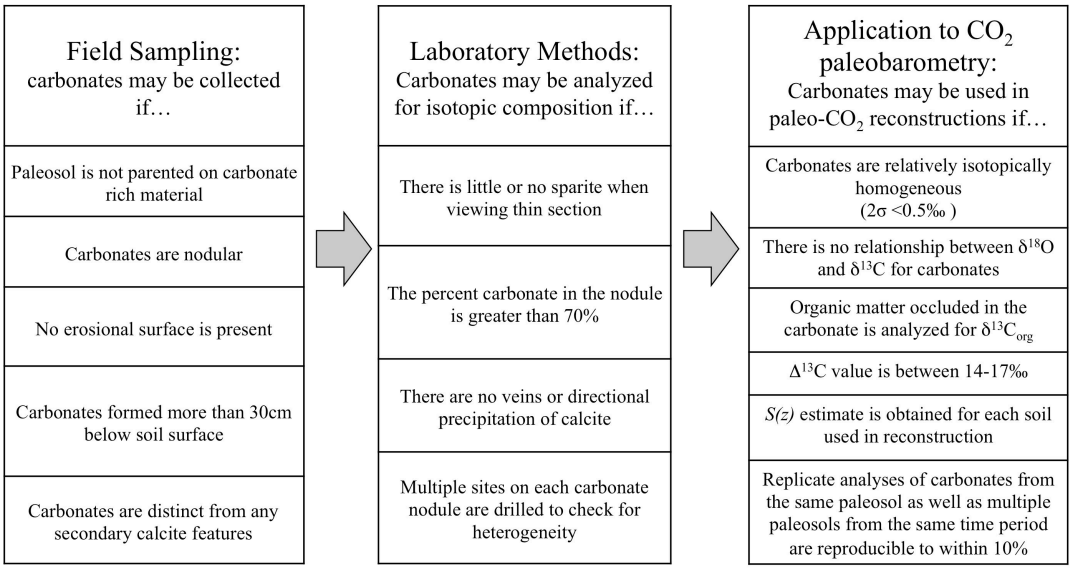

Figure 2.7. Procedural guidelines to follow for use of pedogenic carbonates in atmospheric CO_2 reconstructions, including methods for field sampling, laboratory observations, and isotopic analysis

Paleosol	$\delta^{13}C_c$	$\delta^{13}C_{org}$	T (°C)	$\delta^{13}C_s$	$\delta^{13}C_a$	Depth to Bk (cm)	MAP (mm yr^{-1})	*S(z)*	pCO_2	Error +/-
JB-1	-6.04	-22.43	9.57	-16.69	-6.15	40	374	1858	252	151
JB-2	-6.11	-22.52	9.57	-16.76	-6.15	31	324	1573	215	152
JB-3	-5.95	-22.49	9.57	-16.6	-6.15	40	374	1858	283	170
JB-5	-6.06	-23.48	9.57	-16.71	-6.15	32	330	1607	376	260

Table 2.1. Isotopic data from Montana paleosols used to reconstruct pCO_2 of the late Miocene. Temperature Estimates come from Retallack, 2007. Precipitation estimates are calculated from the Retallack (2005) depth to Bk horizon MAP proxy.

Reference	Formation	Age	Original *S(z)*	MAP (using Bk depth)	MAP (using CIA-K)	Revised *S(z)* Using Bk Depth	Revised *S(z)* using CIA-K	Original pCO_2	Revised pCO_2 using Bk depth	Revised pCO_2 using CIA-K
Cleveland et al. 2008	Chinle - Ghost Ranch Member	199.6	4000	334	619	2163	3782	1811	1145	1714
Cleveland et al. 2008	Chinle - Montoya Member	199.6	3000	348	525	2246	3237	2210	1704	1779
Montañez et al. 2007	Honiker Trail	300.3	2500	451	--	2291	--	1103*	1037	--
Montañez et al. 2007	Cedar Mesa	285	2000	467	--	2381	--	1700*	1149	--
Montañez et al. 2007	Halgaito Shale	298.6	3000	387	--	1929	--	772*	713	--
Ekart et al. 1999	Organ Rock	275	5000	767	--	4079	--	3160	2597	--
Ekart et al. 1999	Cedar Mesa	285	5000	467	--	2381	--	4690	1923	--
Ekart et al. 1999	Halgaito Shale	292	5000	399	--	1991	--	2960	713	--
Ekart et al. 1999	North Horn	66	5000	--	608	--	3177	820	--	506

* pCO_2 estimates from Montañez et al. (2007) are best estimates obtained from Monte Carlo modeling incorporating multiple data points of similar ages, including some with very high *S(z)* estimates, to produce a smoothed pCO_2 curve. This modeling is the reason that the revised *S(z)* estimates for Cedar Mesa are higher than original estimates, yet the revised pCO_2 value is reduced. The modeling also explains why in some cases pCO_2 values do not change significantly despite lower revised *S(z)* estimates.

Table 2.2. Previously published estimates as well as revised estimates for both *S(z)* and atmospheric pCO_2 for Mesozoic and Paleozoic case studies including *S(z)* revisions based on multiple different methods of reconstructing MAP.

2.10 References

Amundson, R., Stern, L., Braisden, T and Wang, Y., 1998. The isotopic composition of soil and soil-respired CO_2. Geoderma 82, 83–114.

Arens, N.C., Jahren, A.H., and Amundson, R., 2000. Can C_3 plants faithfully record the carbon isotopic composition of atmospheric carbon dioxide? Paleobiology 26, 137–164.

Behrensmeyer, A.K., Quade, J., Cerling, T.E., Kappelman, J., Khan, I. A., Copeland, P., Hicks, J., Stubblefield, P., Willis, B.J., and Latorre, C., 2007. The structure and rate of late Miocene expansion of C4 plants: evidence from lateral variation in stable isotopes in paleosols of the Siwalik group, northern Pakistan. Geological Society of America Bulletin 119, 1486–1505

Billups K and Schrag D.P., 2002. Paleotemperature and ice volume of the past 27 Myr revisited with paired Mg/Ca and $^{18}O/^{16}O$ measurements on benthic foraminifera. Paleoceanography 17, 1–11.

Breecker, D.O., Sharp, Z.D., and McFadden, L.D., 2009. Seasonal bias in the formation and stable isotopic composition of pedogenic carbonate in modern soils from central New Mexico, USA. Geological Society of America Bulletin 121, 630–640.

Breecker, D.O., Sharp, Z.D., and McFadden, L.D. 2010. Atmospheric CO_2 concentrations during ancient greenhouse climates were similar to those predicted for A.D. 2100. Proceedings of the National Academy of Sciences 107, 576–580.

Brook, G.A., Folkoff, M.E. and Box, E.O. 1983. A world model for soil carbon dioxide. Earth Surface Processes and Landforms 8, 79–88.

Cerling, T.E. 1984. The stable isotopic composition of modern soil carbonate and its relationship to climate. Earth and Planetary Science Letters 271, 229–240.

Cerling, T.E., 1991. Carbon dioxide in the atmosphere: evidence from Cenozoic and Mesozoic paleosols. American Journal of Science 291, 377–400.

Cerling, T.E., 1999. Stable carbon isotopes in paleosol carbonates. In: Palaeoweathering, Palaeosurfaces and Continental Deposits. eds. M. Thiry and R. Simon-Coincon, International Association for Sedimentology Special Publication 27, 43–60.

Cerling, T.E., Harris, J.M., MacFadden, B.J., Leakey, M.G., Quade, J., Eisenmann, V., and Ehleringer, J. R., 1997. Global vegetation change through the Miocene/Pliocene boundary. Nature 389, 153–157.

Cerling, T.E. and Quade, J., 1993. Stable carbon and oxygen isotopes in soil carbonates. In: Swart, P.K., Lohmann, K.C., McKenzie, J.A., and Savin S. (eds) Climate

change in continental isotopic records. Washington, D.C., American Geophysical Union, 217–231.

Cleveland, D.M., Nordt, L.C., Dworkin, S.I., and Atchley, S.C., 2008a. Pedogenic carbonate isotopes as evidence for extreme climatic events preceding the Triassic-Jurassic boundary: Implications for the biotic crisis? Geological Society of America Bulletin 120, 1408–1415.

Cleveland, D.M., Nordt L.C., and Atchley, S.C., 2008b. Paleosols, trace fossils and precipitation estimates of the uppermost Triassic strata in northern New Mexico. Palaeogeography, Palaeoclimatology, Palaeoecology 257, 421–444.

Davidson, G.R., 1995. The stable isotopic composition and measurement of carbon in soil CO_2. Geochimica et Cosmochimica Acta 59, 2485 – 2489.

Demicco, R.V., Lowenstein, T.K., and Hardie, L.A., 2003. Atmospheric pCO_2 since 60 Ma from records of seawater pH, calcium, and primary carbonate mineralogy. Geology 31, 793–796.

Deutz, P., Montañez, I.P., Monger, H.C., and Morrison, J., 2001. Morphology and isotope heterogeneity of Late Quaternary pedogenic carbonates: Implications for paleosol carbonates as paleoenvironmental proxies. Palaeogeography, Palaeoclimatology, Palaeoecology 166, 293–317.

Ekart, D.D., Cerling, T.E., Montañez, I.P. and Tabor, N.J. 1999. A 400 million year carbon isotopic record of pedogenic carbonate: implications for paleoatmospheric carbon dioxide. American Journal of Science,299, 805–827.

Folk, R.L., 1959. Practical petrographic classification of limestones. American Association of Petroleum Geologists Bulletin 43, 1–38.

Fox, D.L., Koch P.L., 2003. Tertiary history of C_4 biomass in the Great Plains, USA. Geology 31, 809–812.

Garten, Jr., C.T., Cooper, L.W., Post III, W.M., and Hanson, P.J., 2000. Climate controls on forest soil C isotope ratios in the southern Appalachian Mountains. Ecology 81, 1108–1119.

Hoffman, D. S. 1971. Tertiary vertebrate paleontology and paleoecology of a portion of the lower Beaverhead River basin, Madison and Beaverhead counties, Montana. PhD thesis, University of Montana, Missoula, 174 p.

Hijmans, R.J., Cameron, S.E., Parra, J.L., Jones, P.G., and Jarvis, A., 2005. Very high resolution interpolated climate surfaces for global land areas. International Journal of Climatology 25, 1965–1973.

Horton, D.E., Poulsen, C.J., and Pollard, D., 2010. Influence of high latitude vegetation feedbacks on late Paleozoic glacial cycles. Nature Geoscience 3, 572–577.

Hsieh, J.C.C., Yapp, C.J., 1999. Stable carbon isotope budget of CO_2 in a wet, modern soil as inferred from $Fe(CO_3)OH$ in pedogenic goethite: possible role of calcite dissolution. Geochimica et Cosmochimica Acta 63, 767–783.

Kellogg, E.A., 2001. Evolutionary History of the Grasses. Plant Physiology 125, 1198–1205.

Koch, P.L., 1998. Isotopic reconstruction of past continental environments. Annual Review of Earth and Planetary Science 26, 573–613.

Kuenzi, W. D., and Fields, R. W. 1971. Tertiary stratigraphy, structure and geologic history, Jefferson Basin, Montana. Geological Society of America Bulletin 82, 3373–3394.

Kürschner, W.M., Wagner, F., Dilcher, D.L., and Visscher, H., 2001. Using fossil leaves for the reconstruction of Cenozoic paleoatmospheric CO_2 concentrations. In: Gerhard, L.C., Harrison, W.E., and Hanson, B.M. (eds), Geological Perspectives of Global Climate Change. APPG Studies in Geology 47, Tulsa, The American Association of Petroleum Geologists, 169–189.

Machette, M.N., 1985. Calcic soils the southwestern United States. Geological Society of America Special Paper 203, 1–22.

Mintz, J.S., Driese, S.G., Breecker, D.O., and Ludvigson, G.A., 2011. Influence of changing hydrology on pedogenic calcite precipitation in Vertisols, Dance Bayo, Brazoria Country, Texas, U.S.A.: implications for estimating paleoatmospheric pCO_2. Journal of Sedimentary Research 81, 394–400.

Montañez, I.P., Tabor, N.J., Niemeier, D., DiMichele, W.A., Frank, T.D., Fielding, C.R., Isbell, J.L., Birgenheier, L.P. and Rygel, M.C., 2007. CO_2-forced climate and vegetation instability during late Paleozoic glaciation. Science 315, 87–91.

Nordt, L.C., and Driese, S.D., 2010. New weathering index improves paleorainfall estimates from Vertisols. Geology 38, 407–410.

Pagani, M. 2002. The alkenone–CO_2 proxy and ancient atmospheric carbon dioxide: In: D.R. Grocke and M. Kucera (eds.), Understanding Climate Change: Proxies, Chronology, and Ocean-Atmosphere Interactions. Philosophical Transactions of the Royal Society of London Series A, 360, 609–632.

Pagani, M., Freeman, K.H., and Arthur, M.A., 1999. Late Miocene atmospheric CO_2 concentrations and the expansion of C_4 grasses. Science 285, 876–879.

Passey, B.H., Levin, N.E., Cerling, T.E., Brown, F.H., and Eiler, J.M., 2010. High-temperature environments of human evolution in East Africa based on bond ordering in paleosol carbonates. Proceedings of the National Academy of Science 107, 11245–11249.

Quade, J., Breecker, D.O., Daeron, M., and Eiler, J.M., 2011. The paleoaltimetry of Tibet: An isotopic perspective. American Journal of Science 311, 77–115.

Retallack, G.J. 2000. Depth to pedogenic carbonate horizon and a paleoprecipitation indicator? Comment. Geology 28, 572–573.

Retallack, G.J. 2005. Pedogenic carbonate proxies for amount and seasonality of precipitation in paleosols. Geology 33, 333–336.

Retallack, G.J., 2007. Cenozoic Paleoclimate on Land in North America: Journal of Geology 115, 271–294.

Retallack, G.J., 2009. Refining a pedogenic-carbonate CO_2 paleobarometer to quantify a middle Miocene greenhouse spike. Palaeogeography, Palaeoclimatology, Palaeoecology 281, 57–65.

Rosenzweig, M.L., 1968. Net Primary Productivity of Terrestrial Communities: Predictions from climatological data. The American Naturalist 102, 67–74.

Royer, D.L., 1999. Depth to pedogenic carbonate horizon as a paleoprecipitation indicator? Geology 27, 1123–1126.

Royer, D.L., Berner, R.A. and Beerling, D.J., 2001. Phanerozoic atmospheric CO_2 change: evaluating geochemical and abiological approaches. Earth-Science Reviews 54, 349–392.

Royer, D.L., Berner, R.A., Montañez, I.P., Tabor, N.J., and Beerling, D.J. 2004. CO_2 as a primary driver of phanerozoic climate. GSA Today 14, 4–10.

Sheldon, N.D., Retallack, G.J., 2001. Equation for compaction of paleosols due to burial. Geology 29, 247–250.

Sheldon, N.D., Retallack, G.J., Tanaka, S., 2002. Geochemical climofunctions of North American soils and application to paleosols across the Eocene-Oligocene boundary in Oregon. Journal of Geology 110, 687–696.

Sheldon, N.D., Tabor, N.J., 2009. Quantitative paleoenvironmental and paleoclimatic reconstruction using paleosols. Earth–Science Reviews 95, 1–52.

Solomon, D.K., and Cerling, T.E. 1987. The annual carbon dioxide cycle in a montane soil: observations, modeling and implications for weathering. Water Resources Research 23, 2257–2265.

Tabor, N.J., 2007. Permo-Pennsylvanian palaeotemperatures from Fe-Oxides and phyllosilicate $\delta^{18}O$ values. Earth and Planetary Science Letters 253, 159–171.

Tabor, N.J., and Montañez, I.P., 2005. Oxygen and hydrogen isotope compositions of

Permian pedogenic phyllosilicates: Development of modern surface domain rays and implications for paleotemperature reconstructions. Palaeogeography, Palaeoclimatology, Palaeoecology 223, 127–146.

Tabor, N.J., Montañez, I.P., and Scotese, C.R., Mack, G.H., and Poulsen, C.J., 2008. Paleosol Archives of Environmental and Climatic History in paleotropical Western Euramerica during the latest Pennsylvanian through Early Permian. In: Resolving the Late Paleozoic Ice Age in Time and Space, Geological Society of America Special Paper 441, 291–304.

Tabor, N.J., Montañez, I.P., Zierenberg, R., Currie, B.S., 2004. Mineralogical and geochemical evolution of a basalt-hosted fossil soil (Late Triassic, Ischigualasto Formation, northwest Argentina); Potential for paleoenvironmental reconstruction. Geological Society of America Bulletin 116, 1280–1293.

Tabor, N.J., Myers, T.S., Gulbranson, E., Rasmussen, C., and Sheldon, N.D., (In Press), Light stable isotope composition of modern calcareous soil profiles in California: implications for paleoaltimetry and paleoatmospheric pCO_2 reconstructions. SEPM Special Paper, Ed. by L. Nordt and S. Driese.

Tabor, N.J., Yapp, C.J., 2005. Juxtaposed Permian and Pleistocene isotopic archives: Surficial environments recorded in calcite and goethite from the Wichita Mountains, Oklahoma. Geological Society of America Special Paper 395, 55–70.

Tipple, B.J., Meyers, S.R. and Pagani, M., 2010. The carbon isotope ratio of Cenozoic CO_2: a comparative evaluation of available geochemical proxies. Paleoceanography 25, PA3202.

Wanner, H., 1970. Soil respiration, litter fall and productivity of a tropical rainforest. Journal of Ecology 58, 543–547.

Watanabe, Y., Martini, J.E.J., Ohmoto, H., 2000. Geochemical evidence for terrestrial ecosystems 2.6 billion years ago. Nature 408, 574–578.

Wynn, J.G., 2007. Carbon isotope fractionation during decomposition of organic matter in soils and paleosols: Implications for paleoecological interpretations for paleosols. Palaeogeography, Palaeoclimatology, Palaeoecology 251, 437–448

Yapp, C.J. and Poths, H., 1996. Carbon isotopes in continental weathering environments and variations in ancient atmospheric CO_2 pressure. Earth and Planetary Science Letters 137, 71–82.

Zachos, J., Pagani, M., Sloan, L., Thomas, E., and Billups, K., 2001. Trends, rhythms and aberrations in global climate 65Ma to present. Science 292, 686–693.

Chapter 3

Climate controls on soil-respired CO_2 in the United States: Implications for 21st century chemical weathering rates in temperate and arid ecosystems[2]

3.0 Abstract

The most recent IPCC (2007) report predicts that regional-scale precipitation patterns will change significantly in the 21st century as a result of increasing atmospheric CO_2. The amount of respired CO_2 stored in the soil atmosphere is heavily influenced by climate, and the concentration of CO_2 in soils controls the concentration of dissolved CO_2 in pore water involved in chemical weathering. Therefore, we can expect changes to chemical weathering rates as a result of climate change, which can influence the global carbon cycle through the consumption of CO_2 during continental silicate weathering. These changes may even be important on human timescales. To predict changes to the $[CO_{2aq}]$ of soil water, we have produced an extensive literature review of 932 soil-respired CO_2 measurements from 59 soils worldwide to study the spatial variability of soil-respired CO_2. We show that respired CO_2 concentrations and $[CO_{2aq}]$ vary with precipitation. The relationship between summer average soil-respired CO_2 and mean annual precipitation is strong for soils forming in or below 900 mm yr^{-1} precipitation (R^2

[2] Cotton, J.M., Jeffery, M.L., and Sheldon, N.D. Climate controls on soil-respired CO_2 in the United States: Implications for 21st century chemical weathering rates in temperate and arid ecosystems. In Review, Chemical Geology 3/13.

= 0.81). The correlation breaks down when higher mean annual precipitation rates are considered, restricting the use of this relationship to arid to subhumid precipitation regimes, such as those found in the western United States.

We estimate the response of [CO_{2aq}] in soil pore water to projected anthropogenic CO_2 emissions using this new relationship and predicted changes in precipitation simulated by the North American Regional Climate Change Assessment Program for the decade 2051–2060. According to our model, [CO_{2aq}] in soil pore water is expected to decrease by up to 50% in the southwestern United States and to increase by up to 50% in areas of the Northern and Central Great Plains. These results have important implications for CO_2 consumption and changes to terrestrial carbon cycling in the next century.

3.1 Introduction

As anthropogenic emissions of CO_2 to the atmosphere continue to increase (IPCC, 2007), it is important to study how the biosphere reacts to perturbations in the carbon cycle so that future sources and sinks of carbon can be identified. While roughly half of the annual anthropogenic CO_2 emissions are taken up by the biosphere and oceans in various carbon sinks (Schimel et al., 2001; Ballantyne et al., 2012), it is currently unclear whether these sinks will continue to buffer anthropogenic CO_2 emissions at the same rate as the previous two decades (Ballantyne et al., 2012). Terrestrial silicate weathering, which is influenced by ecosystem productivity, is one process that may respond to increasing atmospheric CO_2 concentrations, as silicate weathering drives carbon sequestration by converting atmospheric CO_2 to CO_3^- and moving it to terrestrial and oceanic reservoirs. While originally only thought to influence the carbon cycle on

geologic time scales (Berner, 1992; Berner and Kothavala, 2001), recent studies have shown that chemical weathering rates can instead respond to changes in temperature and precipitation in a matter of years (Gislason et al., 2009; Beaulieu et al., 2012). Such changes in chemical weathering may change atmospheric CO_2 consumption and could possibly offset anthropogenic CO_2 emissions. Thus, identifying regions of change in the rate of chemical weathering may help to pinpoint new sinks and sources of CO_2 in the global carbon cycle.

Chemical weathering is an important component of the global carbon cycle, and influences the fluxes of carbon pools on multiple time scales. The primary driver of chemical weathering is carbonic acid, which is formed from the dissolution of CO_2 into water by the following reactions:

$$CO_{2\,(g)} + H_2O_{\,(l)} \leftrightarrow H_2CO_{3\,(aq)} \quad \text{(Eq. 3.1)}$$

$$H_2CO_{3\,(aq)} \leftrightarrow H^+_{\,(aq)} + HCO_3^-{}_{\,(aq)} \leftrightarrow H^+_{\,(aq)} + CO_3^-{}_{\,(aq)} \quad \text{(Eq. 3.2)}$$

Because concentrations of CO_2 are much greater in soils than the atmosphere (up to hundreds of times atmospheric levels (de Jong and Shappert, 1972; Rightmire, 1978; Brook et al., 1983)), carbonic acid formed in soils is the major source of acid for chemical weathering, and a large proportion of chemical weathering occurs within soils (West et al., 2012). The concentration of dissolved CO_2 ($[CO_{2aq}]$) in the soil water is controlled by Henry's law for the dissolution of gases into a liquid, and increasing pCO_2 in the soil atmosphere will increase concentrations of dissolved CO_2 in soil water. Henry's law is also temperature dependent, with increasing dissolution of CO_2 at lower temperatures. Thus, the concentration of CO_2 in a soil is an important factor in chemical weathering rates (Amundson and Davidson, 1990; Oh and Richter, 2004). Over short

time periods, weathering drives pedogenesis as well as the release of nutrients to plants for photosynthesis (Chadwick et al., 1994). These processes are important to the global carbon cycle on short time scales because soils store three times as much carbon as terrestrial vegetation (Schlesinger, 1977), and twice as much as the carbon stored in the surface ocean (Sigman and Boyle, 2000), so changes in fluxes of organic carbon to and from soils can significantly impact the amount of CO_2 in the atmosphere. Weathering consumes CO_2 and removes it from the atmosphere through the formation of HCO_3^-, which is eventually transported to the oceans to be stored as $CaCO_3$ according to the following simplified equation:

$$CaSiO_3 + H_2CO_3 \rightarrow CaCO_3 + SiO_2 + H_2O \text{ (Eq. 3.3)}$$

where one mole of CO_2 is consumed for every mole of silicate mineral that is weathered (Berner, 1992). While this process has been recognized as the long-term control on the concentration of atmospheric CO_2 for many years (Ebelmen, 1845; Berner et al., 1983), silicate weathering may also play an important role in the global carbon cycle on human timescales. Recent studies have observed increases in chemical weathering in arctic regions corresponding to increases in CO_2 consumption of up to 50% for particular watersheds, showing the that carbon fluxes can change significantly in a matter of decades (Gislason et al., 2009; Beaulieu et al., 2012).

In soils, CO_2 is formed through the respiration of plant roots, through the microbial oxidation of organic material (Witkamp, 1966; Brook et al., 1983), and also enters the soil through the diffusion of atmospheric CO_2 (Amundson and Davidson, 1990; Cerling, 1991; Sheldon and Tabor, in press). The concentration of CO_2 in a soil is dependent on soil properties such as porosity and tortuosity (Raich and Schlesinger,

1992, Royer et al., 2001), the gradient of CO_2 between the soil and the atmosphere, and the CO_2 production rate (Brook et al., 1983), The production rate of soil CO_2 is a function of primary productivity (Wanner, 1970; Raich and Schlesinger, 1992). Primary productivity is controlled by climatic factors such as temperature and precipitation (Rosenzweig, 1968; Raich and Schlesinger, 1992; Raich and Porter, 1995), and so with climate change, one would also expect to observe changes in soil CO_2 concentrations and chemical weathering rates.

3.2 Background

Many recent studies have explored the response of chemical weathering to increases in concentrations of atmospheric CO_2 (Karberg et al., 2005; Oh et al., 2007; Siemens et al., 2012). Experiments using free air CO_2 enrichment (FACE) forest plots have shown that soil CO_2 increases with increasing concentrations of CO_2 in the atmosphere (Andrews and Schlesinger, 2001; Oh and Richter, 2004; Karberg et al., 2005; Oh et al., 2007; Jackson et al., 2009). These increases are due to the mechanism of CO_2 fertilization, by which photosynthesis of C_3 plants becomes more efficient, driving an increase in productivity under higher concentrations of atmospheric CO_2 (Farquhar, 1980, Curtis and Wang, 1998). Increases in productivity have lead to increases in soil CO_2 concentrations, in some instances over 20% (Andrews and Schlesinger, 2001; Jackson et al., 2009), and many studies have observed increased concentrations of dissolved bicarbonate and silica in different ecosystems, such as pine forests (Andrews and Schlesinger, 2001; Karberg et al., 2005; Oh et al., 2007) and crop land (Siemens et al., 2012), even over time scales as short as a few years. Higher concentrations of dissolved

species as well as increased soil acidity suggest higher weathering rates for vegetation plots growing under increased atmospheric CO_2 concentrations.

Though it has been demonstrated that future anthropogenic climate change will cause changes to soil CO_2 concentrations and that these changes to soil CO_2 can drive changes to chemical weathering rates on short time scales, previous work may not be widely applicable to many different biomes due to the limited scope of small-scale free air enrichment experiments and weathering studies that take place in a single ecosystem. In particular, this previous research is not applicable to regions dominated by C_4 vegetation, because C_4 photosynthesis is adapted to low atmospheric CO_2 concentrations (Ehleringer et al., 1997; Sage, 2004) and will not respond to elevated atmospheric CO_2 concentrations in the same way as trees and C_3 grasses. As expected, several studies have found that the increase in photosynthetic production for C_4 plants under elevated CO_2 is less than that of C_3 plants (Ghannoum et al., 2000). However, elevated CO_2 conditions alone do not control soil productivity. Bader and Körner (2010) also demonstrate that increased soil respiration under elevated CO_2 conditions is still controlled by climatic variables such as temperature and soil moisture content. To quantify the response of chemical weathering rates to anthropogenic climate change on a regional scale, we must determine the relationship between soil CO_2 concentrations and climatic/environmental variables.

Previous studies (e.g., Moosdorf et al., 2011) have modeled broad-scale modern chemical weathering and CO_2 consumption for North America by calculating CO_2 consumption based on measured dissolved bicarbonate concentrations from watersheds across the continent and interpolating these concentrations between hydrochemical

monitoring stations. While this method works well for modern estimations of weathering rates, it is not easily adapted for predicting changes to weathering rates in the future. Runoff is dependent on many factors, including precipitation timing, intensity and land use changes, that are not well constrained by models of future climate. We address these issues by modeling future changes in soil-respired CO_2 (called *S(z)* herein) and [CO_{2aq}] directly from climate variables that are predicted by climate models. These results are used to estimate future sources and sinks of carbon from terrestrial weathering.

Though large amounts of CO_2 flux data are available through Ameriflux and the global FluxNet network (http://fluxnet.ornl.gov/), these fluxes do not necessarily correlate to concentration of CO_2 within the soil because of differences in soil porosity and tortuosity, and are often influenced by atmospheric transport (Keppel-Aleks et al., 2011; 2012). Instead we compile previously published measurements of the concentration of CO_2 within soils to determine how [CO_{2aq}] changes with climate. Brook et al. (1983) compiled mean growing season soil CO_2 concentrations from 19 soils worldwide and found relationships with mean annual temperature, mean annual precipitation, potential evapotranspiration (PET), and actual evapotranspiration (AET). Using the relationship between growing season soil CO_2 and AET, Kessler and Harvey (2001) produced a global map for the flux of CO_2 into soil water. Here, we follow similar methods as Kesler and Harvey (2001) to model *S(z)* using its relationship to MAP, but because the previous relationships were based on only 19 soils worldwide, we find it is necessary to test the strength of these relationships with the inclusion of more data. An extensive literature review of 932 *S(z)* measurements from 59 soils worldwide that expands on Brook et al. (1983) has been produced to study the spatial variability of *S(z)* as well as the link

between *S(z)* concentrations and precipitation. Using this expanded dataset, a robust relationship is obtained between mean annual precipitation and *S(z)*, and this relationship is then combined with climate prediction data to explore the range of future *S(z*) and [CO_{2aq}] that can be expected by 2051–2060. An ensemble of high-resolution models from the North American Regional Climate Change Assessment Program (NARCCAP) is used for this analysis. Understanding dissolved CO_2 trends allows us to identify potential sources and sinks of atmospheric CO_2 due to changes in weathering driven by anthropogenic climate change.

3.3 Methods

3.3.1 Modern Soil CO_2 Spatial Variability

Measurements of summer soil CO_2 concentrations from 59 soils worldwide were compiled from the literature (see Appendix B Table B1 for locations), representing all USDA soil orders except Vertisols and Histosols (Soil Survey Staff, 2007). Soil CO_2 measurements are a combination of atmospheric CO_2 derived from diffusion and CO_2 dissolved in precipitation, and respired CO_2 (*S(z)*) produced *in situ* from plant and microbial respiration (Sheldon and Tabor, in press). Because soil CO_2 is composed of both respired CO_2 and atmospheric CO_2, the atmospheric component must be subtracted from the total soil CO_2 measurements according to the following equation:

$$S(z) = C_s - C_a \quad \text{(Eq. 3.4)}$$

where C_s is the total concentration of soil CO_2, and C_a is the concentration of CO_2 in the atmosphere. *S(z)* represents the concentration of soil-respired CO_2 (Cerling, 1991). Given that the concentration of atmospheric CO_2 has been steadily rising due to anthropogenic

emissions, we identified C_a for each measurement based on the month and year of the measurement. Atmospheric CO_2 values were taken from the NOAA Mauna Loa Observatory dataset (from website ftp://ftp.cmdl.noaa.gov/ccg/co2/trends/co2_annmean_mlo.txt: accessed November, 2009). Many sites had soil CO_2 measurements from multiple depths. Depths shallower than 30 cm were excluded because soil CO_2 concentrations often increase with depth (de Jong and Schappert, 1972; Jin et al., 2009) and the concentrations at the surface are not representative of the soil as a whole. *S(z)* concentrations typically reach a constant value around a depth of 30 cm according to both observations and CO_2 diffusion models (Cerling, 1984; 1991; Sheldon and Tabor, 2009).

These *S(z)* concentrations were then coupled with climatic and soil order data for each site. MAP and MAT data were acquired from three different sources. If climatic data was included in the literature along with the soil CO_2 measurements, these values were used. If no climate data was included, MAP and MAT values were obtained based on location. For sites within the United States, NOAA NCDC Climate Normals from 1971–2000 were used. For sites located in Canada, Environment Canada Climate Normals from 1971–2000 were used. For remote sites without climatic data available, WorldClim global climatic data model for ArcGIS (Hijmans et al., 2005) was used to estimate both MAT and MAP. Because the majority of measurements of soil CO_2 in the literature focus on the growing season, summer average (June 21–September 21) *S(z)* concentrations were compared to MAP and MAT. Therefore, this study can only constrain future changes to respired CO_2 and $[CO_{2aq}]$ during the summer months. Given that the major controls on weathering rates are temperature and moisture availability

(Norton and von Blanckenburg, 2010; Jin et al., 2011; Rasmussen et al;, 2011; Goudie and Viles), the majority of chemical weathering in the continental United States likely occurs in the summer months when temperature and precipitation rates are highest. Studies from China using the carbon isotopic composition of dissolved inorganic carbon suggest that chemical weathering rates increase substantially as soil CO_2 concentrations increase in the summer (Li et al., 2010). Therefore, the relationship between summer average *S(z)* and MAP will be important for understanding chemical weathering and terrestrial carbon cycle changes in the future due to anthropogenic climate change (Jin et al., 2009; Beaulieu et al., 2012).

The relationship between MAP and *S(z)* derived using the above method was used to calculate the modern spatial variability of *S(z)*. The modern spatial variability map was constructed using the WorldClim mean annual precipitation dataset (Hijmans et al., 2005) at the resolution of 2.5 arc-minutes (4.6 km). $[CO_{2aq}]$ was then calculated using Henry's law:

$$c = \frac{p}{K_H} \quad \text{(Eq. 3.5)}$$

where c represents the concentration of dissolved CO_2 in water ($[CO_{2aq}]$), p represents the partial pressure of CO_2 in the soil atmosphere, and K_H is Henry's law constant. Because the solubility of gases in water is temperature dependent, the Henry's law constant was adjusted for temperature according changes to the following equation:

$$K_H(T) = K_H(T^0)e^{C\left(\frac{1}{T}-\frac{1}{T^0}\right)} \quad \text{(Eq. 3.6)}$$

Where T^0 is 298K, T is the soil temperature, $K_H(T^0)$ is Henry's law constant at 298K and $K_H(T)$ is Henry's law constant for the soil temperature, and C is a constant equal to -2400

for CO_2 (Sander, 1999). Mean summer temperatures were used as an approximation of mean summer soil temperature. In order to constrain the broad scale spatial variability of *S(z)*, the United States was modeled because it has the largest number of soil sites and the highest data density of any region worldwide. Of the 59 soil sites compiled from the literature, 24 were located in the United States. The regional data density in the rest of the world was not high enough to produce spatially meaningful results.

3.3.2 Future S(z) and [CO_{2aq}] predictions

To predict changes in *S(z)* and [CO_{2aq}], the soil data was coupled with high-resolution precipitation simulations provided by NARCCAP for the United States. Future changes in summer average *S(z)* were modeled based on the relationship between mean annual precipitation and summer average *S(z)* described below in the results section (Eq. 3.7; Section 4.1). Future precipitation estimates were acquired from the NARCCAP models (Mearns et al., 2009). The NARCCAP dataset is comprised of an ensemble of high-resolution regional climate models (RCMs) with boundary conditions provided by Atmosphere Ocean General Circulation Models (AOGCMs). The NARCCAP program specifically aimed to produce climate change scenarios for environmental impacts research and to quantify the uncertainties in these scenarios. All NARCCAP simulations were based on the IPCC A2 scenario, which describes a world with continuing rapid population growth as well as CO_2 emissions. In this scenario, atmospheric CO_2 concentrations were projected to rise to 575 ppm by the year 2050 (Nakicenvoic et al., 2000).

High-resolution models were chosen for this study in order to capture the finer details of precipitation variability, particularly in regions with complex topography such as the western United States (Leung et al., 2003a; 2003b, Di Luca et al., 2011). In order to determine which NARCCAP model(s) best reconstructed current precipitation in North America, simulated modern precipitation conditions were compared to the observed modern precipitation interpolated between weather stations by the WorldClim dataset (Hijmans et al., 2005). From a suite of five models, the two that best simulated modern precipitation rates < 900 mm yr^{-1} were chosen to explore the response of $[CO_{2aq}]$ to climate change in the next century (Appendix B Table B2, http://www.earthsystemgrid.org/project/NARCCAP.html: Data accessed August 2011). The remaining three models are also displayed but the interpretations for future chemical weathering are only based on the two most accurate models. The spatial variability of precipitation and summer average *S(z)* is only examined for areas receiving 900 mm yr^{-1} precipitation or less, due to the fact that the relationship between MAP and summer average *S(z)* is only valid in this precipitation regime.

For each model set, the predicted average mean annual precipitation (MAP) for the period 2051–2060 was compared to the modern average MAP (1971–1996; 20C3M experiment) of the same model set. The change in MAP was then used to determine the associated change in *S(z)* based on the relationship defined using the soil data (Section 3.3.1). $[CO_{2aq}]$ was calculated using Eqs. 3.5 and 3.6, and percent changes in $[CO_{2aq}]$ were calculated based on the difference between modern and future simulated climatic variables for each model.

3.4 Results

3.4.1 Modern Spatial Variability in S(z)

The literature review produced 932 individual measurements of summer *S(z)* concentrations from 59 soils worldwide, including 24 soils located in the United States (Appendix B Table B1, B3). *S(z)* concentrations are highly variable, even within a single soil order (Fig. 3.1). The highest variability is found for Alfisols, Oxisols, and Ultisols. The lowest variability is found in Gelisols, Entisols, and Aridisols. Due to this high variability within each soil order, it is not possible to predict *S(z)* concentrations based on soil order alone; accurate prediction of *S(z)* requires climatic information.

There is a correlation between the average summer *S(z)* and MAP up to a value of 900 mm yr^{-1}, whereas above the 900 mm yr^{-1} threshold the data become highly scattered. The weighted correlation between average summer *S(z)* and MAP for the 16 soils located in the United States forming in 900 mm yr^{-1} precipitation or less, totaling 254 respired CO_2 measurements, is described by:

$$S(z)_{SA} = 13.88(MAP) - 1541.1 \quad \text{(Eq. 3.7)}$$

where $R^2 = 0.91$, SE = ±1206 ppm and $S(z)_{SA}$ represents the summer average soil-respired CO_2 concentration in ppm (Fig. 3.2). A summary of the number of soil CO_2 measurements obtained in this study is located in Table 3.1. Because this study is focusing on the spatial variability of *S(z)* for the United States, only data from sites located in the United States are used in Eq. 3.7, however, it should be noted that essentially the same linear relationship (though with increased scatter) exists between summer average *S(z)* and MAP for all 37 soil sites in the global dataset forming under 900 mm yr^{-1}. Using the *S(z)* data and the relationship outlined by Eq. 3.7, a modern *S(z)*

and [CO_{2aq}] prediction map was created for the continental United States displaying the spatial variability of *S(z)* for areas receiving 900 mm yr^{-1} precipitation or less (Fig. 3.3).

3.4.2 Predictions of Future Spatial Variability of S(z) and [CO_{2aq}]

All of the models capture the main features of spatial variability in modern precipitation, with MAP values increasing with increasing distance from the eastern front of the Rocky Mountains, as well as low MAP values in the Southwestern states. However, some of the models show greater skill at capturing the magnitude of MAP and the spatial extent of the region with precipitation less than 900 mm yr^{-1}. For example, HRM3-HADC3M (Fig. 4C) and MM51-CCSM (Fig. 4E) successfully simulate the lowest (< 100 mm yr^{-1}) precipitation rates in the southwestern United States, whereas RCM3-GFDL (Fig. 4D) overestimates precipitation by 100–200 mm yr^{-1} in this region. Most models also capture some of the spatial variability in precipitation. Arid regions, such as the Snake River Plain in southern Idaho, are clearly visible in some of the precipitation maps (e.g. Fig. 4B, C and E). Most models overestimate MAP in the northwestern states, especially eastern Washington, northern Idaho and western Montana.

No model perfectly simulates the eastern border of the < 900 mm yr^{-1} MAP region. The eastern border of the 900 mm yr^{-1} region simulated by HRM3 and both RCM3 models (Fig. 4A, C and D) is further west than in the WorldClim observation dataset (Fig. 4F). Both WRFG-CCSM and MM51-CCSM models are better at simulating precipitation rates in the Great Lakes region but overestimate precipitation rates in the eastern half of the country. WRFG–CCSM is particularly weak in the eastern United States and underestimates MAP by up to 400 mm yr^{-1} (e.g. Florida, Fig. 4B). MM51–

CCSM (Fig. 4E) is slightly better at simulating the Great Lakes region than RCM3 and HRM3, but not as good as WRFG, and MM51 also underestimates precipitation in the southeastern Great Plains. In general, RCM3 has a wet bias when compared to observations (see also Gao et al., 2011) but does better at reproducing modern conditions when nested in CGCM3 than in GFDL. HRM3–HADCM3 shows the greatest skill in simulating arid regions in the topographically complex west. Overall, WRFG–CCSM and MM51-CCSM compare well with observations in terms of the magnitude of precipitation and the extent of the area with MAP < 900 mm yr^{-1}.

Figure 3.5 displays the predicted changes in [CO_{2aq}] for WRFG-CCSM and MM51-CCSM, the models that simulate best the modern precipitation regime of the United States while Figure 3.6 shows the predicted changes according to the other three models that do not simulate modern precipitation as well. According to the *S(z)* observations described in this study, an increase in MAP will lead to an increase in summer average soil CO_2 and vice versa. NARCCAP simulations are consistent with other climate experiments (e.g., Ruiz-Barradas et al., 2010) in predicting an increase in MAP in the North-Central Great Plains by 2051–2060. *S(z)* and [CO_{2aq}] are therefore also expected to increase (Fig. 3.5). In contrast, most models predict a decrease in MAP (and thus *S(z)*) in the southwestern states, again consistent with prior studies (e.g. Seager et al., 2007). Decreased precipitation rates in this region are expected in a warmer climate due to a poleward expansion of the descending branch of the Hadley cell and extension of the subtropical dry zones (Seager et al., 2007; Seager and Vecchi, 2010). However, there is some disagreement between models in the exact areal extent of these changes. WRFG-CCSM (Fig. 3.5C) predicts large increases in [CO_{2aq}] further west in eastern Montana,

North Dakota as well as regions in north-central Texas. For the North-Central Great Plains, MM51-CCSM (Fig. 3.5D) predicts an increase in [CO_{2aq}] in the eastern edge of the plains as well as northern North Dakota. Both WRFG-CCSM and MM51-CCSM agree there will be a region of decreased *S(z)* and therefore decreased [CO_{2aq}] in the southwestern United States, but in MM51-CCSM, this region is far more extensive both to the north and west than in WRFG-CCSM. Only chemical weathering of silicate minerals consumes atmospheric CO_2. While these figures do not explicitly label regions of the United States with silicate vs. limestone bedrock, the regions identified here with the potential to experience changes in chemical weathering all overlie predominantly silicate bedrock (See detailed geologic map of the region in the Appendix B, Fig. B1). Despite large changes in MAP between the modern and future simulations, the spatial extent of the area with MAP under 900 mm yr^{-1} does not change greatly. For both models, the eastern border of the < 900 mm yr^{-1} region is located slightly further west in the future simulations than in the modern simulations, due to a general increase in MAP in the eastern region of the United States (Figs. 3.5, 3.6).

The magnitude of change in [CO_{2aq}] also varies between models. MM51-CCSM (Fig. 3.5D) predicts decreases of 30–60% in [CO_{2aq}] over a large area of the Southwestern states, and a smaller increase in concentrations of [CO_{2aq}] of 10–30% for the North-Central Great Plains. In comparison, WRFG-CCSM (Fig. 3.5C) predicts the same 30–60% decrease in [CO_{2aq}] in the Southwestern states, but predicts large increases in [CO_{2aq}] of 30–60% in eastern Montana and North Dakota as well as up to 40% in north-central Texas.

While the maximum percent change in [CO_{2aq}] may be similar for both Southwest and Great Plains region, the magnitude of change in the Southwest is smaller because the productivity of the region and initial *S(z)* values are low. Therefore, the overall decreases in [CO_{2aq}] and resulting decreases in chemical weathering due to climate change in the Southwest will be offset by the larger total increases in *S(z)* and [CO_{2aq}] in the Great Plains region (Fig. 3.5A, B).

3.5 Discussion

3.5.1 Modern Spatial Variability of S(z)

From Figure 3.2, the summer average *S(z)* proxy best predicts measured *S(z)* values in areas of lower precipitation. The data then becomes more scattered for areas of higher precipitation. The larger amount of scatter at higher *S(z)* values means that the summer average *S(z)*-MAP proxy is most accurate in arid to semi-arid regions. The strength of this relationship in arid to subhumid precipitation may be explained by the fact that globally, soils are too variable to all respond to precipitation or temperature in a linear way, while soils forming in arid to subhumid climates are typically much more characteristically similar, both in the composition of vegetation and texturally. Soils forming in a precipitation regime of 750 mm yr^{-1} precipitation or less tend to precipitate calcium carbonate (Retallack, 2000). In order to precipitate calcium carbonate, these soils must have low concentrations of soil CO_2 and a high pH (> 7) at the time of precipitation (Cerling, 1984; Breecker et al., 2009). Therefore, the conditions required for the precipitation of calcium carbonate characteristically separate these soils from soils with higher productivity lacking carbonate. This control on *S(z)* is supported by the data in

Figure 3.1, which shows that the maximum levels of *S(z)* are higher for soils that typically do not contain pedogenic carbonates (Alfisols, Oxisols, Ultisols). It is also possible that this relationship only exists for soils forming in less than 900 mm yr^{-1} or less because productivity in these soils may be limited by growing season (summer) precipitation, whereas productivity in wetter areas is controlled by other factors. In areas with greater rainfall such as the eastern United States, vegetation productivity, and thus *S(z),* may instead be controlled by nutrient availability, temperature, or available sunlight (Cotton and Sheldon, 2012). This hypothesis is supported by models showing that the productivity of the western United States is controlled by precipitation while productivity in the eastern United States is generally light limited (Churkina and Running, 1998). Therefore, it is likely that the relationship of *S(z)* and thus $[CO_{2aq}]$ with MAP is strongest in areas of low precipitation because productivity is primarily controlled by precipitation in the western United States.

The soils included in the linear regression for the western United States all lack extensive coverage of trees or closed vegetation canopies. From the increased scatter observed at higher levels of precipitation from forest soil orders (Alfisols, Oxisols, Ultisols) it is likely that respiration in desert scrubland and grasslands responds differently to increased precipitation than in forests. Dörr and Münnich (1987) show that CO_2 production in soils is reduced during both very dry and very wet events, which suggests that for areas where precipitation is seasonal and mainly falls in the summer (where MAP is predominately summer precipitation), the value of summer average *S(z)* will be directly proportional with MAP up to a point, where it will begin to fall with increasing MAP because the precipitation will begin to impede respiration. Amundson

and Davidson (1990) also observed high seasonal variability in soil CO_2 concentrations at sites receiving high precipitation. This variability may also contribute to the break down of the relationship in areas with higher MAP values. Along those lines, differences in water-use efficiency among different plant groups and in open- versus closed-canopy systems are also important, because more densely veined seed plants use water more efficiently than non-angiosperm plants (e.g. ferns; Boyce et al., 2009). Thus, because of the potential for recycling of plant-transpired water in forests (e.g. Boyce et al., 2010), it is unsurprising that differences in MAP are less of a control on productivity in forests (and thus, in forest soils) than with more open ecosystems characterized by lower stature vegetation and less developed soil types. For these reasons the relationship of MAP is stronger in areas of lower MAP such as grasslands and deserts than in areas receiving higher MAP such as forests.

3.5.2 Implications for Future Chemical Weathering and CO_2 Consumption

Given that the modern CO_2 drawdown by chemical weathering in the southwestern United States is minimal compared to more humid regions of the United States (Moosdorf et al., 2011), decreases in $[CO_{2aq}]$ in the southwestern United States will be offset by increases in $[CO_{2aq}]$ in the North and Central Great Plains states. The majority of the chemical weathering in the continental United States currently occurs in the forested regions west of the Mississippi River (Moosdorf et al., 2011). WRFG-CCSM predicts large increases in $[CO_{2aq}]$ in the North-Central Great Plains region, as well as eastern Texas (Fig. 3.5C). Increases in $[CO_{2aq}]$ of up to 60% and resulting increases in chemical weathering to the Great Plains region could increase the area in the United

States where there are significant contributions from chemical weathering to atmospheric CO_2 consumption. This increase in $[CO_{2aq}]$ could cause the region to become an atmospheric CO_2 sink.

Regional changes to $[CO_{2aq}]$ and chemical weathering rates on the scales predicted by this work are supported by many other recent studies. For example, Gislason et al. (2009) show that chemical weathering has increased over the past 40 years in some Icelandic watersheds due to increased temperatures and runoff. Beaulieu et al. (2012) finds that the redistribution of precipitation as well as temperature increases will cause an increase in chemical weathering of up to 50% in the high arctic in response to a doubling of preindustrial concentrations of atmospheric CO_2. These estimates of changes to chemical weathering observed by Gislason et al. (2009) and Beaulieu et al. (2012) are of a similar magnitude to the changes in $[CO_{2aq}]$ predicted by this study and show the possibility for changes to CO_2 consumption and terrestrial carbon cycling in the future due to anthropogenic CO_2 emissions.

This study also highlights the need for further investigation into the potential changes to global chemical weathering and CO_2 consumption. The previous work discussed above both find increases in chemical weathering in Arctic areas, while this study demonstrates that certain regions, such as the southwestern United States, may experience decreases in chemical weathering due to decreases in future precipitation. In the case of this study, the majority of the predicted decreases in $[CO_{2aq}]$ occur in areas that are already very dry and contribute little to CO_2 consumption. However, because global models (IPCC, 2007) predict varying increases and decreases in precipitation depending on the region, we should not expect changes to future chemical weathering to

be globally uniform or even unidirectional. Inferences about global changes to the carbon cycle should not be made until more regional weathering and CO_2 consumption studies have been completed.

3.5.3 Uncertainties in Future Spatial Variability of S(z)

The two main uncertainties associated with future projections of climate change are the rate of emission of greenhouse gases and the response of the Earth to those emissions (Meehl et al., 2007). The uncertainty in climate models increases with increasing time into the future (Meehl et al., 2007) as the uncertainty in predictions of emissions and global response increases. Summer average *S(z)* and $[CO_{2aq}]$ changes were modeled from 2051–2060 because this time period is far enough into the future that differences in summer average *S(z)* should be prominent in the models, but minimizes uncertainty related to model predictions far into the future. Because the A2 scenario represents one of the highest emission rate scenarios, the model predictions likely represent an upper bound of changes in summer average *S(z)* and summer $[CO_{2aq}]$, demonstrating the range of expected changes in response to anthropogenic warming.

Gao et al. (2011) also found that the WRFG and MM51 regional climate models show improvement in simulation of current precipitation compared to simulations using only atmosphere ocean general circulation models. Wang et al. (2009) find that the NARCCAP regional climate models simulate seasonal precipitation variability poorly in the intermountain region between the Cascade and Sierra ranges and the Rocky Mountains, though the RCMs show a marked improvement compared to AOGCMs. In our study, model outputs are averaged over a thirty-year period to obtain modern mean

annual precipitation estimates and to reduce the influence of seasonal and interannual scale variability in the prediction of future *S(z) and* [CO_{2aq}]. Many regions will experience increased seasonal climate variability in the future due to anthropogenically driven climate change (IPCC, 2007), but for the purposes of this study we are only interested in the average change from the present to the future (2050–2060) in an attempt to generalize the direction and scale of expected regional productivity changes. Differences in MAP between models are to be expected due to differences in both the regional models and the AOGCM simulations in which they are nested. The discrepancies between models are a result of different choices of model physics and the parameterization of sub-grid scale processes. Despite the relatively high resolution of the NARCCAP models compared to AOGCMs, precipitation processes occur on a sub-grid scale and MAP can be very sensitive to the way in which these sub-grid processes, such as convective precipitation, are parameterized (e.g., Kain and Fritsch, 1990; Gao et al., 2011). In addition to model differences in the treatment of precipitation, different parameterizations of other model components, such as clouds, land surface properties, and radiation budget can also result in different precipitation rates. Although there are differences in the magnitude of predicted changes, it is reassuring that most models agree on the general pattern of changes in precipitation and *S(z)* that will occur by the middle of this century (Figs. 3.5, 3.6).

3.5.4 Limitations of the Model

Though this study focuses only on the United States, this work is also potentially useful for arid to sub-humid areas world wide because the relationship between *S(z)* and

MAP is similar, albeit with more scatter. Because there are only 37 soils worldwide forming under 900 mm yr^{-1} within this dataset, more data collection is necessary before robust predictions of *S(z)* and [CO_{2aq}] can be made globally.

Weathering rates are controlled by not only temperature and precipitation, but also by the composition of the silicate rock being weathered, particle size, soil bulk density, runoff, and land use (Moosdorf et al., 2011). These factors vary considerably even within a single region, and future changes to runoff and land use are difficult to predict. For this reason our model cannot compute exact rates of weathering and changes to atmospheric consumption of CO_2 at a continental scale. However, the rock type as well as particle size and soil bulk density should remain relatively unchanged on the time scales investigated by this study. (i.e., sub-geological time scales). Assuming that land use changes are minimal in the future, [CO_{2aq}] and climatic variables should remain the major control on chemical weathering rates. Increases to [CO_{2aq}] in combination with increases in temperature represent important increases in chemical weathering rates and CO_2 consumption for the future in the Northern and Central Great Plains region of the United States.

3.6 Conclusions

We have derived a new theoretical relationship between summer average *S(z)* and mean annual precipitation for soils forming under 900 mm yr^{-1} precipitation or less. The relationship between summer average *S(z)* and MAP is useful for the study of chemical weathering and carbon cycling because the concentration of soil CO_2 and [CO_{2aq}] is a major driver of chemical weathering. We find that changes to precipitation by the years 2050–2060 as a result of anthropogenic climate change will cause an increase in [CO_{2aq}]

of up to 60% in regions of the North and Central Great Plains, and also a decrease in [CO_{2aq}] of up to 60% for the southwestern United States. Our results are consistent with other studies in showing that significant changes in chemical weathering are to be expected in the future and that these changes can occur on decadal time scales. These changes to chemical weathering could impact the global carbon cycle in the next century by altering rates of CO_2 consumption. In the Great Plains region, increases in chemical weathering may increase CO_2 drawdown and offset increase atmospheric CO_2 emissions to some degree. Though it is not possible to specify the amount of decrease or increase in summer average *S(z)* for every region of the country due to the uncertainty in climate model predictions, it is possible to predict confidently the direction of change of *S(z)* and thus, the direction of change of chemical weathering.

3.7 Acknowledgements

The authors would like to acknowledge the NSF (NSF1024535 to NDS), Geological Society of America, Evolving Earth Foundation and the Scott Turner Award for Earth Science (to JMC) for funding this research.

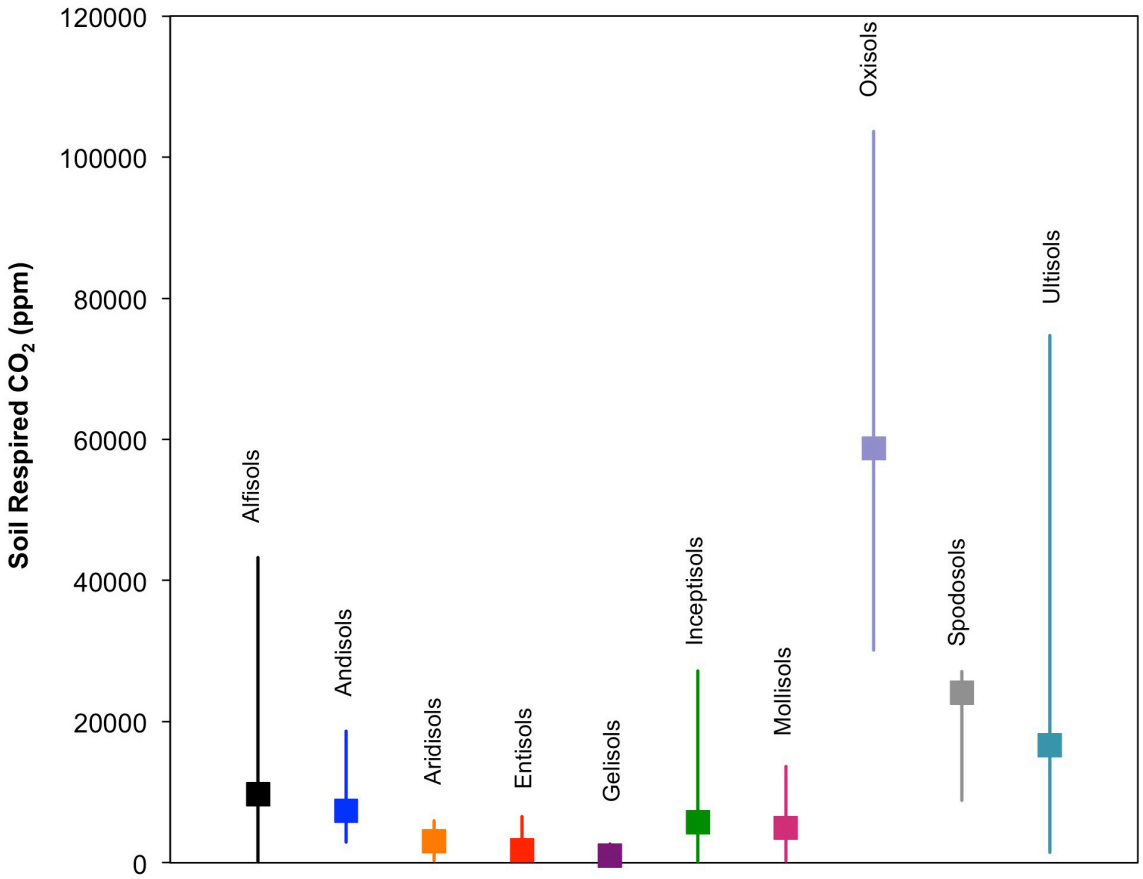

Figure 3.1. Range of values of summer soil-respired CO_2 (*S(z)* by soil order, with the squares showing the summer average *S(z)* and the lines showing the range of values. The largest variability in summer *S(z)* values occurs in Oxisols, Ultisols and Mollisols.

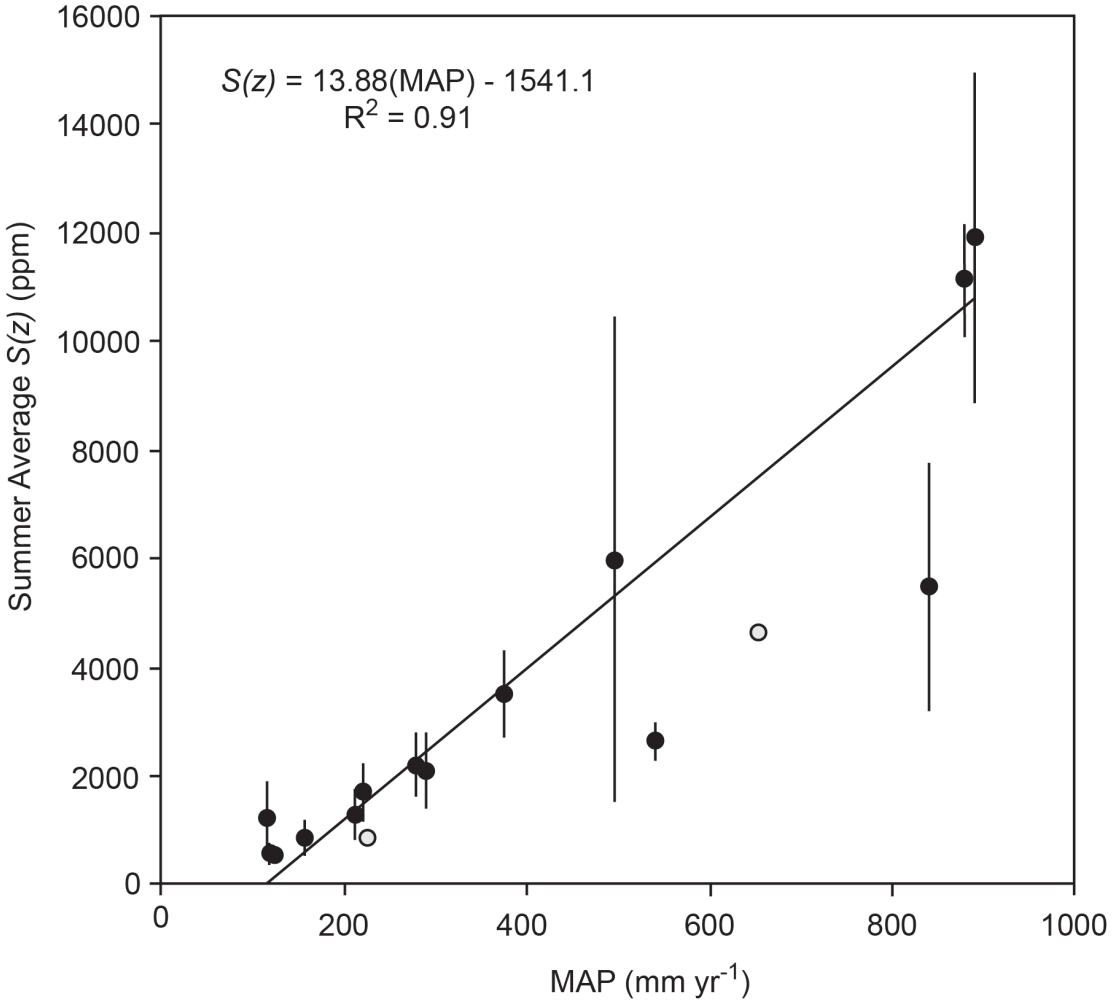

Figure 3.2. Relationship between summer average *S(z)* and mean annual precipitation in the continental United States for soils forming under 900 mm yr^{-1} precipitation or less. Error bars represent one standard deviation around the mean of multiple measurements from each site. The gray data points represent sites in which only one soil CO_2 measurements was available. See Table B1 in Appendix B for site means and standard deviations.

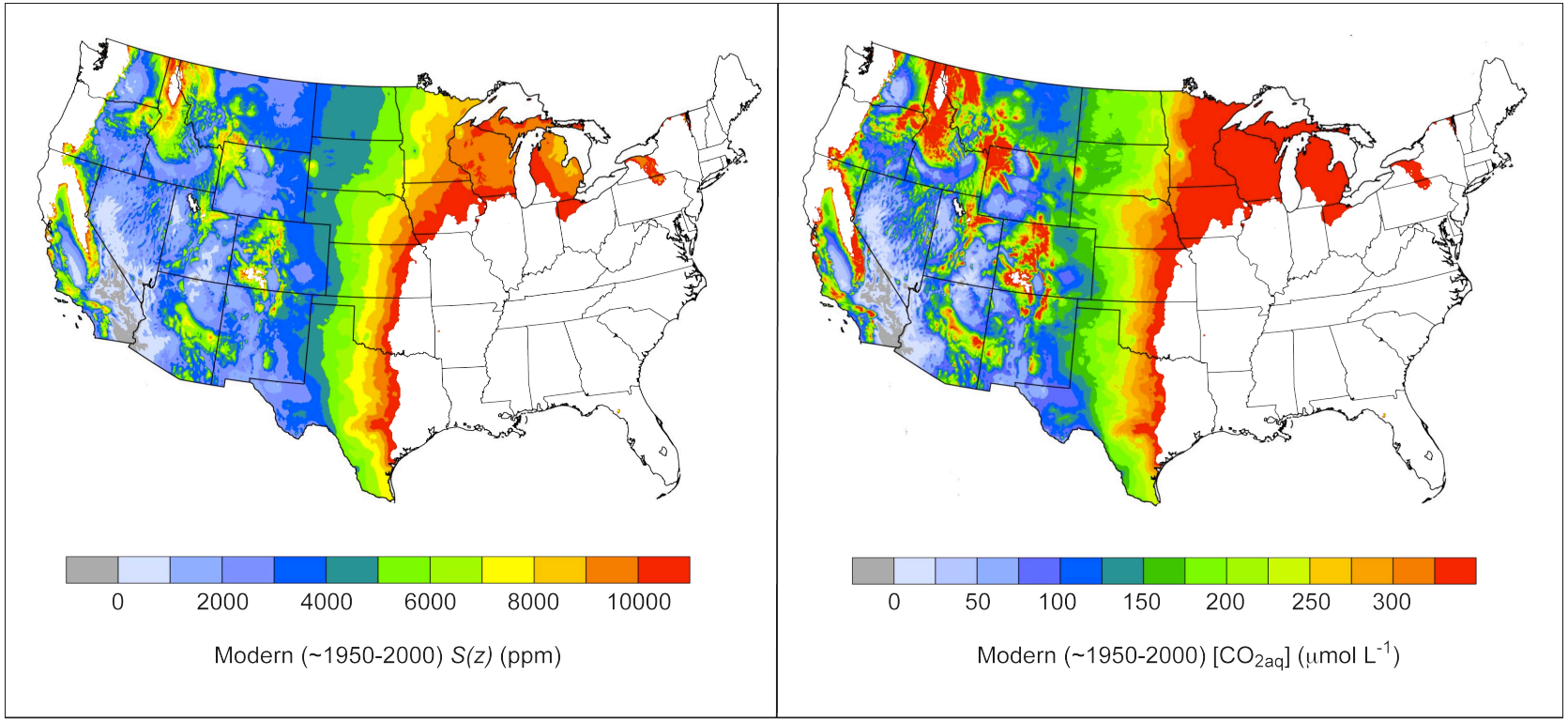

Figure 3.3. A: Calculated modern summer average *S(z)* for areas receiving 900 mm yr^{-1} precipitation or less in the central and Western United States based on the new proxy presented in Eq. 3.5 and Figure 3.2. B: Calculated modern summer average [CO_{2aq}], in μmoles L^{-1} using Henry's Law (Eq. 3.5, 3.6), *S(z)*, and summer average temperature from the Worldclim dataset (Hijmans et al., 2005).

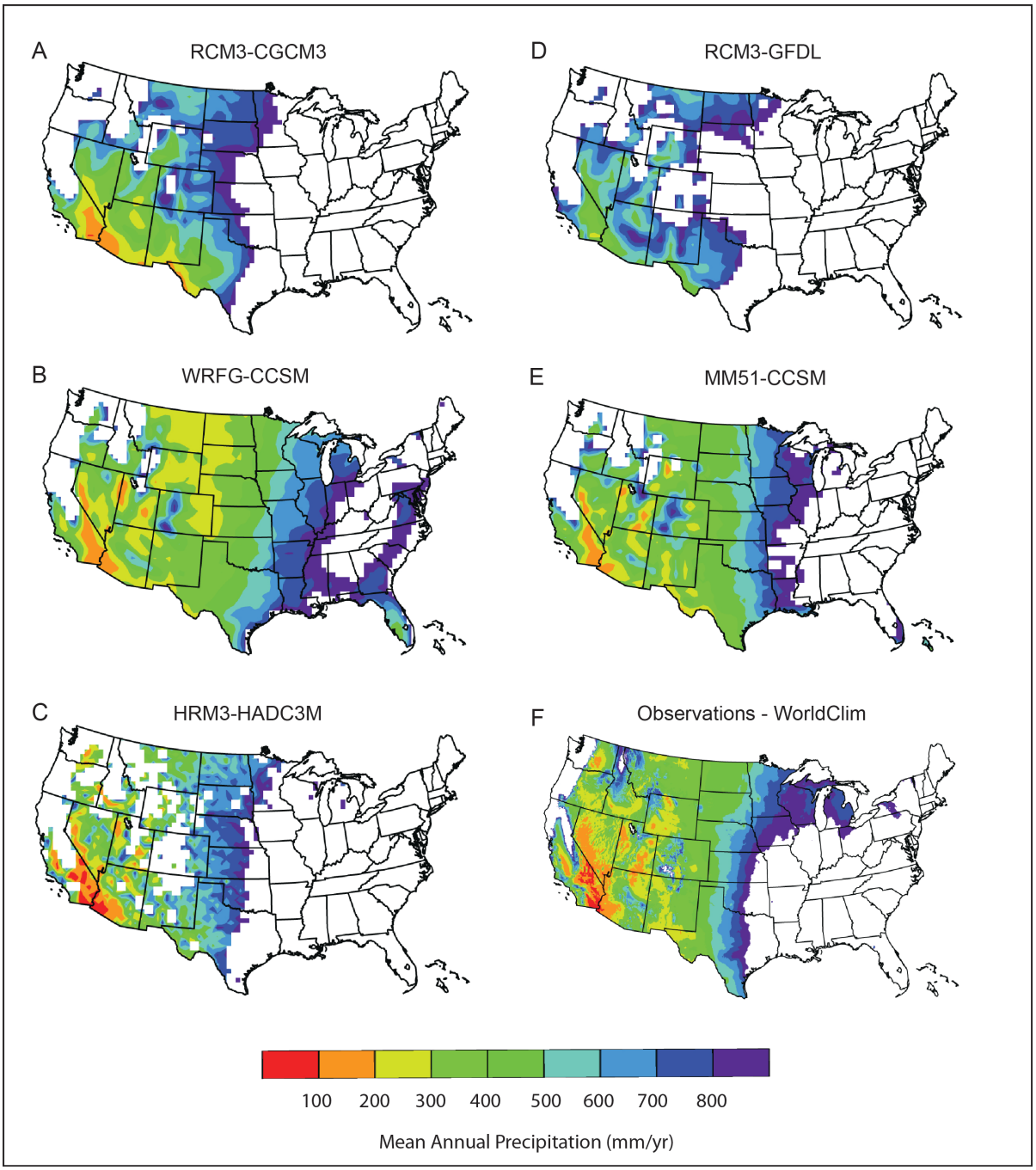

Figure 3.4. Plots of the five regional climate model simulations of current precipitation conditions from 1971 – 2000 compared to average observed precipitation conditions from the WorldClim dataset. The only regions displayed are those forming under 900 mm yr^{-1} annual precipitation or less, because the *S(z)*-MAP relationship is not valid for more humid regions. MM51-CCSM and WRFG-CCSM best simulate modern climate conditions. See the NARCCAP website (http://www.narccap.ucar.edu) for further information about the regional climate model (RCM) characteristics.

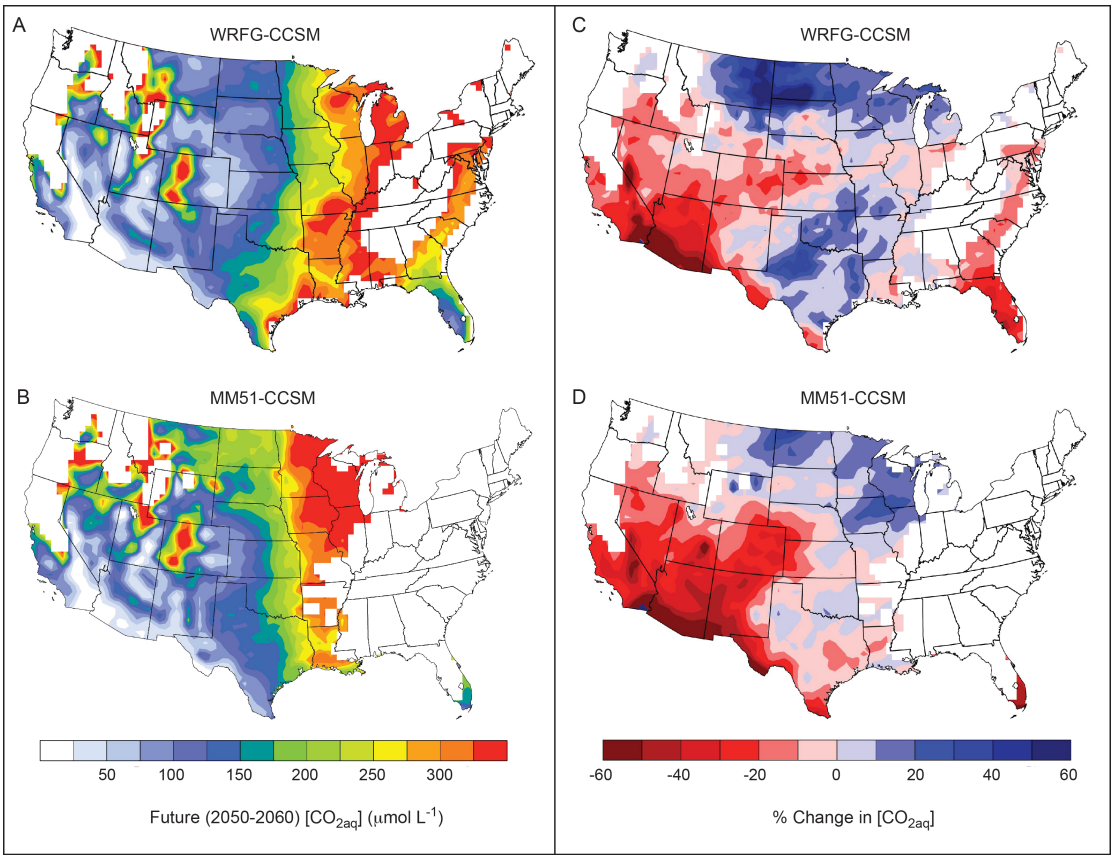

Figure 3.5. Left: Summer average [CO_{2aq}] for the decade 2050–2060 in μmoles L^{-1} H_2O. [CO_{2aq}] and weathering rates are higher in the Great Plains and the in the southwestern United States. A) WRFG-CCSM and, B) MM51-CCSM. Changes to weathering in the Great Plains region are more significant to the carbon cycle than changes to weathering in the southwestern United States. Right: Percent change in summer average [CO_{2aq}] from modern to 2050–2060. [CO_{2aq}] is calculated using the relationship defined in this study (Eq. 3.5) and climate changes simulated by two NARCCAP models, C) WRFG-CCSM and, D) MM51-CCSM.

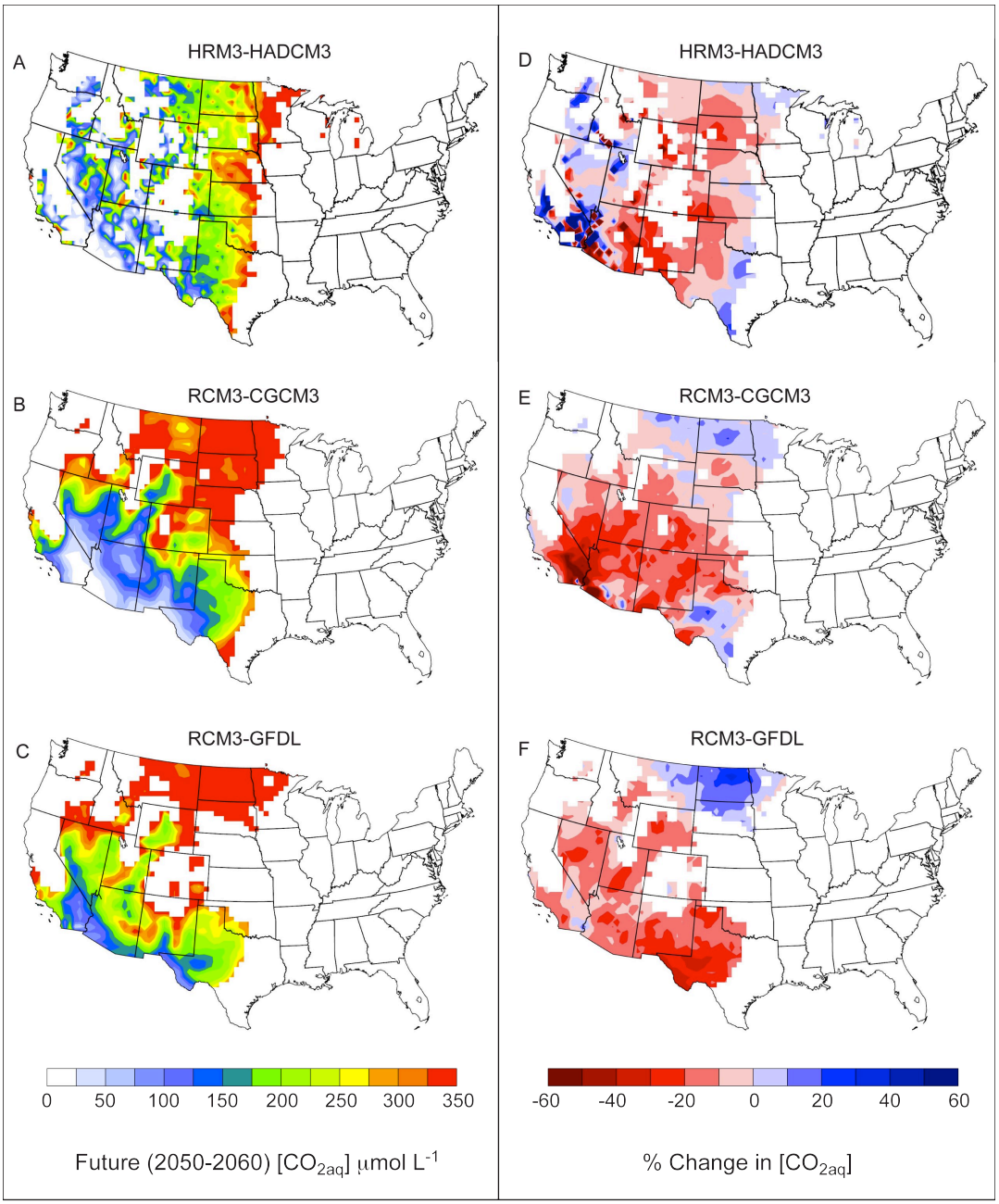

Figure 3.6. A-C: Summer average [CO_{2aq}] for the decade 2050–2060 in µmoles L^{-1} H_2O for the three models that do not accurately simulate modern precipitation variability across the western United States. A: HRM3-HADCM3. B: RCM3-CGCM3. C: RCM3-GFDL. D-F: Percent change in summer average [CO_{2aq}]. D: HRM3-HADCM3. E: RCM3-CGCM3. F: RCM3-GFDL. The models that best simulated modern climate conditions are MM51-CCSM and WFRG-CCSM (Fig. 3.4) and are therefore the most robust predictions of future changes to [CO_{2aq}]. See the NARCCAP website (http://www.narccap.ucar.edu) for further information about the regional climate model (RCM) characteristics.

	Total	Forming under 900 mm yr^{-1}	Located in United States
Number of Soils	59	34	16
Number of Measurements	933	769	254

Table 3.1 Summary of the soil CO_2 data derived from literature review. Though only 16 soils from the United States were used in the derivation of Eq. 3.7, a similar relationship exists (with more scatter) between MAP and *S(z)* for the 34 soils forming under 900mm yr^{-1} precipitation globally.

3.8 References

Amundson, R.G., and Davidson, E.A., 1990. Carbon dioxide and nitrogenous gases in the soil atmosphere. Journal of Geochemical Exploration 38, 13–41.

Andrews, J.A., and Schlesinger, W.H., 2001. Soil CO_2 dynamics, acidification, and chemical weathering in a temperate forest with experimental CO_2 enrichment. Global Biogeochemical Cycles 15, 149–162.

Bader, M.K.F., and Körner, C., 2010. No overall stimulation of soil respiration under mature deciduous forest trees after 7 years of CO_2 enrichment. Global Change Biology 16, 2830–2843.

Ballantyne, A.P., Alden, C.B., Miller, J.B., Tans, P.P., and White, J.W.C., 2012. Increase in observed net carbon uptake by land and oceans during the past 50 years. Nature 488, 70–73.

Beaulieu, E., Godderis, Y., Donnadieu, Y., Labat, D., and Roelandt, C., 2012. High sensitivity of the continental-weathering carbon dioxide sink to future climate change. Nature Climate Change 2, 346–349.

Berner, R.A., Lasaga, A.C., and Garrels, R.M., 1983. The carbonate-silicate geochemical cycle and its effect on atmospheric carbon dioxide over the last 100 million years. American Journal of Science 283, 641–683.

Berner, R.A., 1992. Weathering, plants, and the long term carbon cycle. Geochimica et Cosmochimica Acta 56, 3225–3231.

Berner, R.A., and Kothavala, Z., 2001. GEOCARB III: A revised model of atmospheric CO_2 over Phanerozoic time. American Journal of Science 301, 182–204.

Boyce, C.K., Brodribb, T.J., Field, T.S., and Zwienicki, M.A., 2009. Angiosperm leaf vein evolution was physiologically and environmentally transformative. Proceedings of the Royal Society B 276, 1771–1776.

Boyce, C.K., Lee, J.-E., Field, T.S., Brodribb, T.J., and Zwienick, M.A., 2010. Angiosperms helped put the rain in the rainforests: the impact of plant physiological evolution on tropical biodiversity. Annals of the Missouri Botanical Garden 97, 527–540.

Breecker, D.O., Sharp, Z.D., and McFadden, L.D., 2009. Seasonal bias in the formation and stable isotopic composition of pedogenic carbonate in modern soils from central New Mexico, USA. Geological Society of America Bulletin 121, 630–640.

Brook, G.A., Folkoff, M.E., and Box, E.O., 1983. A world model for soil carbon dioxide.

Earth Surface Processes and Landforms 8, 79–88.

Cerling, T.E., 1984. The stable isotopic composition of modern soil carbonate and its relationship to climate. Earth and Planetary Science Letters 71, 229–240.

Cerling, T.E., 1991. Carbon dioxide in the atmosphere: evidence from Cenozoic and Mesozoic paleosols. American Journal of Science 291, 377–400.

Chadwick, O.A., Kelley, E.F., Merritts, D.M. and Amundson, R.M., 1994. Carbon dioxide consumption during soil development. Biogeochemistry 24, 115–127.

Churkina, G., and Running, S.W., 1998. Contrasting controls on the estimated productivity of global terrestrial biomes. Ecosystems 1, 206–215.

Cotton, J.M. and Sheldon, N.D. 2012. New constraints on using paleosols to reconstruct atmospheric pCO_2. Geological Society of America Bulletin 124, 1411–1423.

Curtis, P.S., and Wang, X., 1998. A meta-analysis of elevated CO2 effects on woody plant mass, form, and physiology. Oecologia 113, 299–313.

de Jong, E., and Schappert, H.J.V., 1972. Calculation of soil respiration and activity from CO_2 profiles in the soil. Soil Science 113, 328–333.

Di Luca, A., de Elia, R., and Laprise, R., 2011. Potential for added value in precipitation simulated by high-resolution nested Regional Climate Models and observations. Climate Dynamics published online, doi: 10.1007/s00382-011-1068-3.

Dörr, H., and Münnich, K.O., 1987. Annual variation in soil respiration in selected areas of the temperate zone. Tellus B 39B, 114–121

Ebelmen, J.J., 1845. Sur les produits de la decomposition de especes mine´rales de la famile des silicates. Annales des Mines 12, 627–654.

Eiriksdottir, E.S., Gislason, S.R., and Oelkers, E.H., 2011. Does runoff or temperature control chemical weathering rates? Applied Geochemistry 26, S346–S349

Ehleringer, J.R., Cerling, T.E., and Helliker, B.R., 1997. C_4 photsynthesis, atmospheric CO_2 and climate. Oecologia 112, 285–299.

Farquhar, G.D., von Caemmerer, S., and Berry, J.A., 1980. A biochemical model of photosynthetic CO_2 assimilation in leaves of C_3 species. Planta, 149, 78–90.

Gao, Y., Vano, J.A., Zhu, C., and Lettenmaier, D.P., 2011. Evaluating climage change over the Colorado River basin using regional climate models. Journal of Geophysical Research, 116, D13104.

Ghannoum, O., von Caemmerer, S., Ziscka, L.H., and Conroy, J.P., 2000. The growth response of C_4 plants to rising atmospheric CO_2 partial pressure: a reassessment. Plant, Cell, and Environment 23, 931–942.

Gislason., S.R., Oelkers, E.H., Eiriksdottir, E.S., Karjilov, M.I., Gisladottir, G., Sigfusson, B., Snorrason, A., Elefsen, S., and Hardardottir, J., 2009. Earth and Planetary Science Letters 277, 213–222.

Goudie, A.S., and Viles, A., 2012. Weathering and the global carbon cycle: Geomorphological perspectives. Earth-Science Reviews 113, 59–71.

Hijmans, R.J., Cameron, S.E., Parra, J.L., Jones P.G., and Jarvis, A. 2005. Very high resolution interpolated climate surfaces for global land areas. International Journal of Climatology 25, 1965–1973.

IPCC, 2007. Climate Change 2007: Synthesis Report. IPCC, Geneva, Switzerland, 104 pp.

Jackson, R.B., Cook, C.W., Pippen, J.S., and Palmer, S.M., 2009. Increased belowground biomass and soil CO_2 fluxes after a decade of carbon dioxide enrichment in a warm-temperate forest. Ecology 90, 3352–3366.

Jin, L., Ogrinc, N., Hamilton, S.T., Szramek, K., Kanduc, T., and Walter, L.M., 2009. Inorganic carbon isotope systematics in soil profiles undergoing silicate and carbonate weathering (Southern Michigan, USA). Chemical Geology, 264, 139–153.

Jin, Z., You, C.-H., Yu, J., Wu, L., Zhang, F., and Liu, H.-C., 2011. Seasonal contributions of catchment weathering and eolian dust to river water chemistry, northeastern Tibetan Plateau: Chemical and Sr isotopic constraints. Journal of Geophysical Research 116, F04006.

Kain, J.S., and Fritsch, J.M., 1990. A One-Dimensional Detraining Plume Model and Its Application in Convective Parameterization. Journal of the Atmospheric Sciences 47, 2784–2802.

Karberg, N.J., Pregitzer, K.S., King, J.S., Friend, A.L., and Wood, J.R., 2005. Soil carbon dioxide partial pressure and dissolved inorganic carbonate chemistry under elevated carbon dioxide and ozone. Oecologia. 124, 296–306.

Kessler, T.J., and Harvey, C.F., 2001. The global flux of carbon dioxide into groundwater. Geophysical Research Letters, 28, 279–282.

Keppel-Aleks, G., Wennberg, P.O., and Schneider, T., 2011. Sources and variations in total column carbon dioxide. Atmospheric Chemistry and Physics 11, 3581–3593.

Keppel-Aleks, G., Wennberg, P.O., Washenfelder, R.A., Wunch, D., Schneider, T., Toon, G.C., Andres, R.J., Blavier, J.-F., Connor, B., Davis, K.J., Desai, A.R., Messerschmidt, J., Notholt, J., Roehl, C.M., Sherlock, V., Stephens, B.B., Vay, S.A., and Wofsy, S.C., 2012. The imprint of surface fluxes and transport on variations in total column carbon dioxide. Biogeosciences 9, 875–891.

Leung, L.R., Qian, Y., and Bian, X., 2003a. Hydroclimate of the western United States based on observations and regional climate simulation of 1981–2000. Part I: Seasonal Statistics. Journal of Climate 16, 1892–1911.

Leung, L.R., Qian, Y., Bian, X., and Hunt, A., 2003b. Hydroclimate of the western United States based on observations and regional climate simulation of 1981-2000. Part II: Mesoscale ENSO anomalies. Journal of Climate, 16, 1912–1928.

Li, S.L., Liu, C.-Q., Li, J., Lang, Y.-C., Ding, H., and Li, L., 2010. Geochemistry of dissolved inorganic carbon and carbonate weathering in a small typical karstic catchment of Southwest China: Isotopic and chemical constraints. Chemical Geology 277, 301–309.

Mearns, L.O. *et al.* (2007) updated 2011. *The North American Regional Climate Change Assessment Program dataset*, National Center for Atmospheric Research Earth System Grid data portal, Boulder, CO. Data downloaded 2011-08-10. [http://www.earthsystemgrid.org/browse/viewProject.htm?projectId=ff3949c8-2008-45c8-8e27-5834f54be50f]

Mearns, L.O., Gutowski, W.J., Jones, R., Leung, L.Y., McGinnis, S., Nunes, A.M.B., and Qian, Y., 2009. A regional climate change assessment program for North America. *EOS* V90, No. 36, 8, 311–312.

Meehl, G. et al., 2007: Global Climate Projections, in: Solomon, S., Qin, M., Manning, M. et al. (eds) Climate Change 2007: The Physical Science Basis. Working Group I Contribution to the Fourth Assessment Report of the IPCC, Cambridge University Press, Cambridge, 996 pp.

Moosdorf, N., Hartmann, J., Lauerwald, R., Hagedorn, B., and Kempe, S., 2011. Atmospheric CO_2 consumption by chemical weathering in North America. Geochimica et Cosmochimica Acta 75, 7829–7854.

Nakicenvoic, N., Alcamo, J., Davis, G., *et al.*, 2000. Special Report on Emissions Scenarios. A Special Report of Working Group III of the Intergovernmental Panel on Climate Change. Cambridge University Press, Cambridge, 599 pp.

Norton, K.P., and Von Blanckenburg, F., 2010. Silicate weatering of soil-manteled slopes in an active Alpine landscape. Geochimica et Cosmochimica Acta 74, 5243–5258

Oh, N-H., and Richter, D.D., 2004. Soil acidification induced by elevated atmospheric

CO_2. Global Change Biology 10, 1936–1946.

Oh, N-H., Hofmockel, M., Lavine, M.L., and Richter, D.D., 2007. Did elevated atmospheric CO_2 alter soil mineral weathering?: an analysis of 5-year soil water chemistry data at a Duke FACE study. Global Change Biology 13, 2626–2641.

Raich, J.W., and Potter, C.S., 1995. Global patterns of carbon dioxide emissions from soils. Global Biogeochemical Cycles 9, 23–26.

Raich, J.W., and Schlesinger, W.H., 1992. The global carbon dioxide flux in soil respiration and its relationship to vegetation and climate. Tellus B 44, 81–99.

Rasmussen, C., Brantley, S., Richter, D. deB., Blum, A., Dixon, J., and White A.F., 2011. Strong climate and tectonic control on plagioclase weathering in granitic terrain. Earth and Planetary Science Letters 301, 521–530.

Retallack, G.J., 2000. Depth to pedogenic carbonate horizon and a paleoprecipitation indicator? Comment: Geology 28, 572–573.

Rightmire, C.T., 1978. Season variation in pCO_2 and ^{13}C content of soil atmosphere. Water Resources Research 14, 691–692.

Rosenzweig, M.L. 1968. Net Primary Productivity of Terrestrial Communities: Predictions from climatological data. The American Naturalist 102, 67–74.

Royer, D.L., Berner, R.A., and Beerling, D.J., 2001. Phanerozoic atmospheric CO_2 change: evaluating geochemical and abiological approaches. Earth-Science Reviews 54, 349–392,

Ruiz-Barradas, A., and Nigam, S. 2010. Great Plains precipitation and its SST links in twentieth-century climate Simulations, and twenty-first- and twenty-second-century climate projections. Journal of Climate 23, 6409–6429.

Sage, R.F., 2004. The evolution of C_4 photosynthesis. New Phytologist 161, 341–370.

Sander, R., 1999. Compilation of Henry's Law Constants for Inorganic and Organic Species of Potential Importance in Environmental Chemistry (Version 3). http://www.mpch-mainz.mpg.de/~sander/res/henry.html

Schimel, D.S., House, J.I., Hibbard, K.A., Bousquet, P., Clais, P., Peylin, P., Braswell, B.H., Apps, M.J., Baker, D., Bondeau, A., Canadell, J., Churkina, G., Cramer, W., Denning, A.S., Field, C.B., Friedlingstein, P., Goodale, C., Heinmann, M., Houghton, R.A., Melillo, J.M., Moore III, B., Murdiyarso, D., Modle, I., Pacala, S.W., Prentice, I.C., Raupach, M.R., Rayner, P.J., Scholes, R.J., Steffen, W.L., and Wirth, C., 2001. Recent patterns and mechanisms of carbon exchange by terrestrial ecosystems. Nature 414, 169–172.

Schlesinger, W.H., 1977. Carbon balance in terrestrial detritus. Annual Review of Ecology and Systematics 8, 51–81.

Seager, R., Ting, M.F., Held, I., Kushnir, Y., Lu, J., Vecchi, G., Huang, H.-P., Harnik, N., Leetmaa, A., Lau, N.-C., Li, C., Velez, J., and Naik, N., 2007. Model projections of an imminent transition to a more arid climate in southwestern North America. Science 316, 1181–1184.

Seager, R., and Vecchi, G.A., 2010. Greenhouse warming of the 21st century hydroclimate of southwestern North America. Proceedings of the National Academy of Sciences of the United States of America 107, 21277–21282.

Siemens, J., Pacholski, A., Heiduk, K., Giesemann, A., Schulte, U., Dechow, R., Kaupenjohann, M., and Weigel, H-J., 2012. Elevated air carbon dioxide concentrations increase dissolved carbon leaching from a cropland soil. Biogeochemistry 108, 135–148.

Sigman, D.M., and Boyle, E.A., 2000. Glacial/interglacial variations in atmospheric carbon dioxide. Science 407, 859–869.

Soil Survey Staff, 2010. Keys to Soil Taxonomy, 11th ed. USDA-Natural Resources Conservation Service, Washington, DC.

Sheldon, N.D., and Tabor, N.J., 2009. Quantitative paleoenvironmental and paleoclimatic reconstruction using paleosols. Earth-Science Reviews 95, 1–52.

Sheldon, N.D., and Tabor, N.J., 2013, Using paleosols to understand paleo-carbon burial. in: Driese, S., Nordt, L. (eds) New Frontiers in Paleopedology and Terrestrial Paleo- climatology, Society for Sedimentary Geology Special Publication 102 (in press).

USDA National Agricultural Statistics Service (2011), Farms, land in farms, and livestock operations 2010 summary, ISSN: 1930–7128.

Wang, S.Y., Gillies, R.R., Takle, E.S., and Gutowski, W.J., 2009. Evaluation of precipitation in the Intermountain Region as simulated by the NARCCAP regional climate models. Geophysical Research Letters 36, L11704.

Wanner, H., 1970. Soil respiration, litter fall and productivity of a tropical rainforest. Journal of Ecology 58, 543–547.

West, A.J., 2012. Thickness of the chemical weathering zone and implications for erosional and climatic drivers of weathering and for carbon-cycle feedbacks. Geology 40, 811–814

Witkamp, M., 1966. Rates of carbon dioxide evolution from the forest floor. Ecology, 47, 492–494.

Chapter 4

Positive feedback drives carbon release from soils to atmosphere during Paleocene/Eocene warming[3]

4.0 Abstract

The Paleocene-Eocene Thermal Maximum (PETM) is the most rapid climatic warming event in the Cenozoic and informs us of how the Earth system responds to large-scale changes to the carbon cycle. Warming was triggered by a massive release of isotopically ^{13}C depleted carbon to the atmosphere, as indicated by negative carbon isotope excursions (CIE) in nearly every carbon pool on Earth. Differences in the magnitude of these CIEs can give insight into the response of different ecosystems to perturbations in the carbon cycle. Here we present records of $\delta^{13}C_{cc}$ of pedogenic carbonates and $\delta^{13}C_{org}$ from preserved soil organic matter in corresponding paleosols to understand changes to soil carbon cycling during the PETM. CIEs during the event are larger in pedogenic carbonates than preserved organic matter for corresponding paleosols at three sites across two continents. The difference in the CIEs within soil carbon pools can be explained by increased respiration and carbon turnover rates of near-surface labile soil carbon. Increased rates of carbon cycling combined with decreases in the amount of

[3] Cotton, J.M., Sheldon, N.D., Hren, M.T., and Gallagher, T.M. Positive feedback drives soil to atmosphere carbon release during Paleocene/Eocene warming. In preparation to be submitted to *Nature*, 3/13.

preserved organic carbon in soils during the PETM suggests a decrease in the size of the soil carbon pool, resulting in an increase in atmospheric pCO_2 and a positive feedback with warming. The magnitude of the PETM is analogous to projections of future climate change, and these results suggest that soils serve as a large source for atmospheric CO_2 during warming events.

4.1 Introduction

Soils contain the largest stock of carbon in the terrestrial biosphere (Schlesinger, 1997), and the primary controls on soil carbon, microbial respiration and plant productivity, are both sensitive to climate (Andrews and Schlesinger, 2001; Nemani et al., 2003). However, the response of this reservoir to a rise in global temperature remains poorly understood, and soils have the potential to become a large source of CO_2 to the atmosphere through positive climate feedbacks (e.g., Giardina et al. 2000; Knorr et al., 2005; Liang and Balser, 2012). Modern soil studies are limited by the amount of time they can observe changes in a certain soil, typically only a few years to a decade, which may not be long enough to determine long-term changes to carbon cycling in soils due to warming and increases atmospheric pCO_2 because carbon stocks can build up or diminish over larger timescales. Ancient soils formed during rapid warming events such as the PETM offer a means of identifying how carbon cycling in soils may change in response to future anthropogenically driven climate change.

The Paleocene/Eocene Thermal Maximum (PETM) is the most rapid warming event in recent geologic history, and is an analog for future climate change (Zachos et al., 2001). The PETM is characterized by a negative carbon isotope excursion (CIE) in

virtually every carbon pool on Earth, both marine and terrestrial (e.g., Koch et al., 1992; Kennet and Stott, 1991; McInerney and Wing, 2011). This CIE is thought to be the result of the release of a large amount of an isotopically ^{13}C depleted source of carbon to the atmosphere, which then was assimilated into marine and terrestrial ecosystems (Dickens et al., 1995; Higgins and Schrag, 2006; Zeebe et al., 2009). The magnitude of this CIE in different carbon pools on Earth is highly variable (McInerney and Wing, 2011), ranging from and average value of -2.5‰ in benthic foraminifera to an average value of -5.5‰ for pedogenic carbonates. Many workers have been interested in determining the true magnitude of the CIE in atmospheric CO_2 from these different carbon pools in an effort to quantify the source, amount of CO_2, and resulting increase in the concentration of atmospheric CO_2 during the rapid warming event (Pagani et al., 2006; Zeebe et al., 2009; Diefendorf et al., 2010 and others). In particular, the differences between the CIE recorded by terrestrial and marine carbon pools have been used to quantify the magnitude of carbon release and resulting climatic changes (Bowen et al. 2004; Schubert and Jahren, 2013). However, the differences in these CIEs between different terrestrial carbon pools also preserve information about the response of different ecosystems to perturbations to the carbon cycle (Bowen et al., 2004; Smith et al. 2007). Here, we examine changes in carbon isotopes ratios in different soils carbon reservoirs during the PETM to determine if soil dynamics and carbon cycling changed during this rapid warming event.

Soil organic matter (SOM) turnover typically occurs on timescale of hundreds of years (Trumbore et al., 1996). The PETM carbon release occurred over thousands of years and was slow enough that changes to the isotopic composition of atmospheric CO_2 were recorded in SOM preserved in paleosols (McInerney and Wing, 2011). Pedogenic

carbonates precipitate within soils in isotopic equilibrium with soil CO_2, which is thought to be predominately derived from the respiration of SOM and root respiration with a smaller contribution from atmospheric CO_2 (Cerling, 1984; 1991; Kuzyakov, 2006). Given that pedogenic carbonates are formed from CO_2 generated from the respiration of SOM, a shift in the isotopic composition of atmospheric CO_2 should result in a CIE of similar magnitude in both the SOM and pedogenic carbonates in a given soil. During the PETM, the magnitude of the CIE in organic and inorganic soil carbon pools is dramatically different, with preserved SOM recording an average CIE of -3.5‰ and pedogenic carbonates recording an average CIE of -5.5‰. Both pedogenic carbonates and soil organic matter are often preserved without diagenetic alteration or isotopic resetting (Koch, 1998; Cotton et al., 2012), and thus the larger magnitude CIE recorded in pedogenic carbonates than in SOM implies that there was a fundamental change to the soil carbon cycle during the PETM. This chapter explores the possible causes of these differing CIE magnitudes in soils. To demonstrate that the differing excursions are not an artifact of sampling bias, we present matching records of the $\delta^{13}C$ of both SOM and pedogenic carbonates from three different sites in North America and Europe.

4.2 Methods

The data from the three sites were derived from both a literature review and isotopic analysis of new samples. We present a new record of the $\delta^{13}C_{org}$ of preserved soil organic carbon from Axhandle Canyon, near Ephraim, Utah. Three vertical transects through the PETM event were measured and correlated one another through their stratigraphic position above or below a distinct 5–10 m thick conglomerate marker bed.

Fresh rock samples for isotopic analysis were collected from the A horizons of paleosols. A horizons were identified based on grain size changes and the presence of preserved root traces. Samples were treated with a 7% solution of HCl to remove carbonate and then rinsed, dried and homogenized according to Cotton et al. (2012). The carbonate-free soil samples were then weighed into tin capsules and analyzed for the isotopic composition of preserved organic material on a Costech elemental analyzer attached to a Finnigan Delta V+ isotope ratio mass spectrometer. Each sample was measured either in duplicate or triplicate depending on the variability of the measured $\delta^{13}C_{org}$ in each sample. More variable samples were measured in triplicate. The analytical uncertainty associated with each $\delta^{13}C_{org}$ measurement is <0.1‰. Pedogenic carbonates were also analyzed for carbon and oxygen isotopic compositions for comparison to the carbonate record published by Bowen and Bowen (2008), and these analyses showed the same excursion in $\delta^{13}C_{cc}$ at approximately the same meter level in the section (Figure C1, Table C4). Analytical errors were determined through repeated measurements of reference materials.

The measured section of $\delta^{13}C_{org}$ of preserved organic carbon at Axhandle Canyon was correlated to the previously published record of $\delta^{13}C_{cc}$ from pedogenic carbonates (Bowen and Bowen, 2008) instead of the new analyses because of the greater sampling resolution in the previous study. Samples were correlated using measured meter levels for the $\delta^{13}C_{org}$ transect and published meter levels for the $\delta^{13}C_{cc}$ transect. The identification of the PETM was based not only on the appearance of the CIE, but also on the magnetostratigraphy and a biostratigraphic age constraint for the early Eocene above the top of the section (Bowen and Bowen, 2008). Paleosols were considered to have

correlated values if the measured $\delta^{13}C_{cc}$ of pedogenic carbonates was within one meter of the measured $\delta^{13}C_{org}$ of preserved organic material. Paleosols with published $\delta^{13}C_{cc}$ values outside this one-meter range were not used in this study. CIE magnitudes in both the SOM and the pedogenic carbonates were calculated and compared. Differences in CIE magnitudes within the same soil are expressed as $\Delta^{13}C$ values, which is defined as:

$$\Delta^{13}C = \delta^{13}C_{cc} - \delta^{13}C_{org} \quad \text{(Eq. 4.1)}$$

where a larger magnitude CIE in pedogenic carbonates than in SOM is represented as a smaller $\Delta^{13}C$ value during the PETM than before and after the warming event.

We also compare the magnitude of CIEs in SOM and pedogenic carbonates from two other sites from which isotopic data has already been published. The first site is Polecat Bench in the northern Bighorn Basin. The record of the CIE in pedogenic carbonates was published by Bowen et al. (2001) and the CIE in the matching organic matter from the same site was published by Magioncalda et al. (2004). The age was constrained by mammalian biostratigraphy and the PETM was identified based on the CIE (Bowen et al., 2001). The second site with data derived from the literature is the Tendruy section in the South-central Pyrenees, Lleida, Spain. For this site, the CIE during the PETM is recorded in the $\delta^{13}C_{cc}$ of pedogenic carbonates published by Schmitz and Pujalte (2003). The $\delta^{13}C_{org}$ from paleosols in the same section was published by Domingo et al. (2009). Identification of the PETM was based on microvertebrate biostratigraphy and the onset of the CIE. Isotopic data was correlated by matching the first appearance and the duration of the CIE in the isotopic record of the pedogenic carbonate to the CIE recorded in the preserved organic material. At the Tendruy section, the density of $\delta^{13}C_{org}$ measurements through the PETM section is far greater than the density of $\delta^{13}C_{cc}$

measurements. Therefore, for this site the isotopic data was considered to be correlated if the $\delta^{13}C_{cc}$ measurement was within three meters of the corresponding paleosol $\delta^{13}C_{org}$ measurement. During the PETM event, $\Delta^{13}C$ values were calculated for correlated meter level according to the methods described above. Because Schmitz and Pujalte (2003) only published one value for the isotopic composition of pedogenic carbonates prior to the PETM, this value was used in the calculation of $\Delta^{13}C$ for each paleosol prior to and after the PETM event. While this method may not accurately describe the $\Delta^{13}C$ values of many of the soils through the section, it does however allow us to investigate the changes to $\Delta^{13}C$ just before and during the PETM. Isotopic data from new and previously published analyses used in this chapter are located in Appendix C.

4.3 Results

For each site, the CIE recorded in the isotopic composition of pedogenic carbonates was larger than the CIE recorded in corresponding preserved organic matter. Each of these localities has slightly different baseline (pre- and post-PETM) $\Delta^{13}C$ values, which is likely due to different soil productivity at each site caused by variable precipitation regimes (Kraus and Riggins, 2007; Bowen and Bowen, 2008; Cotton and Sheldon, 2012). The apparent change in $\Delta^{13}C$ during the PETM can be directly compared at each site by calculating a $\Delta^{13}C$ anomaly value according to the following equation:

$$\Delta^{13}C_{anomaly} = (\delta^{13}C_{cc} - \delta^{13}C_{org})_{sample} - \mu(\delta^{13}C_{cc} - \delta^{13}C_{org})_{pre\text{-}+post\ PETM} \quad \text{(Eq. 4.2)}$$

Where μ represents the average $\Delta^{13}C$ value for soils forming before and after the PETM. Figure 4.1 shows the apparent $\Delta^{13}C$ anomalies at each site. Using Eq. 4.2, the maximum

$\Delta^{13}C$ anomaly observed at Polecat Bench in the Bighorn Basin is -4.4‰ and the average $\Delta^{13}C$ anomaly during the PETM is -2.8‰ (Fig. 4.1A). At Tendruy, Spain (Fig. 4.1B), the maximum $\Delta^{13}C$ value observed during the PETM is -5.7‰, with an average $\Delta^{13}C$ anomaly of -3.2‰ during the event. At Axhandle Canyon, Utah (Fig. 4.1C), the maximum observed $\Delta^{13}C$ anomaly is -2.6‰ with an average $\Delta^{13}C$ anomaly of -1.3‰ through the event. The same temporal trend occurs at all three sites, and the magnitude of these $\Delta^{13}C$ anomalies is also similar. Given the wide distribution of the localities, these $\Delta^{13}C$ anomalies suggest changes to soil carbon cycling during the PETM on a global scale.

4.4 Discussion

There are many factors that control the isotopic composition of pedogenic carbonates and thus, the calculated $\Delta^{13}C$ values for a soil. The following six sections will describe each of these factors and whether or not the mechanism is able to explain the observed trend in decreasing $\Delta^{13}C$ values during the PETM warming.

4.4.1 Increased Atmospheric pCO_2

As pedogenic carbonates precipitate in equilibrium with soil CO_2, changes to the isotopic composition of that CO_2 will influence the $\delta^{13}C_{cc}$ of pedogenic carbonate. Soil CO_2 is comprised of CO_2 derived from root respiration and microbial oxidation of SOM, as well as atmospheric CO_2 diffusing into the soil. The isotopic composition of pedogenic carbonates is then controlled by the ratio of isotopically ^{13}C enriched atmospheric CO_2 (~-6‰) to isotopically ^{13}C depleted respired CO_2 (~-25‰) in the soil at the time of

carbonate formation (Cerling, 1991). During the PETM, a massive release of isotopically light carbon shifted the atmosphere from ~-5‰ (Tipple et al., 2010) to ~-8 to -9‰ (Diefendorf et al., 2010; McInerney and Wing, 2011). An increase in atmospheric pCO_2 would increase the amount of CO_2 derived from the atmosphere in the soil, which would increase ratio of atmospheric CO_2 to respired CO_2 in the soil. For a small release of isotopically very ^{13}C depleted carbon such as biogenic methane (Whiticar, 1999), the effect on the $\delta^{13}C_{cc}$ of pedogenic carbonates would be minimal. For a large release of carbon such as plant biomass, the $\delta^{13}C_{cc}$ of pedogenic carbonates would increase, causing an increase in the $\Delta^{13}C$ value for soils during the PETM, which is the opposite of what is observed (Fig. 4.1). Thus, a release of carbon to the atmospheric during the PETM is not the cause of the observed $\Delta^{13}C$ anomalies.

4.4.2 Increased Temperature and Productivity

If an increase in atmospheric pCO_2 increases $\Delta^{13}C$ values, then an increase in soil-respired CO_2 at the time of pedogenic carbonate formation will cause a decrease in $\Delta^{13}C$ values. The amount of respired CO_2 is controlled by soil productivity, and is influenced by both temperature and precipitation (Brook et al., 1983; Raich and Schlesinger, 1992; Cotton and Sheldon, 2012). With an increase in temperature, one might expect to observe an increase in soil productivity during the PETM, which could lower $\delta^{13}C_{cc}$ and $\Delta^{13}C$ values. The temperature of the soil also influences the isotopic composition of pedogenic carbonates, because the fractionation between soil CO_2 and calcite during carbonate precipitation is temperature dependent (smaller at higher temperatures; Romanek et al., 1992). Therefore, a temperature increase during the PETM would decrease the

fractionation between soil CO_2 and pedogenic carbonates and lower $\Delta^{13}C$ values for the soil. We can quantify the effects of temperature and a possible increase in productivity on $\Delta^{13}C$ by rearranging the Cerling (1999) pedogenic paleobarometer equation to:

$$\frac{CO_{2,atm}}{S(z)} = \frac{\delta^{13}C_s - 1.0044\delta^{13}C_r - 4.4}{\delta^{13}C_a - \delta^{13}C_s} \quad \text{Eq. 4.3}$$

where $\delta^{13}C_r$ represents the isotopic composition of respired CO_2 which is recorded by preserved SOM and $\delta^{13}C_a$ represents the carbon isotopic composition of CO_2 in the atmosphere. $\delta^{13}C_s$ represents the carbon isotopic composition of total soil CO_2 which is recorded by pedogenic carbonates, which is offset from the $\delta^{13}C_{cc}$ according to a temperature dependent fractionation factor (Romanek et al. 1992) that decreases as temperatures increase. *S(z)* represents the amount of respired CO_2 in the soil at the time of pedogenic carbonate formation, and is proportional to soil productivity. Because the concentration of CO_2 in the atmosphere during the PETM is not known, it is necessary to look at possible changes in productivity as a ratio of atmospheric CO_2/*S(z*) in the soil. For a low productivity ecosystem, this value might be as high as 1, for a higher productivity ecosystem, this value might drop to as low as 0.2, and if there was a productivity increase during the PETM, one would expect to observe a decrease in the atmospheric CO_2/*S(z)* values during the event (Breecker et al., 2010).

The calculations of atmospheric CO_2/*S(z)* factor in a mean annual temperature (MAT) increase of 5°C to 10°C during the PETM, consistent with changes predicted by paleotemperature proxies (Zachos et al., 2001; Wing et al., 2005). These calculations also assume a decrease in $\delta^{13}C_a$ from -5‰ to -8‰ (Tipple et al. 2010). For Polecat Bench (Fig. 4.2A), there is a decrease in atmospheric CO_2/*S(z)* values through the PETM, from

an average value of 0.1 for before and after the PETM to negative values during the PETM for both a 5° and 10°C increase in temperature. While the ratios drop during the warming event, negative results from Eq. 4.3 imply negative atmospheric CO_2 contribution to soil CO_2, an impossible result showing that a temperature and productivity increase alone cannot account for the $\Delta^{13}C$ values. At Tendruy (Fig. 4.2B), the atmospheric $CO_2/S(z)$ ratios decrease from ~0.3 prior to the PETM to values very close to zero during the warming event. With a temperature increase of 5°C, many of these values are again negative. For a 10°C temperature increase, most of the atmospheric $CO_2/S(z)$ ratios for soils during the PETM are slightly positive, with an average value of 0.02. However, these ratios are so low that the concentration of respired CO_2 would be ~50x more than the concentration of CO_2 derived from the atmosphere in the soil. These conditions are similar to those found in rainforest soils (Brook et al., 1983; Chapter 2, Cotton et al., in review) which have $S(z)$ values an order of magnitude larger than those found in soils precipitating pedogenic carbonates (Cotton and Sheldon, 2012) and would likely be too acidic for carbonate formation. Even with positive atmospheric $CO_2/S(z)$ values, an increase in temperature and productivity alone cannot explain the $\Delta^{13}C$ anomaly at Tendruy. At Axhandle Canyon (Fig. 4.2C), the atmospheric $CO_2/S(z)$ ratios are highly variable, but show a slight decrease from ~0.4 to ~0.2. These changes suggest an increase in productivity during the PETM equating to a doubling of $S(z)$ during the time of carbonate formation through the warming event. Therefore, an increase in both temperature and productivity could explain the $\Delta^{13}C$ anomaly observed at Axhandle Canyon, but not at Polecat Bench and Tendruy.

4.4.3 Changing Depth to Bk Horizon

The carbon isotopic composition of soil CO_2 is not constant in a soil, and decreases with increasing depth in a soil profile (Cerling, 1991; Amundson et al., 1998). This trend is due to the mixing of atmospheric CO_2 diffusing in from the surface of the soil and the production of soil CO_2 that typically occurs at depth (Fig. 4.3). The depth at which the isotopic composition of soil CO_2 becomes relatively steady with depth is a function of the production rate of soil CO_2 and the concentration of CO_2 in the atmosphere. Increasing atmospheric pCO_2 will increase the depth at which $\delta^{13}C$ of soil CO_2 reaches a steady state, and increasing the production rate of soil CO_2 (i.e., increasing soil productivity) will decrease this depth in the soil. The depth at which pedogenic carbonate forms within a soil is proportional to mean annual precipitation (Retallack, 2005), and increases in precipitation during the PETM could lower the depth at which carbonates are precipitated in a soil such that the carbonates are forming in equilibrium with soil CO_2 that is isotopically more ^{13}C depleted than soil CO_2 higher in the soil profile.

For example, following the diffusion equation for the isotopic composition of soil CO_2 with depth described by Cerling (1991), a pedogenic carbonate forming at Polecat Bench under pre-PETM conditions with a $\delta^{13}C_r$ of -23.5‰ (Magionalda et al., 2004), an atmospheric pCO_2 concentration of 1000 ppm, and precipitating at 50 cm depth with a production rate of 3 mmol m^{-2} hr^{-1} would theoretically be expected to have a $\Delta^{13}C$ of ~16.2‰ (Fig. 4.3A). For a similar soil at Polecat Bench during the PETM, temperature would increase by the observed 5-10°C (Fricke and Wing, 2004; Wing et al., 2005) the $\delta^{13}C$ of respired CO_2 would decrease to -27.5‰, atmospheric pCO_2 could increase to

1500 ppm. Now we will assume that with warming there was also an increase in mean annual precipitation and pedogenic carbonates were now forming at 150 cm depth in the soil. The $\Delta^{13}C$ for this soil, incorporating a 10°C temperature increase would be ~14.5‰. The maximum $\Delta^{13}C$ anomaly based on sampling depth would be ~1.7‰. An increase in production rate of soil CO_2, which would be expected with an increase in precipitation (Cotton and Sheldon, 2012) would increase the predicted $\Delta^{13}C$ anomaly, but even a doubling of production rate would bring the $\Delta^{13}C$ anomaly only to ~2.1‰ (Fig. 4.3B). Therefore, changing the depth at which pedogenic carbonates are precipitated is an unlikely explanation for the full ~3‰ anomaly observed at Polecat Bench and Tendruy. In addition, to increase the depth to carbonate bearing (Bk) horizon by ~1 meter, there would need to be an increase in precipitation on the order of 500 mm yr^{-1} (Retallack, 2005) during the PETM. At Polecat Bench, there is evidence for drying during the event (Kraus and Riggins, 2007; Kraus et al., 2013), which should decrease the depth to the Bk horizon, further showing that the depth at which carbonates are sampled cannot account for the observed $\Delta^{13}C$ anomalies.

4.4.4 Additional Carbon Source

Sediment formation and transport is sensitive to climate, and many models show that increased sedimentation results from climatic changes such as increased run off and vegetation change (Tucker and Slingerland, 1997; Armitage et al., 2011). Depending on the source, sediment may contain previously buried carbon that could be incorporated into soils formed from fluvial deposits. Foreman et al. (2012) find that the Piceance Creek Basin in western Colorado experienced increases in sediment flux and discharge

during the PETM. Schmidt and Pujalte (2003) also find increased erosion rates during the PETM in the Basque Basin in northern Spain, including the Tendruy site. If increased sedimentation rates delivered an allochthonous source of isotopically heavy pre-PETM carbon to soils during the PETM, then the magnitude of the CIE could be masked by the mixed carbon sources. The new carbon would be respired to produce soil CO_2 and the allochthonous recalcitrant carbon would be respired at a slower rate and preserved in the paleosols as soils aggraded. In this situation, the true magnitude of the atmospheric CIE would be recorded by the pedogenic carbonates, while the full CIE in the bulk SOM would be suppressed. Evidence for this mechanism would be seen in the %C preserved in each soil in relation to its $\Delta^{13}C$ anomaly. If increased sedimentation were delivering older recalcitrant carbon to the PETM soils, one would expect to observe a trend of increasing $\Delta^{13}C$ anomaly with increasing %C in a soil. Figure 4.4 shows the $\Delta^{13}C$ anomaly vs. %C for soils at each site. There is no trend of increasing magnitude of $\Delta^{13}C$ anomaly with amount of preserved SOM in each soil. In fact, at Axhandle Canyon and Tenduy, soils forming during the PETM actually tend to have lower %C than before and after the event.

4.4.5 Methane Cycling

Under anaerobic conditions, microbial methanogenesis and methanotrophy within soils can produce CO_2. Biogenic methane is isotopically very depleted, and has typically has a $\delta^{13}C$ of ~-60‰ (Whiticar, 1999). Oxidation of that methane by other microbes would contribute CO_2 to the soil atmosphere that is isotopically more depleted than respired CO_2. Even a small proportion of total soil CO_2 coming from oxidation of methane could shift the isotopic composition of soil CO_2 such that pedogenic carbonates

precipitating in equilibrium with that CO_2 would be isotopically more depleted than expected. Highly negative $\delta^{13}C_{cc}$ values from floodplain limestones in the Bighorn basin have been attributed to oxidation of methane in ponded water and palustrine environments (Bowen and Bloch, 2002). The anoxic or low oxygen environments necessary for methane production require water logged soil conditions. Various continental paleoprecipitation records show increases in seasonality of precipitation in many regions during the PETM (Schmitz and Pujalte, 2007; Handley et al., 2012), which could cause seasonal water logging of soils. However, pedogenic carbonate precipitation requires well-drained soil conditions, which typically occurs during the dry months in a seasonal climate (Breecker et al., 2009). Therefore, the soil conditions required for both the production of methane and the precipitation of pedogenic carbonates should occur at different times of the year in a climate with highly seasonal precipitation or in soils with completely different drainage conditions, and we would not expect CO_2 derived from methane to contribute to soil CO_2 during the time of carbonate formation.

4.4.6 Increased Surface Carbon Cycling

Assuming that the preserved SOM is accurately recording the isotopic composition of plant material, then the isotopic composition of total soil CO_2 (from which the pedogenic carbonates are precipitating) is not tracking respired plant material, which suggests a different isotopically depleted source of carbon for soil CO_2. The $\delta^{13}C_{org}$ of SOM in a soil profile increases with depth due to processes of microbial decomposition which preferentially oxidize ^{12}C, leaving behind SOM more enriched in ^{13}C. The degree of isotopic enrichment at depth is dependent on MAT (Garten et al.,

2000) as well as grain size (Wynn et al., 2005; Wynn, 2007). The difference between the $\delta^{13}C_{org}$ of input leaf litter and $\delta^{13}C_{org}$ of SOM at depth increases with increasing MAT and decreasing grain size. The majority of respired CO_2 in a soil is generated from the microbial decomposition of labile dead plant material and SOM, as well as photorespiration by roots and respiration of root exudates (Hanson et al., 2000; Kuzyakov, 2006), and the proportion of respiration from these different pools is dependent on a variety of factors including vegetation type (Hanson et al., 2000) and climate (Chen et al., 2000; Taneva et al., 2006). Changing temperature and precipitation regimes could change the types of carbon respired in soils and may increase carbon turnover rates in soils (Schimel et al., 1994; Knorr et al., 2005), and also alter the rates at which separate pools of soil carbon are respired (Knorr et al., 2005; Carillo et al., 2011; Liang and Balser, 2012). Labile carbon and carbon derived from root respiration is isotopically depleted in ^{13}C compared to SOM at depth, and increased root respiration or respiration of this labile carbon near the surface of the soil could contribute more isotopically ^{13}C depleted CO_2 to total soil CO_2 and change the $\delta^{13}C$ of total soil CO_2 ($\delta^{13}C_s$) without changing $\delta^{13}C_{org}$ of SOM. In this situation the pedogenic carbonates that precipitated from this soil CO_2 would not track the $\delta^{13}C_{org}$ of respired SOM at depth, but would instead record a mixture of CO_2, with a larger proportion of CO_2 originating from the respiration of root or dead plant material rather than SOM at depth in the soil.

We can compare the $\delta^{13}C_s$ recorded by the pedogenic carbonates at Polecat Bench and Tendruy to the predicted $\delta^{13}C_s$ for soils respiring SOM at depth as well as soil CO_2 derived from varying amounts of root or labile carbon respiration to determine if increased respiration of isotopically depleted labile carbon could explain the observed

$\Delta^{13}C$ anomalies. Figure 4.5 plots the $\delta^{13}C_s$ recorded by the pedogenic carbonates at Polecat Bench and Tendruy accounting for a 5° (Fig. 4.2A) or 10°C (Fig 4.2B) MAT increase in the temperature dependent fractionation between $\delta^{13}C_{cc}$ and $\delta^{13}C_s$ (Romanek et al., 1992). The shaded areas show the predicted $\delta^{13}C_s$ for pre/post-PETM soils respiring only SOM at depth, as well as the predicted $\delta^{13}C_s$ for PETM soils with up to 100% contribution of respired labile and root carbon to soil CO_2. The $\delta^{13}C_{org}$ of surface litter carbon was calculated using the temperature dependent offset between $\delta^{13}C_{org}$ of SOM and $\delta^{13}C_{org}$ of leaf litter published by Garten et al. (2000), and we have assumed that the $\delta^{13}C_{org}$ of leaf litter equals that of labile and root carbon. Table 1 displays the predicted $\delta^{13}C_{org}$ of labile carbon during the PETM at Polecat Bench and Tenduy for both a 5°C and 10°C warming across the event. The predicted $\delta^{13}C_s$ at depth is then calculated following the Cerling (1991) soil CO_2 diffusion model, where $\delta^{13}C_a$ decreases from -5‰ (Tipple et al., 2010) to -8‰ (McInerney and Wing, 2011) and atmospheric pCO_2 increases from 500 to 1500 ppm during the PETM (McInerney and Wing, 2011) and temperature warms by 5° and 10°C. Predicted $\delta^{13}C_s$ values are reported for 100 cm depth.

Figure 4.5 shows that the $\delta^{13}C_s$ values recorded by pedogenic carbonates have some contribution of respired labile and root carbon to soil CO_2. The Axhandle Canyon $\Delta^{13}C$ anomalies are most likely explained by an increase in productivity and temperature and data for that site are not displayed. For Polecat Bench, the majority of pedogenic carbonates record soil CO_2 that is comprised of 25 to 75% respired labile or root carbon. For a 5°C (Fig. 4.5A) warming during the PETM, three of these carbonates show greater than 100% contribution of labile or root carbon to soil CO_2, however with a 10°C warming (Fig. 4.5B), all carbonates fall within a reasonable range (below 100%

contribution of respired labile carbon to soil CO_2) of $\delta^{13}C_s$ values. Many the pre/post-PETM carbonates at Polecat Bench also record soil CO_2 that is isotopically depleted in ^{13}C compared to preserved SOM. These carbonates are from the rising limb of the CIE (meter level 1498–1500) as well as one carbonate that may be recording a pre-PETM carbon release event that has been documented in $\delta^{13}C_{org}$ records from multiple sites in the Bighorn Basin as well as at Tendruy (Domingo et al., 2009). The Tendruy carbonates exhibit a similar but slightly smaller contribution of labile or root carbon to soil CO_2 than Polecat Bench. For a 5°C temperature increase, there is one carbonate that records a greater than 100% contribution of labile carbon to soil CO_2, which is remedied when temperature is increased by 10°C. This plot suggests that the mechanism causing the $\Delta^{13}C$ anomalies was likely increased respiration and carbon cycling of near-surface labile litter and/or root carbon. Given that pedogenic carbonates form over hundreds to thousands of years (Retallack, 2005), a prolonged change in the type of carbon respired must have occurred to sustain $\Delta^{13}C$ anomalies throughout the PETM. These results also imply that temperature increases during the PETM may have been closer to 10° than 5°C during the time of carbonate formation. This observation is supported by multiple temperature reconstructions from the Bighorn Basin and Axhandle Canyon that show larger increases in summer temperatures, the time of pedogenic carbonate formation, than in MAT during warming events (Fricke and Wing, 2004; Snell et al., 2013; VanDeVelde et al., 2013).

Modern soil studies demonstrate that warming and increased atmospheric pCO_2 could increase rates of carbon cycling and thus, increase root respiration and respiration labile carbon. This prediction is supported by the $\Delta^{13}C$ anomalies found during the

PETM. Many studies (e.g. Schimel et al., 1994; Trumbore et al. 1996; Chen et al., 2000; Knorr et al., 2005) show increased rates of carbon cycling and increased respiration of labile or root carbon under warming conditions. However, these increased carbon turnover rates seem to be restricted to only labile carbon. Cardon et al. (2001) show that microbes shift from respiring old SOM to new more labile root biomass in California grasslands under warming and increased atmospheric pCO_2. Carillo et al. (2011) also find that for prairie soils in Wyoming, increased warming and atmospheric CO_2 increase the amount of labile carbon as well as labile carbon decomposition rates in the top 5 cm of soil, but respiration rates for resistant SOM do not change. Therefore, one could expect to observe increased rates of carbon cycling and increased respiration of labile carbon near the surface of soils under climatic warming and increased atmospheric pCO_2 during the PETM. The $\Delta^{13}C$ anomalies observed at Polecat Bench, Tendruy, and, to a lesser extent, Axhandle Canyon likely preserve a record of changing soil respiration and increased carbon turnover rates during the PETM.

4.5 Implications for Carbon Cycle

Increased rates of respiration and turnover in labile carbon may change the size of the terrestrial carbon pool and consequently affect the global carbon cycle. Trumbore et al. (1996) suggest that changing soil carbon dynamics due to anthropogenic climate change could alter the amount of carbon stored in soils. An increase in soil respiration would need to be matched by an equivalent increase in plant biomass production to maintain the size of the terrestrial carbon stock. However, it is currently unclear whether plant productivity will continue to respond to CO_2 fertilization (Friedlingstein et al.,

2006; Pan et al., 2011; Ballantyne et al., 2012), as net primary productivity is limited by other nutrients such as phosphorus and nitrogen (Vitousek and Howarth, 1991; Vitousek and Farrington, 1997). If an increase in respiration outpaced increases in plant biomass production, then warming could create a positive feedback in which increased respiration decreased soil carbon stocks and increases the reservoir of atmospheric CO_2. In order to change the amount of carbon buried in soils, an increase in overall respiration is not necessary. Because soils aggrade and labile carbon is eventually buried as SOM, increasing respiration at the surface of the soil removes labile carbon at a faster rate and decreases the amount of surface carbon available to be buried in the recalcitrant stable pool of SOM at depth. This decrease in the amount of carbon entering the SOM pool has been observed under warming and elevated atmospheric pCO_2 in modern grassland soils (Cardon et al., 2001), and extrapolated over hundreds to thousands of years, decreases in amount of carbon buried as soils aggrade would eventually decrease the amount of carbon stored on land in soils.

The $\Delta^{13}C$ anomalies suggest an increase in carbon turnover rates for labile soil carbon that was nearly constant throughout the PETM. Given the length of the PETM warming event (ca. 100 Kyr), these increased turnover rates likely caused a decrease in the size of the soil carbon pool. Evidence for such a decrease in terrestrial carbon storage could be recorded in the rock record as a decrease in the amount of carbon preserved at depth in the PETM paleosols. This decrease in amount of SOM is observed in many paleosols during the PETM, including the paleosols at Axhandle Canyon and Tenduy, and also at Claret, Spain (Domingo et al., 2009) and Cabin Fork in the Bighorn Basin (Wing et al. 2005) as shown in Figure 4.6. Preliminary evidence from the Bighorn Basin

Coring Project also shows decreases in the abundance of preserved n-alkanes (Baczynksi et al. 2012) as well as pollen (Harrington and Jardine, 2012) during the PETM. Measured $\Delta^{13}C$ anomalies and decreases in preserved organic carbon abundances occur at multiple sites with differing ecosystems. Axhandle Canyon was an arid, low productivity ecosystem (Bowen and Bowen, 2008), whereas Polecat Bench and Tendruy were temperate forests (Wing et al. 2005; Domingo et al., 2009), suggesting that changes to soils occurred on a global scale. Thus, increased root respiration or respiration of labile carbon during the PETM suggests a net flux of carbon out of soils and a significant decrease in the size of the terrestrial reservoir of carbon stored in soils.

A decrease in terrestrial carbon stored in soils translates to an increase in the size of the atmospheric carbon reservoir (Trumbore et al., 1996). This processes of changing respiration rates and its effect on the carbon cycle is summarized in Figure 4.7, where the thickness of the line is proportional to the relative size of the fluxes. Because the CIE in different carbon pools on Earth remains stable during the PETM (McInerney and Wing, 2011), it has been suggested that the warming event was caused by a continued release of carbon to the atmosphere and that this carbon may have come from more than one source (Zeebe et al., 2009). It is possible that a first pulse of warming from a release of carbon to the atmosphere from methane clathrates or another source initiated a positive feedback in soils, causing increased carbon turnover rates in the surface of soils. This increase in respiration reduced the amount of carbon that was able to buried as stable SOM, and thereby increased the flux of carbon back to the atmosphere (Fig. 4.7). The release of this carbon back to the atmosphere would contribute to the atmospheric CIE, as respired CO_2 is isotopically more depleted than atmospheric CO_2. Given that the magnitude of

temperature change during the PETM is analogous to future climate change over the next 100+ years (Kump, 2011), a positive feedback system by which increased carbon turnover rates decreases carbon burial in soils and increases the concentration of atmospheric CO_2 could occur as a result of anthropogenic CO_2 emissions.

4.6 Conclusions

The carbon isotope excursion during the Paleocene-Eocene Thermal Maximum is larger in pedogenic carbonates than in corresponding soil organic matter for the same soils. These different CIEs result in $\Delta^{13}C$ anomalies at three sites around the world. The differing CIEs and resulting $\Delta^{13}C$ anomalies are likely caused by increased carbon turnover rates for labile and root derived carbon. Increased labile carbon turnover rates likely initiated a positive feedback system in which decreased carbon stored in soils lead to increased concentrations of atmospheric CO_2. Modern soil studies support the conclusion that warming increases respiration rates for labile carbon pools, however due to length limitations of these experiments it is not possible to determine how respiration changes influence the carbon cycle over hundreds to thousands of years from modern studies. Isotopic evidence from PETM paleosols show long term changes to soil respiration as a result of climatic warming and suggest that these changes can decrease the amount of carbon buried in soils and affect the global carbon cycle. Therefore, it is possible that future climate warming will alter soil carbon cycling rates resulting in increasing fluxes of carbon to the atmosphere.

4.7 Acknowledgements

The authors would like to acknowledge the American Association for Petroleum Geologists, the Society for Sedimentary Geology, the University of Michigan Scott Turner Award and the University of Michigan Rackham Graduate School and NSF Award 1024535 to NDS for funding this research. The authors would also like to thank Lora Wingate for sample analysis and Ethan G. Hyland for helpful discussions.

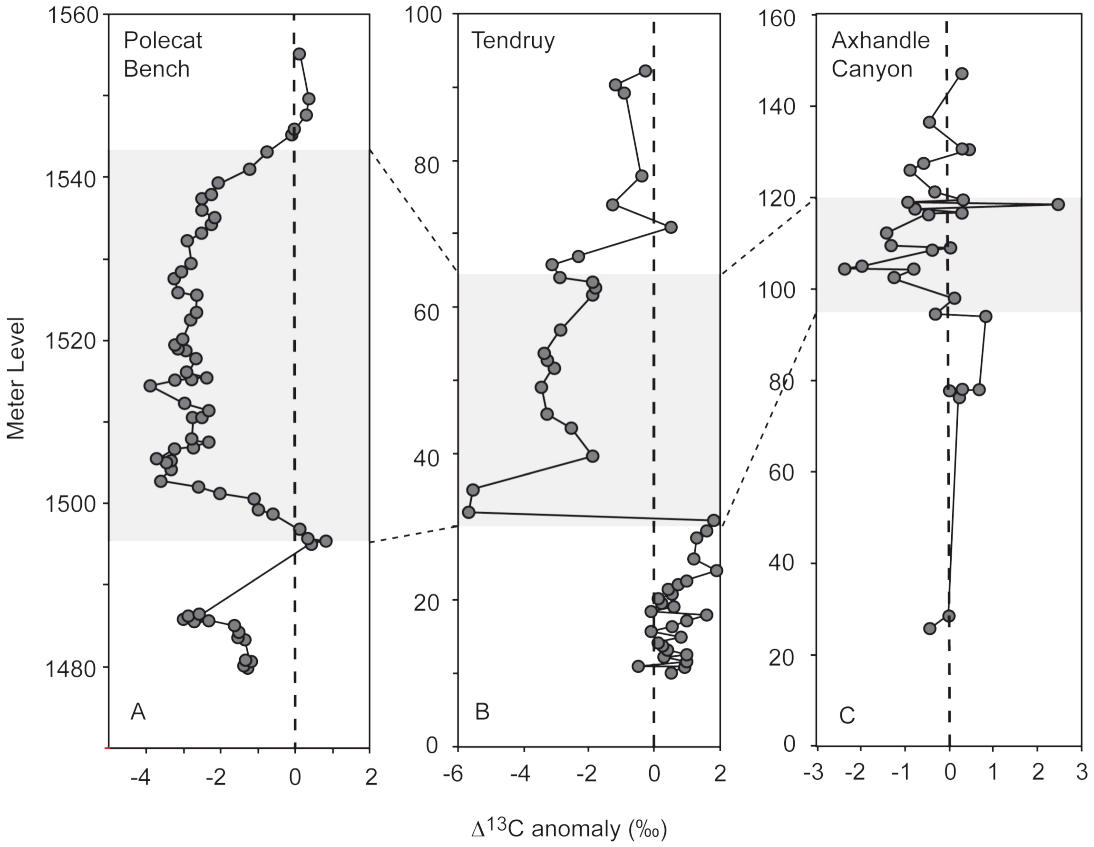

Figure 4.1. $\Delta^{13}C$ anomalies for Polecat Bench (A), Tendruy (B), and Axhandle Canyon (C) calculated using Eq. 4.2. The gray shaded areas highlight the PETM event. The anomalies are similar in magnitude for each site. The $\mu\Delta^{13}C$ value used in Eq. 4.2 for Polecat bench was calculated using only post-PETM soils because the pre-PETM soils are likely recording a brief negative atmospheric CIE prior to the PETM (Domingo et al., 2009).

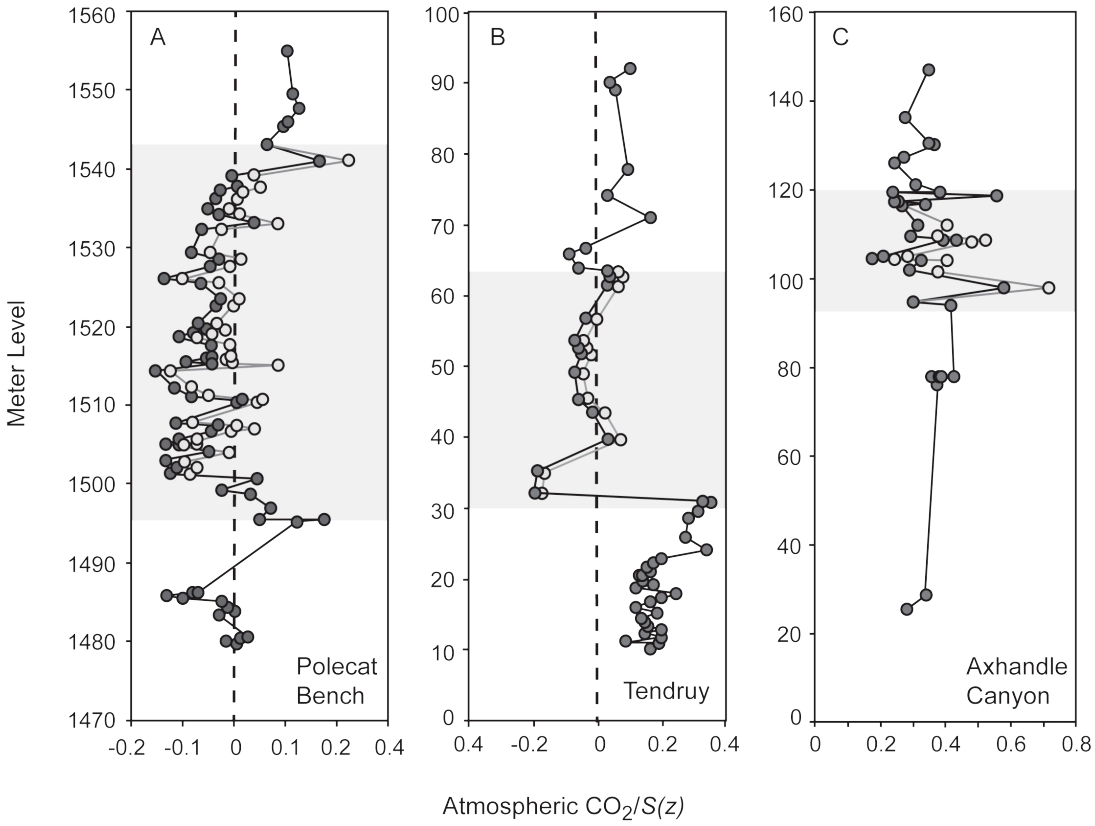

Figure 4.2. Atmospheric $CO_2/S(z)$ ratios for each site calculated using Eq. 4.3. Dark gray circles are calculated changes in atmospheric$CO_2/S(z)$ for a 5°C increase in temperature during the PETM. Light gray circles are for a 10°C increase in temperature. Decreasing values are caused by increasing productivity under warming, but at Tendruy and Polecat Bench, many atmospheric $CO_2/S(z)$ values are negative, implying negative atmospheric CO_2 concentrations. These negative values show that productivity and temperature increases alone cannot explain the full $\Delta^{13}C$ anomalies at Polecat Bench and Tendruy.

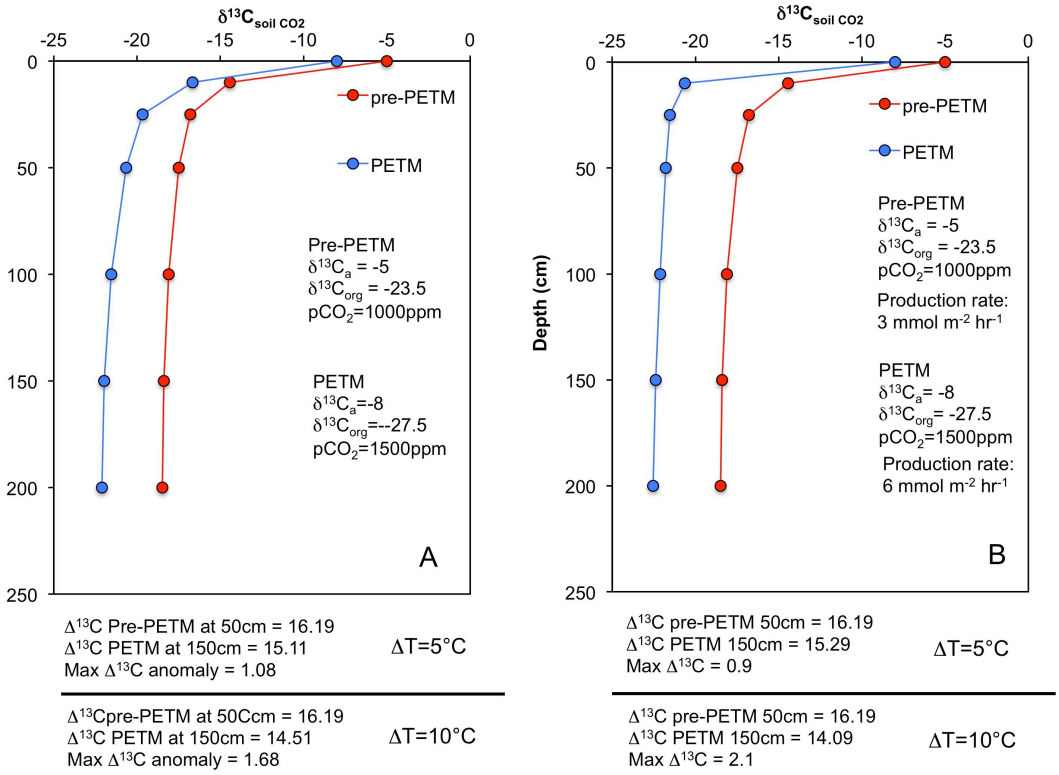

Figure 4.3. The isotopic composition of soil CO_2 with depth in a hypothetical soil. Because the isotopic composition of soil CO_2 is not steady with depth in a soil, a negative $\Delta^{13}C$ anomaly could be observed by changing the depth of carbonate formation. A pre-PETM soil is plotted in red, with a $\delta^{13}C_r$ value of -23.5‰, a $\delta^{13}C_a$ value of -5‰, and an atmospheric CO_2 concentration of 1000 ppm. In blue is an example PETM soil, with a $\delta^{13}C_r$ value of -27.5‰, a $\delta^{13}C_a$ value of -8‰, an atmospheric CO_2 concentration of 1500 ppm (A). In panel B, the same conditions apply except that productivity has increased from 3 mmol m^{-2} hr^{-1} to 6 mmol m^{-2} hr^{-1}. The maximum $\Delta^{13}C$ that could be caused by increasing the depth of carbonate formation by 100 cm is only 2.1. Under this scenario the increase in atmospheric pCO_2 is only 500 ppm. It is likely that atmospheric pCO_2 increased more than this during the PETM. Higher atmospheric pCO_2 during the PETM or lower atmospheric pCO_2 before the PETM would decrease the maximum observed $\Delta^{13}C$ anomaly from changing the depth of carbonate formation. Therefore, this mechanism cannot explain the full $\Delta^{13}C$ anomalies observed at Polecat Bench and Tendruy.

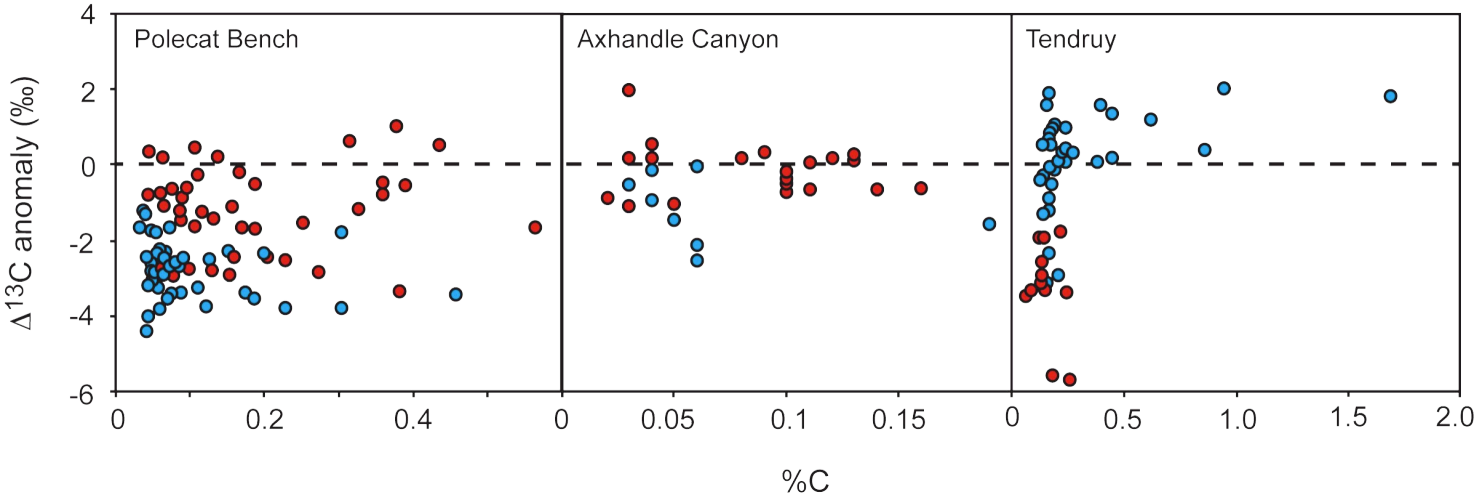

Figure 4.4. $\Delta^{13}C$ anomaly vs. %C for each PETM site. If increased sedimentation delivered an older source of carbon to the soils that muted the CIE in bulk soil organic material, we would expect to see a trend of increasing %C preserved with increasing magnitude of $\Delta^{13}C$ anomalies. This trend is not visible in the data, and many soils with the highest magnitude $\Delta^{13}C$ anomalies have very low %C, especially for Tendruy and Axhandle Canyon.

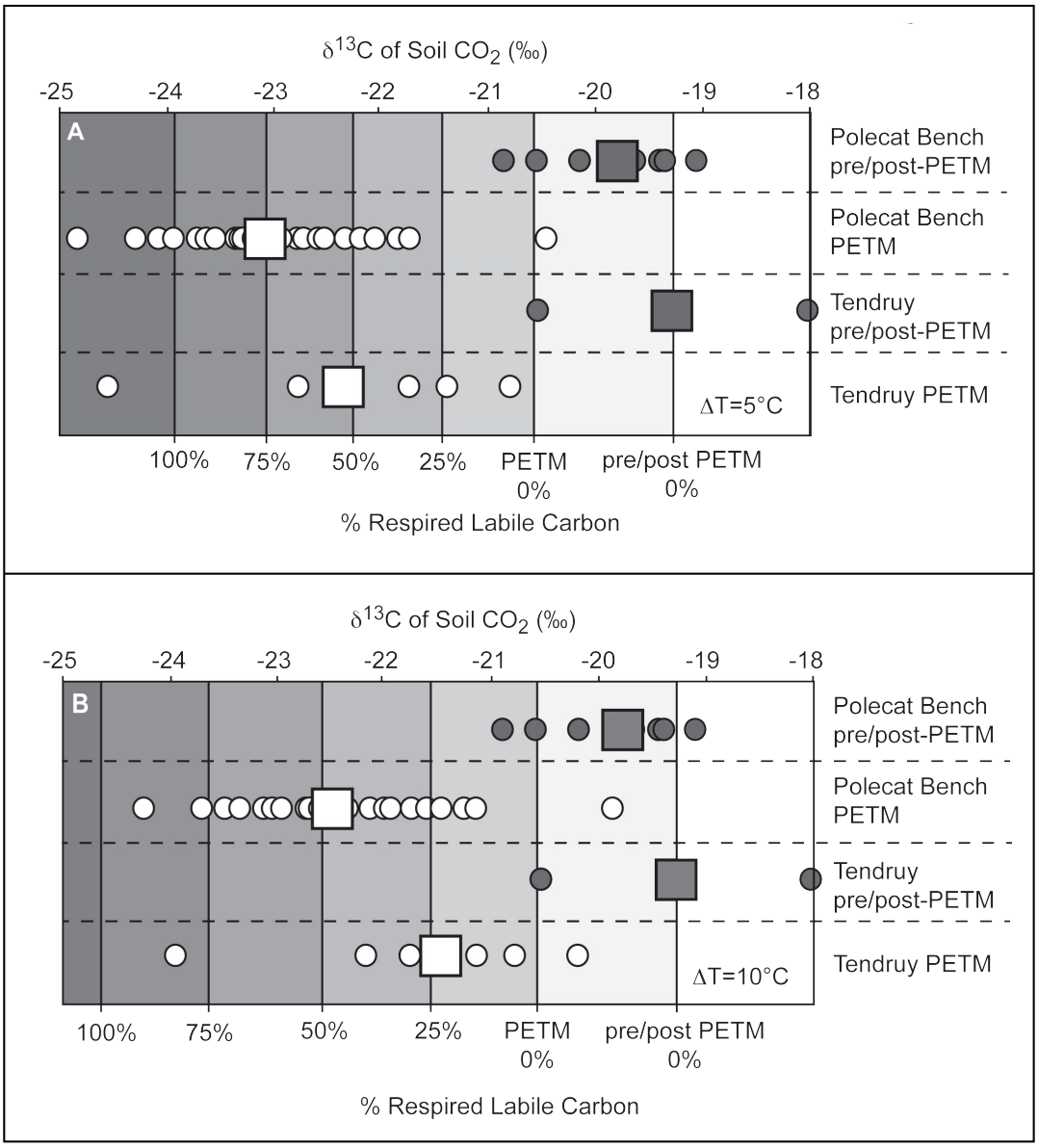

Figure 4.5. Predicted $\delta^{13}C_s$ and $\delta^{13}C_s$ recorded by the isotopic composition of pedogenic carbonates from Polecat Bench and Tendruy for the pre/post PETM. The predicted $\delta^{13}C_s$ is based on a change in atmospheric pCO_2 of 500 ppm to 1500 ppm, a change in $\delta^{13}C$ of atmospheric CO_2 of -5 to -8‰, and no overall productivity change during the PETM. Each predicted $\delta^{13}C_s$ value is for 100 cm depth in the soil. $\delta^{13}C_{org}$ of labile carbon values were calculated using the dependence of $\delta^{13}C_{litter} - \delta^{13}C_{som}$ on MAT (Garten et al., 2000). These values are summarized in Table 1. Also plotted is the $\delta^{13}C_s$ recorded by pedogenic carbonates. Each $\delta^{13}C_{cc}$ value is converted to $\delta^{13}C_s$ using the temperature dependent fractionation between CO_2 and calcite (Romanek et al., 1992). The top panel assumes $\Delta T=5°C$ and the bottom assumes $\Delta T=10°C$ during the PETM.

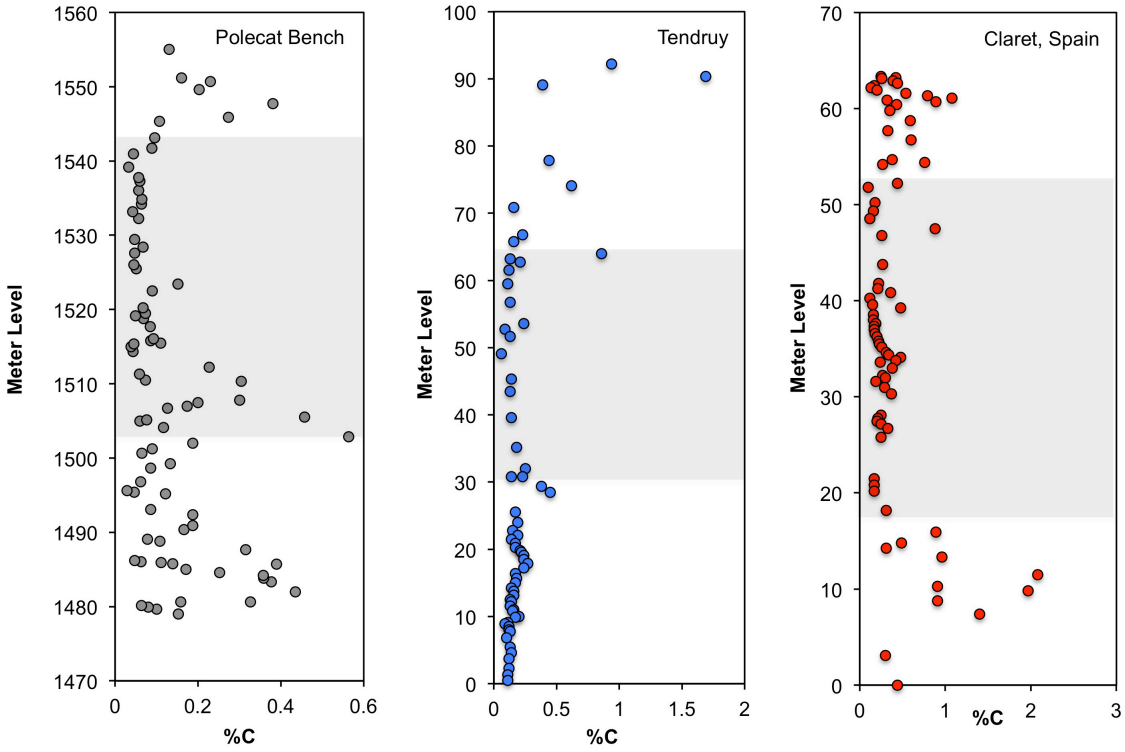

Figure 4.6. Percent carbon preserved in paleosols during the PETM from three different sites. At Polecat Bench (Magioncalda et al., 2004) and Claret, Spain (Domingo et al., 2009), the percent carbon drops during the PETM and then rises again after the PETM. At Tendruy (Domingo et al., 2009), the percent carbon is low before and during the event, but then increases after. These sites support the hypothesis that the soil carbon pool decreased in side during the PETM.

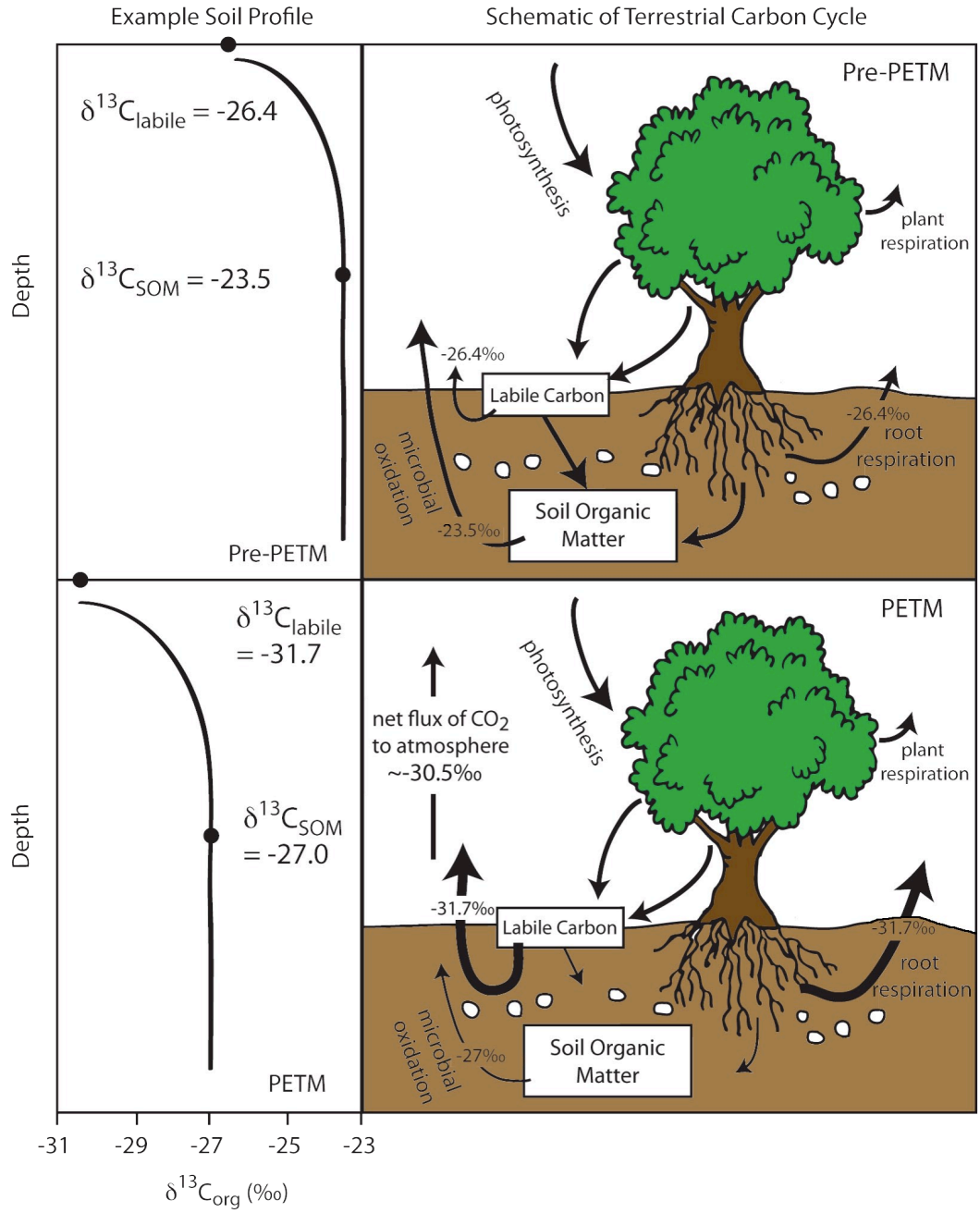

Figure 4.7 Left: Diagram of the $\delta^{13}C_{org}$ enrichment with depth in a hypothetical Pre-PETM and PETM soil displayed Rayleigh fractionation. Representative isotopic values for SOM are taken from measured values at Polecat Bench (Bowen and Bowen 2008). Surface $\delta^{13}C_{litter}$ values were calculated using the temperature dependent offset between $\delta^{13}C_{som}$ and $\delta^{13}C_{litter}$ of Garten et al. (2000) assuming a 5°C MAT increase. Right: Schematic diagram of changing soil respiration during the PETM. The arrows represent fluxes of carbon into terrestrial pools and fluxes of respired carbon back to the atmosphere. The thickness and length of the lines and size of the arrows represent the

relative magnitude of the fluxes of carbon. During the PETM, an increase in respiration rates of labile carbon reduced the amount of carbon converted to stable SOM, which over time could have caused an increase in the net flux of CO_2 to the atmosphere. The hypothetical isotopic composition of CO_2 released from soils to the atmosphere assumes CO_2 is sourced 75% from the respiration of litter and 25% from respiration of SOM.

	SOM at Depth		Surface Litter	
Site	pre/post-PETM	PETM	T=20°C	T=25°C
Polecat Bench	-24.16	-26.42	-30.16	-30.99
Tendruy	-24.60	-26.32	-30.06	-30.80

Table 4.1. $\delta^{13}C_{org}$ values used to calculate $\delta^{13}C_s$ with varying contributions of respiration from surface litter. $\delta^{13}C_{org}$ of surface litter is dependent on MAT, and was calculated using the following equation derived from Garten et al. (2000).

$$\delta^{13}C_{som} - \delta^{13}C_{litter} = 0.166(MAT)+0.41 \; R^2 = 0.54$$

4.8 References

Andrews, J.A., Schlesinger, W.H., 2001. Soil CO_2 dynamics, acidification, and chemical weathering in a temperate forest with experimental CO_2 enrichment. Global Biogeochemical Cycles 15, 149–162.

Armitage, J.J., Duller, R.A., Whittaker, A.C., and Allen, P.A., 2011. Transformation of tectonic and climatic signals from source to sedimentary archive. Nature Geoscience 4, 231–235.

Baczynski, A.A., McInerney, F.A., and Wing, S.L., 2012. Preliminary n-alkane results from Basin Substation, BBCP. Abstract 1499156 presented at 2012 Fall Meeting, AGU, San Francisco.

Ballantyne, A.P., Alden, C.B., Miller, J.B., Tans, P.P., and White, J.W.C., 2012. Increase in observed net carbon uptake by land and oceans during the past 50 years. Nature 488, 70–73.

Bowen, G.J., Beerling, D.J., Koch, P.L., Zachos ,J.C., and Quattlebaum, T., 2004. A humid climate state during the Palaeocene/Eocene thermal maximum. Nature 432, 495–499.

Bowen, G.J., and Bowen, B.B., 2008. Mechanisms of PETM global change constrained by a new record from central Utah. Geology 36, 379–382.

Bowen, G.J. and Bloch, J.I., 2002. Petrogrpahy and geochemistry of floodplain limestones from the Clarks Fork Basin, Wyoming, U.S.A.: Carbonation deposition and floodplain accumulation on a Paleocene-Eocene floodplain. Journal of Sedimentary Research 72, 46–58.

Bowen, G.J., Koch, P.L., Gingerich, P.D., Norris, R.D., Bains, S. and Corfield, R.M., 2001. Refined isotope stratigraphy across the continental Paleocene-Eocene boundary on polecat bench in the northern Bighorn Basin. University of Michigan Papers on Paleontology 33, 73–88.

Breecker, D.O., Sharp, Z.D., and McFadden, L.D., 2010. Atmospheric CO_2 concentrations during ancient greenhouse climates were similar to those predicted for A.D. 2100. Proceedings of the National Academy of Sciences 107, 576–580.

Brook, G.A., Folkoff, M.E. and Box, E.O., 1983. A world model of soil carbon dioxide. Earth Surface Processes and Landforms 8, 79–88.

Cardon, Z.G., Hungate, B.A., Cambardella, C.A., Chapin III, F.S., Field, C.B., Holland, E.A., and Mooney, H.A. 2001. Contrasting effects of elevated CO_2 on old and new soil carbon pools. Soil Biology and Biochemistry 33, 365–373.

Carillo, Y., Pendall, E., Dijkstra, F.A., Morgan, J.A., and Newcomb, J.M. 2011. Response of soil organic matter pools to elevated CO_2 and warming in a semi-arid grassland. Plant and Soil 347, 339–350.

Cerling, T.E. 1984. The stable isotopic composition of modern soil carbonate and its relationship to climate. Earth and Planetary Science Letters 271, 229–240.

Cerling, T.E., 1991. Carbon dioxide in the atmosphere: evidence from Cenozoic and Mesozoic paleosols. American Journal of Science 291, p. 377–400.

Cerling, T.E., 1999. Stable carbon isotopes in paleosol carbonates, *in* Thiry, M., and Simon-Coinco, R., eds., Palaeoweathering, Palaeosurfaces and Continental Deposits. International Association for Sedimentology Special Publication 27, p. 43–60.

Chen, H., Harmon, M.E., Griffiths, R.P. and Hicks, W., 2000. Effects of temperature and moisture on carbon respired from recomposing woody roots. Forest Ecology and Management 138, 51–64.

Cotton, J.M., and Sheldon, N.D., 2012. New constraints on using paleosols to reconstruct atmospheric pCO_2. Geological Society of America Bulletin 124, 1411–1423.

Cotton, J.M., Sheldon, N.D., and Stromberg, C.A.E., 2012. High resolution isotopic record of C_4 photosynthesis in a Miocene grassland. Palaeogeography, Palaeoclimatology, Palaeoecology 337-338, 88–98.

Cotton, J.M., Jeffery, M.L. and Sheldon, N.D. Climate controls on soil-respired CO_2 in the United States: Implications for 21st century chemical weathering rates. In review, Chemical Geology.

Dickens, G.R., Castillo, M.M., and Walker, J.C.G., 1997. A blast of gas in the latest Paleocene: simulating first-order effects of massive dissociation of oceanic methane hydrate. Geology 25, 259–62

Diefendorf, A.F., Mueller, K.E., Wing, S.L., Koch, P.L., and Freeman, K.H., 2010. Global patterns in leaf ^{13}C discrimination and implications for studies of past and future climate. Proceedings of the National Academy of Sciences 107, 5738–5743.

Domingo, L., López-Martínez, N., Leng, M.L. and Grimes, S.T., 2009. The Paleocene-Eocene Thermal Maximum record in the organic matter of the Claret and Tendruy continental sections (South-central Pyrenees, Lleida, Spain). Earth and Planetary Science Letters 281, 226–237.

Fricke, H.C. and Wing, S.L., 2004. Oxygen isotope and paleobotanical estimates of temperature and $\delta^{18}O$-latitude gradients over North America during the early

Eocene. American Journal of Science 304, 612–635.

Friedlingstein, P., Cox, P., Betts, R., Bopp, L., von Bloh, W., Brovkin, V., Cadule, P., Doney, S., Eby, M., Fung, I., Bala, G., John, J., Jones, C., Joos, H., Kato, T., Kawamiya, M., Knorr, W., Lindsay, K., Matthews, H.D., Raddatz, T., Rayner, P., Reick, C., Roeckner, E., Schnitzler, K.-G., Schnur, R., Strassmann, K., Weaver, A.J., Yoshikawa, C., and Zeng, N., 2006. Climate-carbon cycle feedback analysis: Results from the C^4MIP model intercomparison. Journal of Climate 19, 3337–3353.

Foreman, B.Z., Heller, P.L., and Clementz, M.T., 2012. Fluvial response to abrupt global warming at the Paleocene/Eocene boundary. Nature 491, 92–95.

Garten, Jr., C.T., Cooper, L.W., Post III, W.M. and Hanson, P.J., 2000. Climate controls on forest soil C isotope ratios in the southern Appalachian Mountains. Ecology 81, 1108–1119.

Giardina, C.P. and Ryan, M.G., 2000. Evidence that decomposition rates of organic carbon in mineral soil do not vary with temperature. Nature 404, 858–861.

Handley, L., O'Halloran, A., Pearson, P.N., Hawkins, E., Nicholas, C.J., Schouten, S., McMillan, I., and Pancost, R.D. 2012. Changes in the hydrologic cycle in tropical East Africa during the Paleocene-Eocene Thermal Maximum. Palaeogeography, Palaeoclimatology, Palaeoecology 329-330, 10–21.

Hanson, P.J., Edwards, N.T., Garten, C.T. and Andrews, J.A., 2000. Separating root and soil microbial contributions to soil respiration: A review of methods and observations. Biogeochemistry 48, 115–146.

Harrington, G. and Jardine, P. 2012. Bighorn Basin Coring Project: Palynofloral changes and taphonomy through the Paleocene-Eocene Thermal Maximum in the Bighorn Basin, Wyoming, USA. Abstract 1469447 presented at 2012 Fall Meeting, AGU, San Francisco.

Higgins, J.A., and Schrag, D.P., 2006. Beyond methane: Toward a theory for the Paleocene-Eocene Thermal Maximum. Earth and Planetary Science Letters 245, 523–537.

Kennett J.P., and Stott L.D., 1991. Abrupt deep-sea warming, palaeoceanographic changes and benthic extinctions at the end of the Palaeocene. Nature 353, 225–229.

Knorr, W., Prentice, I.C., House, J.I., and Holland, E.A., 2005. Long-term sensitivity of soil carbon turnover to warming. Nature 433, 298–301.

Koch, P.L., Zachos, J.C. and Gingerich, P.D., 1992. Correlation between istope record in

marine and continental resevoirs near the Paleocene/Eocene boundary. Nature 358, 319–322.

Kraus, M.J. and Riggins, S., 2007. Transiet drying during the Paleocene-Eocene Thermal Maximum (PETM): Analysis of paleosols in the bighorn basin, Wyoming. Palaeogeography, Palaeoclimatology, Palaeoecology 245, 444–461.

Kraus, M.J., McInerney, F.A., Wing, S.L., Secord, R., Bacynscki, A.A. and Bloch, J. I., 2013. Paleohydrologic response to continental warming during the Paleocene-Eocene Thermal Maximum. Palaeogeography, Palaeoclimatology, Palaeoecology In Press. DOI: 10.1016/j.palaeo.2012.12.008.

Kump, L.R., 2011. The last great global warming. Scientific American 305(1), 56–61.

Kuzyakov, Y., 2006. Sources of CO_2 efflux from soil and review of partitioning methods. Soil Biology and Biochemistry 38, 425–448.

Liang, C., and Balser, T.C., 2012. Warming and nitrogen deposition lessen microbial residue contribution to soil carbon pool. Nature Communications 3, 1222.

Magioncalda, R., Dupuis, C., Smith, T., Steurbat, E., and Gingerich, P.D., 2004. Paleocene-Eocene carbon isotope excursion in organic carbon and pedogenic carbonate: Direct comparison in a continental stratigraphic section. Geology 32, 553–556.

McInerney, F.A. and Wing, S.L., 2011. The Paleocene-Eocene Thermal Maximum: A perturbation of carbon cycle, climate, and biosphere with implications for the future. Annual Review of Earth and Planetary Sciences 39, 489–516.

Nemani, R.R., Keeling, C.D., Hashimoto, H., Jolly, W.M., Piper, S.C., Tucker, C.J., Myneni, R.B., and Running S.W., 2003. Climate driven increases in global terrestrial net primary production from 1982-1999. Science 300, 1560–1563.

Pagani, M., Caldiera, K., Archer, D. and Zachos, J.C., 2006. An ancient carbon mystery. Science 314, 1556–1557.

Pan, Y., Birdsey, R.A., Fang, J., Houghton, R., Kauppi, P.E., Kurz, W.A., Phillips, O.L., Shvidenko, A., Lewis, S.L., Canadell, J.P., Ciais, P., Jackson, R.B., Pacala, S.W., Mcguire, A.D., Piao, S., Rautiainen, A., Sitch, S. and Hayes, D., 2011. A large and persistent carbon sink in the world's forests. Science 333, 988–993.

Raich, J.W. and Schlesinger, W.H., 1992. The global carbon dioxide flux in soil respiration and its relationship to vegetation and climate. Tellus 44B, 81–99.

Retallack, G.J., 2005. Pedogenic carbonate proxies for amount and seasonality of precipitation in paleosols. Geology 33, 333–336.

Romanek, C.S., Grossman, E.L., and Morse, J.W., 1992. Carbon isotopic fractionation in synthetic aragonite and calcite: Effects of temperature and precipitation rate. Geochimica et Cosmochimica Acta 56, 419–430.

Schlesinger, W.H. 1997. Biogeochemistry: An Analysis of Global Change. Academic Press, San Diego

Schimel, D.S., Braswell, B.H., Holland, E.A., McKeown, R., Ojima, D.S., Painter, T.H., Parton, W.J., and Townsend, A.R., 1994. Climatic, edaphic and biotic controls over storage and turnover of carbon in soils. Global Biogeochemical Cycles 8, 279-293.

Schmitz, B., and Pujalte, V., 2003. Sea-Level, humidity and land-erosion records across the initial Eocene thermal maximum from a continental-marine transect in northern Spain. Geology 31, 689–69.

Schubert, B.A., and Jahren, A.H., 2013. Reconciliation of marine and terrestrial carbon isotope excursions based on changing atmospheric CO_2 levels. Nature Communications 4, 1653.

Smith, F.A., Wing, S.L., and Freeman, K.H., 2007. Magnitude of the carbon isotope excursion at the Paleocene-Eocene Thermal Maximum: the role of plant community change. Earth and Planetary Science Letters 262, 50–65.

Snell, K.E., Thrasher, B.L., Eiler, J.M., Koch, P.L., Sloan, L.C. and Tabor, N.J., 2013. Hot summers in the Bighorn Basin during the early Paleogene. Geology 41, 55–58.

Taneva, L., Pippen, J.S., Schlesinger, W.H. and Gonzalez-Meler, M.A., 2006. The turnover of carbon pools contributing to soil CO_2 and soil respiration in a temperature forest exposed to elevated CO_2 concentration. Global Change Biology 12, 983–994.

Tipple, B.J., Meyers, S.R., and Pagani, M., 2010. Carbon isotope ratio of Cenozoic CO_2: A comparative evaluation of available geochemical proxies. Paleoceanography 25, PA001851.

Trumbore, S.E., Chadwick, O.A., Amundson, R. 1996. Rapid exchange between soil carbon and atmospheric carbon dioxide driven by temperature change. Science 272, 393–396.

Tucker, G.E., and Slingerland R., 1997. Drainage basin responses to climate change. Water Resources Research 33, 2031–2047.

VanDeVelde, J.H., Bowen, G.J., Passey, B.H. and Bowen, B.B., 2013. Climatic and

diagenetic signals in the stable isotope geochemistry of dolomitic paleosols spanning the Paleocene-Eocene boundary. Geochemica et Cosmochimica Acta 109, 254–276.

Vitousek, P.M. and Howarth, R.W., 1991. Nitrogen limitation on land and in the sea: How can it occur? Biogeochemistry 13, 87–115.

Vitousek P.M. and Farrington H., 1997. Nutrient limitation and soil development: Experimental test of a biogeochemical theory. Biogeochemistry 37, 63–75.

Whiticar, M.J., 1999. Carbon and hydrogen isotope systematics of bacterial formation and oxidation of methane. Chemical Geology 161, 291–314.

Wing, S.L., Harrington, G.J., Smith, F.A., Bloch, J.I., Boyer, D.M., and Freeman, K.H., 2005. Transient floral change and rapid global warming at the Paleocene-Eocene boundary. Science 310, 993–996.

Wynn, J.G., 2007. Carbon isotope fractionation during decomposition of organic matter in soils and paleosols: Implications for paleoecological interpretation of paleosols. Palaeogeography, Palaeoclimatology, Palaeoecology 251, 437–448.

Wynn, J.G., Bird, M.I. and Wong, V.N.L., 2005. Rayleigh distillation and the depth profile of $^{13}C/^{12}C$ ratios of soil organic carbon from soils of disparate textures in Iron Range National Park, Far North Queensland, Australia. Geochimica et Cosmochimica Acta 69, 1961-1973.

Zachos, J.C., Pagani, M., Sloan, L., Thomas, E., and Billups, K., 2001. Trends, rhythms and aberrations in global climate 65 Ma to present. Science 292, 686–693.

Zeebe, R.E., Zachos, J.C., and Dickens, G.R., 2009. Carbon dioxide forcing alone insufficient to explain Palaeocene- Eocene Thermal Maximum warming. Nature Geoscience 2, 576–580.

Chapter 5

Summary of Major Results and Conclusions

This chapter presents a summary of the major results of this dissertation, and puts the conclusions into context within the larger framework of paleoclimatic reconstructions, carbon cycling and implications for future anthropogenic climate change.

5.1 Chapter 2

At present, CO_2-temperature sensitivity is poorly constrained, in part due to reconstructions of atmospheric pCO_2 concentrations that contain large uncertainties as well as inconsistencies between different geochemical proxy methods (Paleosens Project Members, 2012). The pedogenic carbonate paleobarometer is the most widely applicable method for atmospheric pCO_2 reconstructions that can be applied back to the Silurian. However, until recently a key variable necessary for pCO_2 reconstructions has been unconstrained. The concentration of respired CO_2 in the soil at the time of pedogenic carbonate formation ($S(z)$) is a commonly assumed value, and in many instances has lead to overestimation of atmospheric pCO_2 compared to other proxy reconstructions that suggest CO_2-temperature coupling throughout the Phanerozoic (Retallack, 2009; Breecker et al., 2010). In this chapter I have derived a relationship between the

concentration of respired CO_2 in a soil at the time of carbonate formation and mean annual precipitation. The relationship was first determined through a literature review of soil-respired CO_2 measurements and climatic data, and was verified using isotopic analyses of moderns soils along a precipitation transect in the United States. This new proxy allows for a unique value of *S(z)* to be applied to each paleosol used with the pedogenic carbonate paleobarometer, which reduces the uncertainty in this method of pCO_2 reconstruction. After revising previously published pedogenic carbonate derived estimates of atmospheric pCO_2, we find the concentration of atmospheric CO_2 to be lower during key times in the geologic past with ample evidence of glaciation in the rock record, and that atmospheric CO_2 was coupled to temperature throughout the Phanerozoic.

The chapter also emphasizes a specific set of guidelines to be followed to make the most accurate reconstructions of atmospheric pCO_2, including only using soils with $\Delta^{13}C$ values from 14–17‰. Montañez (2013) determined the average *S(z)* concentration for different soil orders (including Alfisols) and suggested that only soils with $\Delta^{13}C$ values from 16.6–20.2‰ should be used for atmospheric pCO_2 reconstructions, which is 2–3‰ higher than the range suggested in Chapter 2. Restricting soils to a high $\Delta^{13}C$ range removes a large number of soils forming in moderate to high productivity areas from the potential suite of useful soils for atmospheric pCO_2 reconstructions. For example, many of the Miocene paleosols from the Beaverhead locality discussed in Chapter 2 had $\Delta^{13}C$ less than 16.6‰. These pedogenic carbonates produced pCO_2 estimates consistent with many other pCO_2 proxies and are suitable for atmospheric pCO_2 reconstructions.

As discussed previously, large $\Delta^{13}C$ values are typical in low productivity ecosystems because decreased respiration rates allow for total soil CO_2 to be comprised of a greater proportion of isotopically enriched atmospheric CO_2. As a result of low productivity, soils with a large $\Delta^{13}C$ have low *S(z)* concentrations at the time of carbonate formation. Applying an *S(z)* value typical of a reasonably productive soil ($\Delta^{13}C \approx 16.0$) to a soil with a $\Delta^{13}C$ larger than ~17‰ will result in an overestimation of atmospheric pCO_2. To illustrate, the Beaverhead locality paleosols had an average $\Delta^{13}C$ of 16.6‰ that resulted in an atmospheric pCO_2 estimate of ~280ppm for the late Miocene. One paleosol from the section had a $\Delta^{13}C$ value of 17.9‰, and applying a similar *S(z)* value as the other soils resulted in a pCO_2 estimate of ~460 ppm, higher than all other contemporaneous proxy records. Therefore, while Montañez (2013) appears to have expanded the types of soils useful for pedogenic carbonate paleobarometry beyond the work presented in Chapter 2 with the inclusion of Alfisols, it is likely that applying the relatively large average *S(z)* values determined for each soil order to soils with large (>17‰) $\Delta^{13}C$ values will result in the overestimation of atmospheric pCO_2 for many reconstructions.

5.2 Chapter 3

While anthropogenic CO_2 emissions currently total ~8 gigatonnes per year, roughly half of those annual emissions are taken up by the biosphere and oceans in various carbon sinks (Schimel et al., 2001; Le Quéré et al., 2009; Ballantyne et al., 2012). However, it is currently unclear whether the biosphere will continue to take up carbon and buffer anthropogenic CO_2 emissions at the same rate as the previous two decades

(Ballantyne et al., 2012). Soils store nearly four times as much carbon as the terrestrial biosphere (Fig. 1.1) and have the potential to become either sinks or sources of carbon to the atmosphere (Trumbore et al., 1996; Chapter 4) depending on changes to rates of photosynthesis, respiration and weathering, and studying soil productivity is important for constraining changes to the carbon cycle on decadal timescales.

The long-term control on the concentration of CO_2 in the atmosphere is the chemical weathering of silicate minerals (Berner et al., 1983; Berner and Kothavala, 2001; Berner, 2006). Until recently, the rates of chemical weathering and thus the consumption of atmospheric CO_2 were not thought to change significantly on decadal timescales (Gislason et al., 2009; Beaulieu et al., 2012; Sheldon and Tabor, 2013). Given that the majority of chemical weathering occurs in soils (West et al., 2012), the concentration of soil CO_2 and thus, of $[CO_{2aq}]$ is an important factor in chemical weathering rates. We show that the concentration of soil-respired CO_2 and $[CO_{2aq}]$ can vary significantly with climate and that these changes can occur on human timescales. Due to projected changes in precipitation, the North-Central Great Plains region of the United States is expected to experience increases in $[CO_{2aq}]$ by up to 50% by the decade 2050–2060 and a consequent increase in chemical weathering and atmospheric CO_2 consumption. On the other hand, $[CO_{2aq}]$ is expected to decline by up to 50% in the Southwestern United States. A decrease in future weathering should not substantially impact CO_2 consumption by soils because little chemical weathering currently occurs in the southwestern United States. This work highlights the importance of further studies to determine other regions in which soils may become sources or sinks for atmospheric CO_2 on decadal timescales that may act to buffer or enhance anthropogenic CO_2 emissions.

5.3 Chapter 4

In Chapter 3, we identified a region that may become a sink for carbon in the coming decades due to increases in the concentration of dissolved CO_2 and accompanying weathering. However, it is currently not clear whether the large stock of carbon stored in soils will be stable under warming over longer timescales (e.g., Trumbore et al., 1996; Giardina et al., 2000; Knorr et al., 2005). In Chapter 4, I examine the carbon isotopic compositions of preserved soil organic material and pedogenic carbonates in an effort to constrain soil carbon cycling during a time of rapid warming analogous to future climate change. Paleosol $\Delta^{13}C$ values decrease substantially for soils formed during the Paleocene/Eocene Thermal Maximum at three different sites. The magnitude of these decreases cannot be explained by temperature or productivity increases, or by a different, older source of carbon being delivered to the soils through sedimentation. Given that pedogenic carbonates are precipitated in equilibrium with soil CO_2, the decreases in $\Delta^{13}C$ can show that the carbonates must have precipitated from CO_2 that had an isotopically lighter composition than the preserved soil organic material. This CO_2 likely came from near-surface labile carbon that experienced increased rates of respiration due to the PETM warming. Higher rates of surface carbon respiration likely drove a decrease in carbon storage in soils and acted as a net source of carbon to the atmosphere. This work demonstrates that soils may have become a source of carbon to the atmosphere under rapid warming conditions, and may also become a new source of carbon to the atmosphere in the future due to anthropogenic warming.

5.4 Implications for Future Climate Change

This dissertation demonstrates the potential for large changes in the carbon cycle due to anthropogenic CO_2 emissions on multiple time scales. Changes to $[CO_{2aq}]$ in soil pore water can change chemical weathering rates (Chapter 4; West et al., 2012). On million-year time scales, $[CO_{2aq}]$ can be altered by the changing composition of the atmosphere in addition to changing climate and its effect on vegetation. However, rapid climate change due to anthropogenic CO_2 emissions has proven that these processes can alter $[CO_{2aq}]$ and resulting atmospheric CO_2 consumption on human timescales as well. In Chapter 4, we use the PETM as an analog for future anthropogenic climate change and show that over longer timescales of hundreds to thousands of years, increases in soil respiration rates can decrease the rate of carbon burial in soils. However, the rates of release of carbon to the atmosphere and consequent warming during the PETM were at least an order of magnitude slower than warming that is occurring today (Zachos et al., 2001; Cui et al., 2011). It is possible that increases to labile carbon respiration and decreases in carbon storage in soils may become an important source of carbon to the atmosphere on shorter timescales as well. Therefore, the possible short-term gains in CO_2 consumption due to increased chemical weathering could be outpaced by reduced carbon burial as soils begin to respire greater amounts of carbon under warming conditions.

This work highlights the fact that carbon reservoirs on Earth are more susceptible to flux changes on multiple time scales than previously thought. While roughly half of the annual anthropogenic CO_2 emissions are currently being taken up by the biosphere and oceans, these sinks for atmospheric CO_2 may not continue take up carbon at the same rate in the future due to vegetation and climatic changes (Le Quéré et al., 2009;

Ballanyne et al., 2012). In the next 100 years as the concentration of atmospheric CO_2 rises and the Earth continues to warm, positive feedback will likely drive soils to become a new source of carbon to the atmosphere. Increased chemical weathering of silicate minerals is one mechanism that may act to enhance terrestrial carbon uptake, but without further study to determine soil CO_2 and [CO_{2aq}] changes in other regions of the world, one cannot say precisely whether increases in soil respiration will outpace possible increases in CO_2 consumption from chemical weathering.

Coupled climate-carbon cycle models used in the IPCC 4th assessment to project changes to carbon cycling due to anthropogenic warming show a consistent decrease in the size of the terrestrial carbon sink and a consequent increase in the rate of accumulation of atmospheric CO_2 due to climate feedbacks (Friedlingstein et al., 2006; IPCC, 2007). These models (C^4MIP, Friedlingstein et al., 2006) treat the decomposition of organic material variably, classifying soil organic carbon into various numbers of labile and recalcitrant pools depending on the particular model. However, for each of the eleven coupled climate-carbon cycle models compared by the IPCC 4th assessment report, the rates of soil organic carbon decomposition are driven by changes in temperature and precipitation. All but one of these models (UMD, Zeng et al., 2004) assumes that different soil carbon pools decompose at the same rate and none takes into consideration changing proportions of soil carbon decomposition and different possible responses to warming between the labile and recalcitrant carbon pools as shown to occur during the PETM in Chapter 4 (Friedlingsetin et al., 2006; IPCC, 2007). While many other variations exist between the coupled climate-carbon cycle models, it is interesting to note that the UMD model that does treat labile and recalcitrant soil carbon pools

differently also shows the largest increases in atmospheric pCO_2, as well as the second lowest level of carbon uptake by the terrestrial biosphere by 2100. These results as well as the conclusions from Chapter 4 of this dissertation suggest that the terrestrial carbon storage may decline faster than is modeled in the IPCC 4th assessment report.

Coupled climate-carbon cycle models used in the 4th IPCC assessment report also do not vary terrestrial weathering on decadal timescales (Friedlingstein et al., 2006). Increases in vegetation productivity across many ecosystems may counteract decreases in terrestrial carbon sinks largely driven by recovery from land use change. To determine how changes to soil CO_2 may affect the global carbon cycle, it is necessary to produce a global model for changes in soil [CO_{2aq}]. Therefore, it is important to continue studying how soils respond to rapid climate warming to determine the most accurate projections of future climate and environmental change because weathering and respiration of soil carbon can have large impacts on the global carbon cycle.

5.5 Future Work

Future work beyond this dissertation will focus on further refining the pedogenic carbonate paleobarometer as well as understanding how $\Delta^{13}C$ varies in modern soils for application to past environmental reconstructions. One way to increase the precision of the pedogenic carbonate paleobarometer would be to derive specific relationships between *S(z)* and MAP for certain types of soils. Montañez (2013) find that *S(z)* is most similar for soils within the same order. It is possible that because soils within the same order behave more similarly, there would be a stronger relationship between *S(z)* and climatic variables when only comparing specific soil orders. A stronger relationship

would reduce the error associated with *S(z)* predictions and reduce the uncertainty in atmospheric pCO_2 reconstructions. Preliminary data show that a strong correlation exists between MAP and both summer average and summer minimum *S(z)* for Mollisols (R^2 = 0.96 and 0.93, respectively), as well as Aridisols (R^2 = 0.57 and 0.83, respectively). The slope of preliminary relationship between *S(z)* and MAP for Mollisols has twice the slope of that for Aridisols, which could explain some of the variability in the overall relationship presented in Chapter 2.

Further work to increase the precision on the pedogenic carbonate paleobarometer will focus on the differences between the $\delta^{13}C_{org}$ of SOM at depth, surface leaf litter and overlying vegetation of modern soils. The carbon isotopic composition of SOM is not constant within a soil profile, but becomes more enriched in ^{13}C with increasing depth due to the microbial oxidation of organic material (Wynn et al., 2005; Wynn, 2007). Because microbial decomposition is faster at higher temperatures (Raich and Schlesinger, 1992; Raich and Potter, 1995), the difference between the $\delta^{13}C_{org}$ of leaf litter and the $\delta^{13}C$ of SOM at depth is temperature dependent. Garten et al. (2000) present a relationship between MAT and the offset between the $\delta^{13}C_{org}$ of leaf litter and SOM at depth. This relationship was based on a limited amount of data, and expanding on this idea with the incorporation of new data could present a method for refining previously published estimates of atmospheric pCO_2.

Many previous studies have used the $\delta^{13}C_{org}$ of preserved plant material as a proxy for the $\delta^{13}C_{org}$ of respired SOM (e.g., Montañez et al., 2007; Cleveland et al., 2008; Retallack, 2009) in the pedogenic carbonate paleobarometer (Eq. 2.1). However, the $\delta^{13}C_{org}$ of SOM is often 2–3‰ more enriched in ^{13}C compared to leaf litter, and using a

value for $\delta^{13}C_r$ that is isotopically heavier than the true value will cause underestimations in atmospheric pCO_2 reconstructions. Defining a strong relationship between the offset between $\delta^{13}C_{org}$ of leaf litter and SOM and MAT could allow one to correct the leaf $\delta^{13}C_{org}$ to SOM $\delta^{13}C_{org}$ in previously published estimates of atmospheric pCO_2 if a MAT estimate is available for the locality. This correction factor could be used to revise previous work and may increase the accuracy of these estimates of atmospheric pCO_2. For the modern soil calibration of the *S(z)*-MAP proxy (Chapter 2), I collected samples from depth profiles for 54 modern soils that can be paired with measured climatic data for each site. These new soils can then be added to the set of 25 soils published by Garten et al. (2000) to determine if the original relationship between $\delta^{13}C_{org}$ and MAT holds with the inclusion of more data. Because the relationship published by Garten et al. (2000) only included temperate forest soils, one should expect that this relationship would behave similarly to the *S(z)*-MAP proxy in that the inclusion of more data may decrease the strength of the relationship due to varying controls on microbial decomposition and soil productivity within different ecosystems. Separating the data by soil order or ecosystem type will likely be an important step in constraining the controls on the offset between leaf and SOM $\delta^{13}C_{org}$.

Stable carbon isotopes of modern soil organic material and carbonates can also be used to understand the controls on $\Delta^{13}C$ for soils that fall outside of the typical 14–17‰ range to determine if there are modern soil analogs with both low and high $\Delta^{13}C$ values that can be used to interpret disequilibrium paleosols. The modern soil dataset used to calibrate the *S(z)*-MAP proxy discussed in Chapter 2 also includes many soils with high and low $\Delta^{13}C$ values for further study. In the future, I will use these soils to try to

constrain the ecological controls on $\Delta^{13}C$. Preliminary analysis shows that many of the soils with $\Delta^{13}C$ values outside the range of 14–17‰ occur in areas that have been disturbed for agricultural purposes, which suggests that careful sampling of modern soils is necessary to exclude anthropogenic effects from the variations in $\Delta^{13}C$. While $\Delta^{13}C$ should be a measure of the productivity of a soil, compilations of modern soil $\Delta^{13}C$ values do not show a clear relationship with climate (Cerling and Quade, 1993; Cotton and Sheldon, unpublished). Factors other than productivity such as parent material, soil order or grain size must also strongly influence $\Delta^{13}C$. I can determine the relative influence of each of these factors by comparing the $\Delta^{13}C$ for soils divided into different categories by soil characteristic. For example, separating $\Delta^{13}C$ for soils by parent material will allow me to exclude geologic controls on $\Delta^{13}C$ and should help to decipher the effects of climate on $\Delta^{13}C$. Future work will investigate how these factors of soil development influence the isotopic composition of different soil carbon pools. Identifying processes in soils that control the fractionation between pedogenic carbonates and SOM, including differences in disturbance regime, diffusion, respiration and varying times of carbonate precipitation can give clues to paleoenvironment that may not be determined from soil morphology and trace fossils alone (Breecker et al., 2009; Mintz et al., 2011).

This dissertation and related future work demonstrates that soils are a dynamic and important component and recorder of the global carbon cycle that warrants more investigation into their potential to contribute to climate change in the future as well as to help us predict and prepare for future ecosystem changes due to anthropogenic CO_2 emissions.

5.6 References

Ballantyne, A.P., Alden, C.B., Miller, J.B., Tans, P.P., and White, J.W.C., 2012. Increase in observed net carbon uptake by land and oceans during the past 50 years. Nature 488, 70–73.

Beaulieu, E., Godderis, Y., Donnadieu, Y., Labat, D., Roelandt, C., 2012. High sensitivity of the continental-weathering carbon dioxide sink to future climate change. Nature Climate Change 2, 346–349.

Berner, R.A., 2006. GEOCARBSULF: A combined model for Phanerozoic atmospheric O_2 and CO_2. Geochimica et Cosmochimica Acta 70, 5653–5664.

Berner, R.A., Lasaga, A.C., Garrels, R.M., 1983. The carbonate-silicate geochemical cycle and its effect on atmospheric carbon dioxide over the last 100 million years. American Journal of Science 283, 641–683.

Berner, R.A., Kothavala, Z., 2001. GEOCARB III: A revised model of atmospheric CO_2 over Phanerozoic time. American Journal of Science 301, 182–204.

Breecker, D.O., Sharp, Z.D., and McFadden, L.D., 2009. Seasonal bias in the formation and stable isotopic composition of pedogenic carbonate in modern soils from central New Mexico, USA. Geological Society of America Bulletin 121, 630–640.

Breecker, D.O., Sharp, Z.D., and McFadden, L.D. 2010. Atmospheric CO_2 concentrations during ancient greenhouse climates were similar to those predicted for A.D. 2100. Proceedings of the National Academy of Sciences 107, 576–580.

Cerling, T.E., and Quade, J., 1993. Stable carbon and oxygen isotopes in soil carbonates, *in* Swart, P.K., Lohmann, K.C., McKenzie, J.A., and Savin, S., eds., Climate Change in Continental Isotopic Records: Washington, D.C., American Geophysical Union, p. 217–231.

Cleveland, D.M., Nordt, L.C., Dworkin, S.I., and Atchley, S.C., 2008. Pedogenic carbonate isotopes as evidence for extreme climatic events preceding the Triassic-Jurassic boundary: Implications for the biotic crisis? Geological Society of America Bulletin 120, 1408–1415.

Cui, Y., Kump, L.R., Ridgwell, A.J., Charles, A.J., Junium, C.K., Diefendorf, A.F., Freeman, K.H., Urban, N.M., and Harding, I.C., 2011. Slow release of fossil carbon during the Paleocene-Eocene Thermal Maximum. Nature Geoscience 4, 481–485.

Friedlingstein, P., Cox, P., Betts, R., Bopp, L., von Bloh, W., Brovkin, V., Cadule, P., Doney, S., Eby, M., Fung, I., Bala, G., John, J., Jones, C., Joos, H., Kato, T.,

Kawamiya, M., Knorr, W., Lindsay, K., Matthews, H.D., Raddatz, T., Rayner, P., Reick, C., Roeckner, E., Schnitzler, K.-G., Schnur, R., Strassmann, K., Weaver, A.J., Yoshikawa, C., and Zeng, N., 2006. Climate-carbon cycle feedback analysis: Results from the C^4MIP model intercomparison. Journal of Climate 19, 3337–3353.

Garten, Jr., C.T., Cooper, L.W., Post III, W.M., and Hanson, P.J., 2000. Climate controls on forest soil C isotope ratios in the southern Appalachian Mountains. Ecology 81, 1108–1119.

Giardina, C.P. and Ryan, M.G., 2000. Evidence that decomposition rates of organic carbon in mineral soil do not vary with temperature. Nature 404, 858–861.

Gislason., S.R., Oelkers, E.H., Eiriksdottir, E.S., Karjilov, M.I., Gisladottir, G., Sigfusson, B., Snorrason, A., Elefsen, S., Hardardottir, J., 2009. Earth and Planetary Science Letters 277, 213–222.

Knorr, W., Prentice, I.C., House, J.I., and Holland, E.A., 2005. Long-term sensitivity of soil carbon turnover to warming. Nature 433, 298–301.

IPCC, 2007. Climate Change 2007: Synthesis Report. IPCC, Geneva, Switzerland, 104 pp.

Le Quéré, C., Raupach, M.R., Canadell, J.G., Marland, G., Bopp, L., Ciais, P., Conway, T.J., Doney, S.C., Feely, R.A., Foster, P., Friedlingstein, P., Gurney, K., Houghton, RA., House, J.I., Huntingford, C., Levy, P.E., Lomas, M.R., Maijkut, J., Metzl, N., Ometto, J.P., Peters, G.P., Prentice, I.C., Randerson, J.T., Running, S.W., Sarmiento, J.L., Schuster, U., Sitch, S., Tacahashi, T., Viovy, N., van der Werf, G.R., and Woodward, F.I., 2009. Trends in the sources and sinks of carbon dioxide. Nature Geoscience 2, 831–836.

Mintz, J.S., Driese, S.G., Breecker, D.O., Ludvigson, G.A., 2011. Influence of changing hydrology on pedogenic calcite precipitation in Vertisols, Dance Bayou, Brazoria, Texas, U.S.A.: implications for estimating paleoatmospheric pCO_2. Journal of Sedimentary Research 81, 394–400.

Montañez, I.P., 2013. Modern soil system constraints on reconstructing deep time atmospheric CO_2. Geochimica et Cosmochimica Acta 101, 57–75.

Montañez, I.P., Tabor, N.J., Niemeier, D., DiMichele, W.A., Frank, T.D., Fielding, C.R., Isbell, J.L., Birgenheier, L.P. and Rygel, M.C., 2007. CO_2-forced climate and vegetation instability during late Paleozoic glaciation. Science 315, 87–91.

Paleosens Project Members, 2012. Making sense of paleoclimate sensitivity. Nature 491, 683–691.

Raich, J.W., and Schlesinger, W.H., 1992. The global carbon dioxide flux in soil

respiration and its relationship to vegetation and climate. Tellus 44B, 81–99.

Raich, J.W., and Potter, C.S., 1995. Global patterns of carbon dioxide emissions from soils. Global Biogeochemical Cycles 9, 23–36.

Retallack, G.J., 2009. Refining a pedogenic-carbonate CO_2 paleobarometer to quantify a middle Miocene greenhouse spike. Palaeogeography, Palaeoclimatology, Palaeoecology 281, 57–65.

Schimel, D.S., House, J.I., Hibbard, K.A., Bousquet, P., Clais, P., Peylin, P., Braswell, B.H., Apps, M.J., Baker, D., Bondeau, A., Canadell, J., Churkina, G., Cramer, W., Denning, A.S., Field, C.B., Friedlingstein, P., Goodale, C., Heinmann, M., Houghton, R.A., Melillo, J.M., Moore III, B., Murdiyarso, D., Modle, I., Pacala, S.W., Prentice, I.C., Raupach, M.R., Rayner, P.J., Scholes, R.J., Steffen, W.L., and Wirth, C., 2001. Recent patterns and mechanisms of carbon exchange by terrestrial ecosystems. Nature 414, 169–172.

Sheldon, N.D., and Tabor, N.J., 2013, Using paleosols to understand paleo-carbon burial: SEPM Special Publication 104, 71-78. Doi: 10.2110/sepmsp.104.11

Trumbore, S.E., Chadwick, O.A., and Amundson, R., 1996. Rapid exchange between soil carbon and atmospheric carbon dioxide driven by temperature change. Science 272, 393–396.

West, A.J., 2012. Thickness of the chemical weathering zone and implications for erosional and climatic drivers of weathering and for carbon-cycle feedbacks. Geology 40, 811–814.

Wynn, J.G., 2007. Carbon isotope fractionation during decomposition of organic matter in soils and paleosols. Implications for paleoecological interpretations of paleosols. Palaeogeography, Palaeoclimatology, Palaeoecology 251, 437–448.

Wynn, J.G., Bird, M.I., Wong, V.N.L., 2005. Rayleigh distillation and depth profile of $^{13}C/^{12}C$ ratios of soil organic carbon from soils of disparate texture in Iron Range National Park, Far North Queensland, Australia. Geochimica et Cosmochimica Acta 69, 1961–1973.

Zachos, J., Pagani, M., Sloan, L., Thomas, E., and Billups, K., 2001. Trends, rhythms and aberrations in global climate 65 Ma to present. Science 292, 686–693,

Zeng, N., H. Qian, E. Munoz, and R. Iacono, 2004: How strong is carbon cycle-climate feedback under global warming? Geophysical Research Letters 31**,** L20203.